

Czech University of Life Sciences Prague
Faculty of Environmental Sciences



The Use of Laser Scanning Data in the Environmental Sciences

Michal Fogl

This dissertation is submitted for the degree of *Doctor of Philosophy*
at the Department of Applied Geoinformatics and Spatial Planning.

Prague

August 2019

The Use of Laser Scanning Data in the Environmental Sciences

Dissertation Thesis

Author: Michal Fogl

Supervisor: Dr. Vítězslav Moudrý
Czech University of Life Sciences Prague

Reviewers: Dr. Marta Szostak
University of Agriculture in Krakow

Dr. Vincent Lecours
University of Florida

Dr. Peter Surový
Czech University of Life Sciences Prague

I hereby declare that the dissertation entitled “*The Use of Laser Scanning Data in The Environmental Sciences*” submitted for the Degree of Philosophy of Applied and Landscape Ecology is my original work guided by my supervisor. All sources of information, text, illustration, tables and images have been specifically cited. The dissertation was not published elsewhere.

.....

Acknowledgements

I would like to thank my supervisor Vítězslav Moudrý for his support, motivation, willingness and knowledge. I would like to acknowledge everyone who contributed towards this thesis, all my colleagues at the Department of Applied Geoinformatics and Spatial Planning and all my co-authors. I would like to particularly thank Jaroslav Janošek for his useful editorial and linguistic advice. Finally, my great thanks go to my fiancée and to my family.

I would also like to express my thanks to everyone who is going to read this study and hope that the readers will find it interesting and enriching.

The scientific papers included in this thesis was funded by the following research projects:

- 17-17156Y
Czech Science Foundation
- SGS18/055/OHK1/1T/11
Grant Agency of the Czech Technical University in Prague
- SGS16/060/OHK1/1T/11
Grant Agency of the Czech Technical University in Prague
- IGA 20154229
*Internal Grant Agency of the Faculty of Environmental Sciences,
Czech University of Life Sciences Prague*
- IGA 20174234
*Internal Grant Agency of the Faculty of Environmental Sciences,
Czech University of Life Sciences Prague*

Abstract

Remote sensing (RS) has significantly enhanced the possibilities of describing the environment and become an irreplaceable data source for analyses in environmental sciences. Capabilities of RS were further improved by introduction of airborne laser scanning (LiDAR), which facilitated a direct collection of relatively accurate three-dimensional spatial data from extensive areas. The presented thesis aims to at least partially respond to the challenges that are associated with the use of LiDAR in environmental sciences, including (a) data collection using laser scanners mounted on unmanned aerial vehicles (UAVs); (b) filtering point clouds acquired from laser scanning; (c) accuracy of digital terrain models acquired using airborne laser scanning and those derived from UAV imagery; and (d) application of laser scanning data in the urban environment.

The results of the thesis showed a great potential of UAV laser scanning for capturing terrain and vegetation. The combination of LiDAR and UAVs is for some projects much more cost-efficient than acquisition of data from conventional airborne laser scanning. It is however necessary to use a suitable UAV platform as the use of an airship in our study proved to be problematic. Under certain circumstances, photogrammetric processing of UAV-acquired imagery may prove to be a suitable alternative to LiDAR for terrain mapping. In the off-leaf season, this method yields a similar accuracy to airborne laser scanning in deciduous forests and in places with low vegetation. In any case, the accuracy of resulting models can be affected by the choice of the filtering algorithm. We have tested filtering algorithms across multiple types of environment and revealed that when choosing the filtering algorithm, it is crucial to

take the character of vegetation (e.g. steppe vs. forest) and terrain into consideration. Finally, the thesis also includes a case study utilizing the existence of freely available LiDAR data. The study discusses the effect of shadows on the rooftop solar potential estimates. The results imply that the effect of shadows cast by vegetation plays a much greater role at a local scale than at a larger scale and when for example considering the solar potential of an entire agglomeration, the effect is negligible.

Abstrakt (Czech)

Dálkový průzkum Země významným způsobem ovlivnil možnosti popisu prostředí a stal se nepostradatelným zdrojem dat pro analýzy v environmentálních vědách. Významnou měrou pak tyto možnosti rozšířilo letecké laserové skenování (LiDAR), které umožnilo přímý sběr relativně přesných trojrozměrných dat z rozsáhlých oblastí. Předkládaná práce si klade za cíl alespoň částečně odpovědět na výzvy, které při používání LiDARu v environmentálních vědách vyvstávají a mezi něž patří následující témata: (a) sběr dat bezpilotními leteckými prostředky (UAVs) využívajícími laserové skenování; (b) filtrace bodových mračen z laserového skenování; (c) přesnost digitálních modelů terénu vytvořených ze snímkování pomocí bezpilotních leteckých systémů a z leteckého laserového skenování a (d) aplikace dat leteckého laserového skenování v urbánním prostředí.

Výsledky práce ukázaly vysoký potenciál UAV laserového skenování pro zachycení struktury vegetace a terénu. Kombinace LiDARu a UAV je pro některé projekty z ekonomického hlediska mnohem dostupnější než pořízení dat konvenčního leteckého laserového skenování. Nicméně je potřeba zvolit vhodný bezpilotní prostředek, neboť zde použitá autonomní vzducholod se ukázala jako problematická. V určitých případech lze jako alternativu LiDARu pro mapování terénu využít metodu fotogrammetrického snímkování pomocí UAV. V mimovegetačním období dosahuje tato metoda v listnatých lesích a v místech s nízkou vegetací obdobné přesnosti jako laserové skenování. Přesnost výsledného modelu terénu může být v každém případě ovlivněna volbou filtračního algoritmu. Ve studii byly testovány filtrační algoritmy napříč různými typy prostředí a ukázalo se, že kritická je zejména volba algo-

ritmu s ohledem na charakter vegetace (např. les versus step) a terénu. Nakonec se práce zabývá konkrétní případovou studií, která byla možná zejména díky existenci volně dostupných LiDARových dat. Zpracovaná studie řeší efekt zastínění vegetací na odhad solárního potenciálu střešních ploch. Z výsledků je patrný předpoklad, že vliv zastínění okolní vegetací u solárního potenciálu střešních ploch hraje mnohem vyšší roli v lokálním měřítku. Naopak při řešení napříč rozlehlými urbánními oblastmi je již tento vliv zanedbatelný.



Contents

I	Introduction and Theory	19
1	Thesis Preface	21
1.1	Foreword	21
1.2	Scientific Motivation	22
1.3	Thesis Structure	23
2	Objectives of the Thesis	25
3	Theoretical Background	27
3.1	Introduction	27
3.2	Airborne Laser Scanning: Data Acquisition and Processing	29
3.2.1	The principle of laser ranging	30
3.2.2	Airborne LiDAR	32
3.2.3	Types of LiDAR sensors	33
3.2.4	LiDAR data	34
3.2.5	Availability of existing LiDAR datasets	36
3.2.6	Point cloud filtering and classification	36
3.2.7	Errors, accuracy and quality of data	38
3.3	Laser Scanning Data: Common Derived Features and Variables	41

3.3.1	Structure of terrain and vegetation	41
3.3.2	Digital model of the terrain and of the surface .	42
3.3.3	Canopy height model	43
3.3.4	Ecological applications and three-dimensional structure	45

II Research 47

4 Suitability, Characteristics, and Comparison of an Airship UAV with LiDAR 49

4.1	Introduction	51
4.2	Technologies Used	51
4.2.1	AMA	51
4.2.2	Photogrammetry from fixed wing UAV	56
4.2.3	LiDAR from conventional aircraft	57
4.3	Measuring	58
4.3.1	Locality	58
4.3.2	Notes about UAV legislation	59
4.3.3	AMA	60
4.3.4	Photogrammetry from fixed wing UAV	61
4.3.5	LiDAR from conventional aircraft	63
4.4	Accuracy Analysis	64
4.4.1	Results	65
4.5	Comparison of Other Characteristics	68
4.5.1	Vegetation penetrability	68
4.5.2	Data density	70

4.5.3	Data collection speed	71
4.5.4	Economic aspects	71
4.6	Conclusion	72
5	Assessment of LiDAR Ground Filtering Algorithms	75
5.1	Introduction	77
5.2	Material and Methods	80
5.2.1	Study area	80
5.2.2	LiDAR and Reference data acquisition	82
5.2.3	Ground points classification algorithms	83
5.2.4	Quantitative and Qualitative validation	85
5.3	Results	88
5.3.1	Selection of best parameters	88
5.3.2	Quantitative assessment: Vertical accuracy, Type I and Type II errors	88
5.3.3	Effect of vegetation and terrain	90
5.4	Discussion	93
5.5	Conclusions	97
6	Comparison of Leaf-off and Leaf-on Combined UAV Imagery and Airborne LiDAR	103
6.1	Introduction	105
6.2	Materials and Methods	109
6.2.1	Study area	109
6.2.2	ALS and UAV image data collection	110
6.2.3	Ground control points and verification data survey	111
6.2.4	Point clouds processing and DTM generation	112

6.2.5	Comparison of LiDAR and SfM point clouds	113
6.2.6	DTM accuracy assessment	115
6.2.7	Analysis of vegetation cover effect on DTM accuracy	115
6.3	Results	116
6.3.1	Comparison of point clouds	116
6.3.2	Combination of point clouds acquired under leaf-on and leaf-off conditions	117
6.3.3	Comparison of DTMs	118
6.3.4	The effect of the vegetation on DTMs accuracy	119
6.4	Discussion	119
6.5	Conclusion	124

7 Influence of Vegetation Canopies on Solar Potential in Urban Environments 127

7.1	Introduction	129
7.2	Methodology	131
7.2.1	Study area	131
7.2.2	LiDAR data	132
7.2.3	LiDAR-derived footprint and DSM	133
7.2.4	Estimating the incident solar irradiation	135
7.3	Results	137
7.3.1	Annual solar potential and losses due to vegetation	137
7.3.2	Monthly changes in solar potential lost	138
7.3.3	Comparison of estimated solar irradiation rasters	139
7.4	Discussion	139
7.4.1	Temporal changes in shadowing effects	140

7.4.2	Solar radiation models based on 2.5D	141
7.5	Conclusion	143
8	Discussion and Summary	147
8.1	Conventional Platforms vs. UAVs for LiDAR Data Collection	148
8.2	Comparison of UAV Imagery and ALS for Evaluation of DTM and Vegetation Structure	150
8.3	Filtering Algorithms for Processing Laser Scanning Data	152
8.4	Application of Laser Scanning Data in Urban Environ- ments	154
8.5	Conclusions	155
8.6	Further Research	158
8.7	Afterword	159
9	References	161
10	Curriculum Vitae & List of Publications	195

Part I

Introduction and Theory

Chapter 1

Thesis Preface

1.1 Foreword

Laser scanning has become one of the most prominent data sources for Earth surface mapping. Over the last decades, many new processing techniques of airborne LiDAR (Light Detection And Ranging) data have been developed and, nowadays, the use of LiDAR is well established in the fields of environmental sciences. LiDAR technology can penetrate through gaps in vegetation canopies and register multiple returns representing both above ground objects and terrain (Wehr and Lohr, 1999; Dubayah and Drake, 2000). Thanks to the capability of direct acquisition of 3D data in high vertical and horizontal resolution, airborne LiDAR data provide complementary data to other remote sensing techniques that are suitable for vast range of applications in environmental sciences. Many reviews have been published, focused for example on the use of LiDAR for mapping three-dimensional habitat structure (Lefsky et al., 2002; Vierling et al., 2008), its application for assessment of species-environment relationships (Davies and Asner, 2014; Bakx et al., 2019) or land cover classification (Yan et al., 2015) and new possibilities of the use of LiDAR are still being discovered (Eitel et al., 2016). Although LiDAR is a well-established technique and its usage is extensive, there are still challenges to be met. Various data acquisition and processing techniques need to be properly investigated

and validated. Mounting LiDAR sensors on UAVs may represent one of such challenges as it is still in its infancy, especially due to the relatively high weight of laser scanners and UAVs' low load bearing capacity (e.g. [Esposito et al., 2014](#); [Pilarska et al., 2016](#); [RIEGL, 2019](#); [Velodyne, 2019](#)). Development of new ground filtering techniques of LiDAR point cloud represents another active field of research. Although the fundamental principles of filtering were laid out relatively long ago ([Sithole and Vosselman, 2004](#)), existing algorithms are being continuously improved ([Pingel et al., 2013](#)) and new ones being developed (see [Meng et al., 2010](#); [Rashidi and Rastiveis, 2017](#); [Zhang et al., 2016](#)). Despite the widespread use of remote sensing data across various areas of environmental sciences, there are still specialized fields where the application of remote sensing is underdeveloped, such as restoration ecology ([Cordell et al., 2017](#)). All the above topics therefore still offer a broad field of research opportunities and the presented thesis aims to at least partially answer challenges presented by the gaps in the current state of the art.

1.2 Scientific Motivation

The availability of LiDAR data for common users is ever growing, which is among other things being helped by the existence of free point cloud data repositories (e.g. opentopography.org). Another valuable source of LiDAR data is represented by open data national datasets, which are available in some countries. Nevertheless, many existing LiDAR datasets are not available to public or are only available for purchase, which is also true about the national dataset of the Czech Republic. Personally, I believe that it is necessary to increase the public awareness about the existence of LiDAR data and, in effect, to increase the pressure on their release. At the same time, a gradual decrease in costs of LiDAR data acquisition can be expected; in particular, a combination of LiDAR with UAVs can contribute towards improving

the data availability even in relation to local scales, higher density or an increased mapping frequency. Laser scanning can capture a complex landscape structure, which gives it a huge advantage over traditional field mapping methods as it can capture the condition of the landscape at a particular time. Besides, availability of such data due to shared repositories will make the data available also to researchers in a hundred years. In contrast, standard field mapping methods usually only measure selected landscape features, which are only rarely standardized and typically only available to those who collected them so their potential for future use is limited. This perspective is especially important if we take into consideration that three-dimensional environmental processes such as growth, vegetation disturbance, snow and ice accumulation or melt, fluvial and soil erosion processes and other aspects of landscape development are inherently dynamic.

1.3 Thesis Structure

The thesis consists of three published and one submitted studies. It is divided into two Parts and seven Chapters. **Part I** contains this preface and a general introduction into the field of remote sensing, airborne laser scanning and its application in the environmental research. **Part II** contains chapters with texts of the individual published or submitted studies: **Study I**: Suitability, characteristics, and comparison of an airship UAV with LiDAR for middle size area mapping; **Study II**: Assessment of LiDAR ground filtering algorithms for determining ground surface of non-natural terrain overgrown with forest and steppe vegetation; **Study III**: Comparison of leaf-off and leaf-on combined UAV imagery and airborne LiDAR for assessment of a post-mining site terrain and vegetation structure: Prospects for monitoring hazards and restoration success and **Study IV**: Influence of vegetation canopies on solar potential in urban environments. The last Chapter contains comments to and summary of the findings of individual studies.

Chapter 2

Objectives of the Thesis

The aims of this Thesis are: **1)** to investigate the possible use of airborne laser scanning for mapping of a three-dimensional structure of the landscape, in particular a) suitability of various unmanned aerial vehicles (UAVs) for LiDAR data collection, b) to evaluate existing filtering algorithms important for processing laser scanning data, c) to compare UAV imagery and airborne LiDAR for evaluation of the terrain and vegetation structure, and d) to investigate the feasibility of application of laser scanning data for evaluation of the influence of vegetation on solar potential; and **2)** based on the acquired results, to discuss the contribution of airborne laser scanning in the field of environmental research.

Chapter 3

Theoretical Background

3.1 Introduction

The knowledge of three-dimensional structure of the environment is crucial for environmental sciences as such structure affects natural processes to a great degree. Various mapping methods are utilized for capturing the landscape structure – terrestrial, airborne or spaceborne technologies of modern mapping that may use both passive and active remote sensing (RS) methods. The most common representation of the mapped structure for research applications comes in the form of products such as digital terrain models (DTMs) or digital surface models (DSMs). DSMs and DTMs are used in many areas as the shape of the terrain plays an important role in atmospheric, geomorphological, hydrogeological or ecological processes (Wilson, 2012). The typical applications of those models can be found in the fields of geodesy, geology, geophysics, civil or military engineering, landscape design, urban planning, or environmental management (Petrie and Kennie, 1987; Li et al., 2004).

At present, airborne photogrammetry and airborne laser scanning (ALS) are the most widely used mapping methods. ALS is an accurate tool for measuring ground topography, land cover or three-dimensional structure of vegetation. Recently, even newer methods of “computer vision” such as structure from motion (SfM) and multi-view stereo (MVS) have grown in popularity and complement the ALS method (e.g. Iglhaut

et al., 2019; Nowak et al., 2019; Ren et al., 2019). These methods of RS yield similar data to those generated by ALS, they however do not provide comparably detailed spatial information, especially the information about vegetation structure (Lisein et al., 2013). Their principal benefit however lies in their lower price, especially where the data acquisition is done by unmanned aerial vehicles (UAVs).

The beginnings of the use of the laser technology for RS application go back into 1960s and 1970s when the possibility of their use for long ranging purposes has been first demonstrated, especially in view of ambitious space projects (Flood, 2001). Since then, and especially in the recent years, the availability and accessibility of laser scanning systems for mapping the Earth surface have increased. Those systems are widely known under the name of light detection and ranging (LiDAR). LiDAR technology as an active RS method brought many new options and new applications in various research areas as well as in engineering. It has won such a prominent position especially due to the ability to provide data with (until then) unimaginable speed, accuracy and density. Besides, data from widespread passive RS methods (such as visible light or multispectral imagery) are usually unable to provide information about the vertical component of landscape structure as their use cannot penetrate the uppermost layer of the vegetation cover. LiDAR systems, on the other hand, are usually able to acquire data on the internal vegetation structure. They have thus proved to be a desirable complement to the passive sensors. Combination of laser scanning data with those obtained from other RS sensors can result in a very sophisticated system for collection of data on the vertical landscape structure.

LiDAR or laser scanning systems are nowadays no longer only used as airborne laser profilers and scanners (ALS), other modifications mounted on various platforms have also been developed. Representatives of such systems especially include dynamic mobile laser scanners (MLS) or static terrestrial laser scanners (TLS). Laser altimeters or spaceborne

laser profilers constitute a separate category. MLS are most frequently used for corridor mapping of linear elements such as roads, railroads or watercourses. This system is typically mounted on cars, trains, or boats (Michoud et al., 2014). When compared to ALS, TLS provides usually much higher point density and measurement accuracy. The limited range of scanning and high time demands however prevent the use of this method for more extensive mapping. The choice of a suitable platform depends on the properties of the studied surface, extent of the mapped area, required accuracy and resulting data density (Baltsavias, 1999b). The presented thesis is especially focused on airborne laser scanning and its use for the needs of environmental sciences where it is often necessary to collect data from large areas.

3.2 Airborne Laser Scanning: Data Acquisition and Processing

Airborne laser scanning is a modern remote sensing method for direct collection of spatial data. Under optimal circumstances, its absolute vertical accuracy is ± 0.15 m, which makes it one of the most accurate RS methods (Charlton et al., 2009; Wei and Bartels, 2014). Due to its accuracy and speed of data collection even over extensive areas, it plays a very important role in many areas of research and/or commercial applications including archaeological exploration, (Crow et al., 2007), ecology (Clawges et al., 2008), hydrological modelling (French, 2003; Mandlbürger et al., 2008), glaciology (Arnold et al., 2006), geology and geomorphology (Johnson et al., 2015), forestry (Hyypä et al., 2004; Dubayah and Drake, 2000) and many others, see Harpold et al. (2015).

The term LiDAR is an acronym for Light Detection And Ranging. Some authors abbreviate the system as LADAR (LAsER Detection And Ranging), in which case the acronym is created in the same way as RADAR (RAdio Detection And Ranging). Other names for this method

in literature include laser scanning, laser mapping, or laser altimetry. As the title suggests, the technology uses laser beams to measure distances and, in effect, to determine positions of objects (Wehr and Lohr, 1999).

3.2.1 The principle of laser ranging

The word laser is an acronym on itself, standing for Light Amplification by Stimulated Emission of Radiation. Laser is an optical device producing, upon activation by an external energy source, a monochromatic radiation – a laser beam. Laser is used for measurement of distances due to its unique characteristics such as its coherence and capability of emitting a huge amount of photons in a defined direction in very short impulses of pre-defined frequency and wavelength (Heritage and Large, 2009).

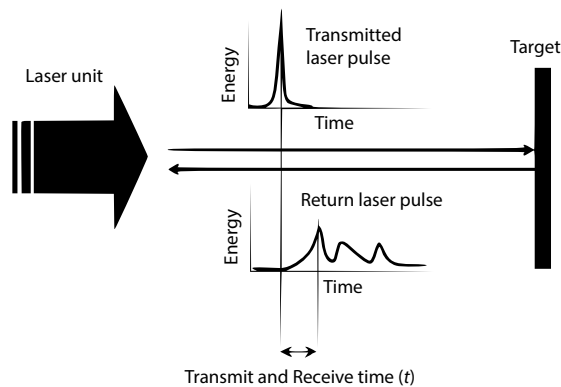


Figure 3.1: The time of flight principle (Heritage and Large, 2009).

In general, two types of lasers can be used for laser ranging, namely pulsed laser and continuous wave (CW) laser. The method of distance calculation differs according to the type of utilized laser. The physical principle of pulsed laser rangefinder lies in the emission of photons that are subsequently reflected back from the measured surface into the recording unit. The distance from the device to the object is then determined from the difference between the emission and reception of the impulse, i.e., from the time it takes to the light beam to travel

to the object and back. This principle based on the speed of light is called time of flight. CW lasers calculate the distances from the phase difference between the emitted and returned beam. In commercially available systems, however, the time of flight method of laser ranging is the more common (Baltsavias, 1999a,b).

The record of the emitted and received impulses can be expressed as the amount of energy or intensity as a function of time. The time period between individual detected incoming impulses is recorded and forms the basis for calculation (Fig. 3.1).

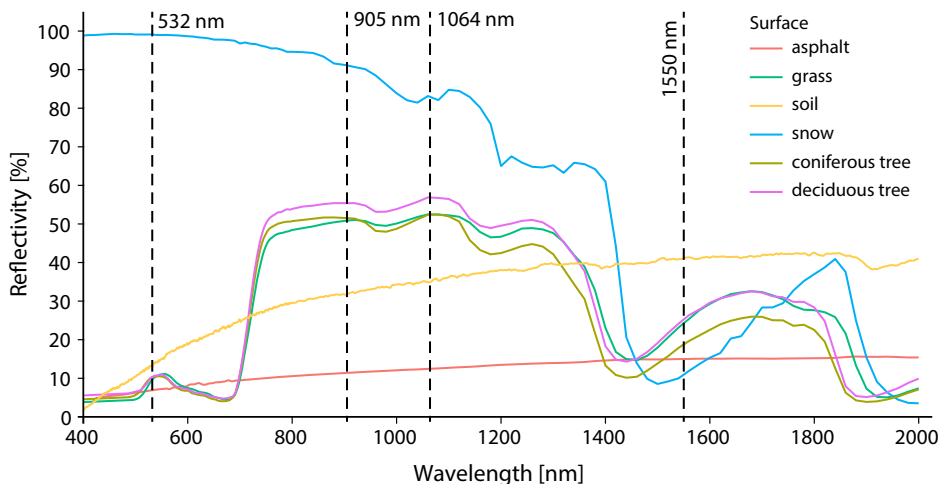


Figure 3.2: The relationship between the laser wavelength and surface reflectivity (JHU Spectral Library, NASA JPL).

Many types of lasers are used in LiDAR systems. Based on the laser type and application, various wavelengths can be utilized. Many commercial systems for general topographic mapping operate with infrared radiation (a wavelength of approx. 1064 nm), while for example bathymetric LiDAR systems developed for mapping of watercourse and water body bottoms use a wavelength of 532 nm (Baltsavias, 1999b). Recently, even universal multispectral LiDAR systems performing a simultaneous recording in several wavelengths (such as a combination of 532 nm, 1064 nm and 1550 nm) have appeared on the market (Teledyne, 2019).

The advantage brought by a simultaneous use of several wavelengths lies in different interactions of the beams with the material of the scanned surfaces. The object reflectivity is to a certain extent even more important than their size due to the differences in the reflectivity rates of individual materials. For example, a laser scanner may be capable of recording a 1 cm power line wire while missing a 3 cm wide branch of a tree (Baltsavias, 1999b) (see Fig. 3.2). For example, it is beneficial to use laser with 810 nm wavelength when mapping glaciers as its reflectivity from ice and snow is higher than that of other wavelengths (Wehr and Lohr, 1999). Reflectivity of the studied material thus affects the rate and effectiveness of its capture during scanning.

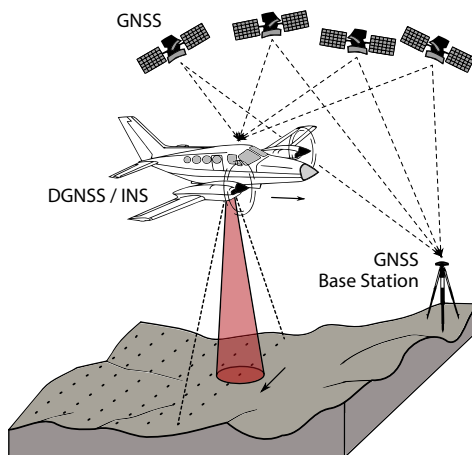


Figure 3.3: Airborne LiDAR system structure.

3.2.2 Airborne LiDAR

Airborne LiDAR is a complex multisensor system consisting most importantly of the control, monitoring and recording unit (CMR), position and orientation system (POS) and laser scanner (Fig. 3.3) (May and Toth, 2007). The system can be complemented with additional sensors such as photogrammetric chamber, video system, multispectral sensor, etc. (Baltsavias, 1999b). Such a system can be mounted on

various types of airborne carriers including airplanes, helicopters or UAVs (Charlton et al., 2009). The airborne LiDAR gradually records the surface under the moving airplane using a laser scanner – a device, the function of which is to distribute the beams that are typically emitted every 5-10 ns (Wagner et al., 2004). It consists of an optomechanical scanner, memory unit and a laser distance meter consisting of the laser emitter and electro-optical receiver (Wehr and Lohr, 1999). The most commonly used optomechanical device is a rotating mirror directing the laser beam in the axis perpendicular to the flight direction. The movement of the beam in the axis of the flight is then of course ensured by the flight of the carrier itself. The maximum crosswise extent of the device is called swath width. As scanning is performed in swaths, some authors also use the abbreviation ALSM (Airborne Laser Swath Mapping) instead of ALS (Slatton et al., 2007).

If an airborne system is used, it is of course also necessary to have accurate information about the position of the carrier. To be able to determine the spatial coordinates of every reflecting surface, the scanner position and orientation of the laser unit at any time must be known, which is ensured by the integrated POS. POS consists of an inertial measurement unit (IMU), differential global navigation and satellite systems (DGNSS) positioning system and a control unit. The position of the carrier is detected using several DGNSS and elements of carrier orientation (pitch, roll and heading) of the inertial navigation system (INS/IMU). A combination of the control unit, laser scanner, DGNSS and INS then ensures the capture of all recorded points in a unified coordinate system (Wehr and Lohr, 1999).

3.2.3 Types of LiDAR sensors

Several types of construction of the airborne LiDAR systems are available, usually categorized on the basis of one of two criteria – either according to the footprint size (small-footprint and large-footprint) or

based on the processing of returns (discrete return systems and full-waveform LiDAR systems). Small-footprint systems are characterized by a small diameter of the laser footprint on the surface (< 100 cm), usually with a very high recording frequency, thus creating a dense point cloud, while large-footprint systems are characterized by a greater diameter of the laser footprint (10–100 m) and a lower recording frequency.

The classification according to the method of reflection processing differentiates between discrete return systems and full-waveform LiDAR systems (Devereux and Amable, 2009). Discrete return systems record a single (Single pulse LiDAR), two or more returns (Multi pulse LiDAR). Conversely, a full-waveform LiDAR can record the full intensity curve of the return. The undisputed advantage of such system when compared to the discrete return systems is the possibility to analyse the waveform of the reflected beam and thus to provide information on the structure and physical properties of the reflecting surface such as reflectivity, roughness or geometry. Typical attributes derived from the full waveform analysis include range, elevation variation and reflectance, which can be subsequently used in data classification or filtering (Mallet and Bretar, 2009; Reitberger et al., 2008, 2009). Nowadays, new types of LiDAR sensors such as Multi-spectral LiDAR (Teledyne, 2019) or Geiger Mode LiDAR/Single Photon LiDAR (Stoker et al., 2016) are also available.

3.2.4 LiDAR data

The output from LiDAR scanning is an irregular distribution of points in a three-dimensional space, known as point cloud (Straub et al., 2009) (Fig. 3.4). These points are a result of a direct measurement of the surface structure. Every single point in the point cloud is termed a “return” as it denotes a position of a detected return of the laser beam from the studied surface. In this text, the terms point and return will be

used interchangeably. It is also necessary to point out that the amount of data originating from laser scanning is usually very high. Within an hour of scanning, typically tens of millions of points are generated (depending on the type of the scanning system, speed of the carrier and spatial resolution). A typical LiDAR system provides a spatial resolution (or scanning density) of 10 points per square meter where the carrier is an airplane or 200 points per square meter if the scanner is mounted on a helicopter (Devereux and Amable, 2009). Every point in the point cloud is associated with attributes recorded at the moment of the receipt of the return of the laser beam by a scanning device. At the first sight, it may appear beneficial to always strive for as dense a point cloud as possible; a high density however, besides increasing costs of data acquisition significantly, also complicates subsequent data processing.

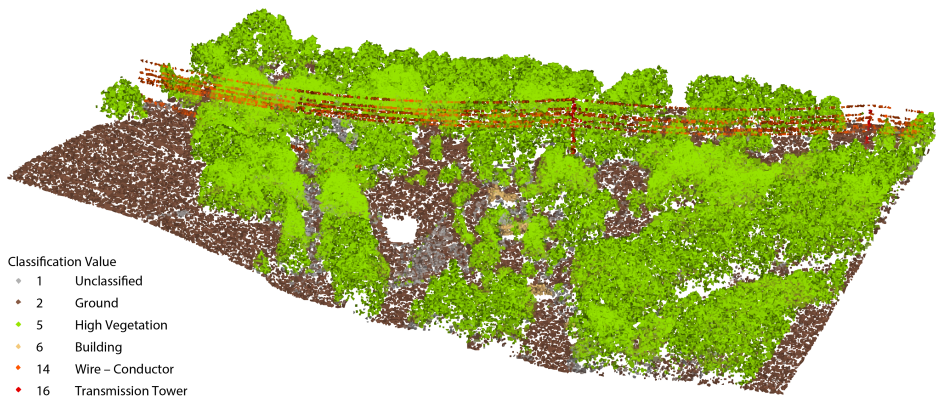


Figure 3.4: Classified ALS point cloud.

Many special data formats have been developed for storage of the acquired data, the most commonly used of which (and supported by almost all LiDAR and GIS tools) are a binary LAS data format or ASCII XYZ format. LAS is a universal format serving for recording and editing point data originating in particular from laser scanning, regardless of the hardware or software used. Every data file contains information on the used LiDAR system, coordinate system, total extent

of the data and the point data themselves. Besides the positional X , Y , Z coordinates, every return is associated with data on the intensity of the return, order of the return, the total number of returns in the pulse, class, scanner angle, GNSS record time and, if present, additional data from various sensors (NIR or RGB values). A derived format, LAZ, is a LAS format that underwent lossless data compression ([ASPRS, 2013](#)).

The other widely used format of data recording is the ASCII format, i.e. TXT, CSV or DBF files. These are in principle text files containing records of individual points, similar to LAS. This format however usually records only the positional coordinates and sensor altitude, possibly including intensity values in columns ([Samberg, 2007](#)).

3.2.5 Availability of existing LiDAR datasets

Especially in Europe (it can be however to a certain degree observed worldwide), there is an increasing trend of the usage of laser scanning for national programs of improving the elevation and topographic maps. Some datasets have been in recent years released by national policies and made accessible to public, research institutes and/or commercial organizations, so-called open data. The data can be obtained free of charge in several countries, albeit in some, it is just for a partial area. At present, such states include for example Finland, Denmark, Netherlands, United Kingdom, Slovenia, Spain or Switzerland. ALS data are also available for the entire Czech Republic, they are however not freely available but must be purchased. Individual datasets differ in the degree of coverage, in their up-to-dateness, accuracy or resolution.

3.2.6 Point cloud filtering and classification

Regardless of the application and the final product needed, an inevitable and at the same time the most critical step of the LiDAR point cloud processing is ground filtering – a process of detection of ground points,

i.e., points lying on the terrain. This can be achieved using various filtering algorithms that have been developed for ALS data processing (Zhang et al., 2003; Meng et al., 2009; Susaki, 2012). Numerous filtering algorithms have been reviewed e.g. by Sithole and Vosselman (2004). The output of ground filtering is a file containing points classified as ground and non-ground points. The correct filtering is crucial for creating final products such as digital terrain models (DTMs), digital surface models (DSMs) or feature extractions (Sithole and Vosselman, 2004; Chen et al., 2017).

Non-ground points can be also further classified. Usually, buildings and vegetation are two such classes. Other classes may include noise (gross errors), low, medium and high vegetation, road surfaces, water bodies, power lines (wires) and transmission towers, or specific points of the skeleton of terrain relief. Data classification is a process performed in several cycles, during which individual points representing the returns of the terrain and objects on it are assigned into individual classes (Filin, 2004; ASPRS, 2013). At this stage, a maximum automation is desirable. For improving the accuracy or determination of specific objects of interest, manual classification may play a complementary role; a full manual classification is however, from the perspective of the immense extent of the point cloud and sheer volume of data, a laborious and time consuming process, often practically non-feasible. Classification of the point cloud can be based on the height characteristics, shape of the local structure of the point cloud and reflection intensity. The definition of the individual classes is actually standardized in the LAS format specification (see Tab. 3.1). The intensity of the reflected beam can therefore be utilized for distinguishing between individual land cover categories and data classification as its value is dependent on the reflectivity and physical properties of the material of the scanned object or surface (Song et al., 2002; Charaniya et al., 2004; Kashani et al., 2015).

For classification and processing of laser scanning data, specialized software is used, e. g. LAStools (rapidlasso.com), FUSION/LDV (forsys.cfr.washington.edu), CloudCompare (danielgm.net/cc) or standalone libraries, e. g. Point Cloud Library (pointclouds.org) or Point Data Abstraction Library (pdal.io). Limited tools for processing point clouds are available in some GIS software such as ArcGIS, GRASS GIS (Petras et al., 2016) or SAGA (Jochem et al., 2010). Besides DTM or DSMs, products generated from ALS data may include contoured maps, 3D building models or vegetation models.

Table 3.1: ASPRS Standard LIDAR point classes.

Value	Meaning	Value	Meaning
0	Created, never classified	11	Road Surface
1	Unclassified	12	<i>Reserved</i>
2	Ground	13	Wire – Guard (Shield)
3	Low Vegetation	14	Wire – Conductor (Phase)
4	Medium Vegetation	15	Transmission Tower
5	High Vegetation	16	Wire-structure Connector
6	Building	17	Bridge Deck
7	Low Point (noise)	18	High Noise
8	<i>Reserved</i>	19–63	<i>Reserved</i>
9	Water	64–255	User definable
10	Rail		

Source: (ASPRS, 2013)

3.2.7 Errors, accuracy and quality of data

To ensure a required quality of the products of the project, it is necessary to do the preparations and flight planning prior to the data collection itself. A proper flight planning affects, among other things, the price of the resulting product, and maximum effectiveness is thus desirable. The quality of the point cloud is of course affected both by systematic and random errors in the scanning process. This means that it is necessary to perform proper evaluation of the LiDAR data quality in order to

minimize the rate of erroneous values that would have negative impact on the resulting products. While scanning, incorrect positioning of some points or a record of a non-existent return caused by a high radiation noise can occur. Inaccurate measurements are often caused by an interaction of the laser beam with atmospheric particles, which means that dust particles or smoke in the studied area have a detrimental effect on scanning accuracy. The ideal conditions for scanning are represented by clean and dry environment with a minimum of carbon dioxide and without any form of water in the air (rain, fog, humidity). The best results are achieved at night while the worst results during clear sunny days (Baltsavias, 1999a). Errors caused by such conditions can to a certain degree be removed by suitable filtering algorithms in specialized software.

To ensure the required accuracy, quality assurance and quality control (QA/QC) processes should be adhered to. Quality Assurance (QA) denotes processes related especially to the management of quality such as calibration, planning, implementation and supervision of the data collection process. Examples of QA may include pre-flight terrain reconnaissance in the scanned area and rough determination of the surface (such as the vegetation extent and density or high-rise buildings) allowing selection of optimum flight parameters. In forested areas, those mean slower speed, lower scanning angle, higher swath overlap, or a lower flight altitude to ensure a higher point density. For the best possible accuracy of the determination of the position of the carrier using DGNSS, it is also important to choose a proper time frame combining a good visibility and ideal positions of the satellites (Habib and Rens, 2009).

The term Quality Control (QC) is used for evaluation of the quality of the final products (typically DTMs or DSMs). End users who only receive the final product are often not informed about the methods used for its creation and even if they were, they are often unable to judge the suitability of the used methods. For this reason, a proper

evaluation of the accuracy of acquired models is crucial. To evaluate the accuracy of the final product, ground control points (GCPs), well-recognizable points with geodetically determined positions inside the scanned area are usually used. The quality control is then performed by comparing the final product created from the filtered LiDAR point cloud (typically DTM) with the independently selected GCPs. In addition, data from the overlapped areas of scanning can be also used for evaluating the quality of the data and system calibration. Differences between individual swaths in the overlapped areas are then aligned using various mathematical methods. In this way, systematic component of error can be usually detected, reduced and/or even eliminated and data accuracy can be improved (Habib and Rens, 2009).

Nevertheless, despite all efforts for quality assurance and accuracy, measured data always contain errors, regardless of the used method of measurement. Such errors originate from inaccuracies in the source data, in the data collection, human errors in the process of data collection, errors stemming from coordinate system transformations or in data processing. It must be however taken into account that the absolute accuracy of mapping is not the only parameter of creating products such as DTMs and others – a much more reasonable approach lies in determining a required accuracy, which subsequently allows creating sufficiently accurate and economically feasible products. It is of course possible to improve the accuracy by selecting appropriate methods and algorithms for surface modelling combined with increased density of data. Any increase in the data density is however inherently associated with higher costs of data acquisition and, in effect, of the final product. Hence, decision on a data density optimal for the project in question must be made, which however may not be always a simple one (Li et al., 2004).

3.3 Laser Scanning Data: Common Derived Features and Variables

3.3.1 Structure of terrain and vegetation

The capability of the beam to penetrate through canopy gaps and to capture terrain or objects under the canopy constitutes one of the greatest advantages of ALS as it allows the researchers to capture even terrain in the forested areas with a relatively good accuracy. In areas covered with vegetation, the laser beams are usually reflected by various layers of the vegetation cover. The interaction of the laser beam with the canopy is thus characterized by multiple returns from several depths of the vegetation cover. The first return typically comes from the vegetation canopy surface. The gaps in the non-continuous surface allow the beams to penetrate deeper so a second and possibly other returns follow, with the last one ideally being a return from the terrain. Such a penetration of the beam and evaluation of multiple returns can be used for modelling or deriving vegetation characteristics and metrics in both vertical (e.g. canopy height, standard deviation of height) and horizontal (e.g. canopy cover, canopy gap density) directions (Bakx et al., 2019). In addition, individual treetops can be distinguished and trees in the tree stand counted, crown diameter, canopy density, the volume of wood matter and/or biomass, vertical structure of the individual vegetation levels or even of individual vegetation species can be determined (Dubayah and Drake, 2000; Hyypä et al., 2004; Næsset et al., 2004). Terrain returns are however not always detected – the possibility of their recording depends on the spatial distribution of the vegetation canopy (or gaps therein), scan angle, laser beam divergence and reflectivity of the surface for the wavelength of the laser beam (Hofton et al., 2002; Næsset et al., 2004).

Unlike ALS, other remote sensing methods such as photogrammetry are only able to provide a partial information on the vegetation structure (Fig. 3.5). They can be for example used for acquisition of imagery that can be used for classification of woody plant species (Holmgren and Persson, 2004) or to derive information about the tree stand health (Hyypä et al., 2004) but they usually cannot provide data on the vertical structure of vegetation (Lefsky et al., 2002).

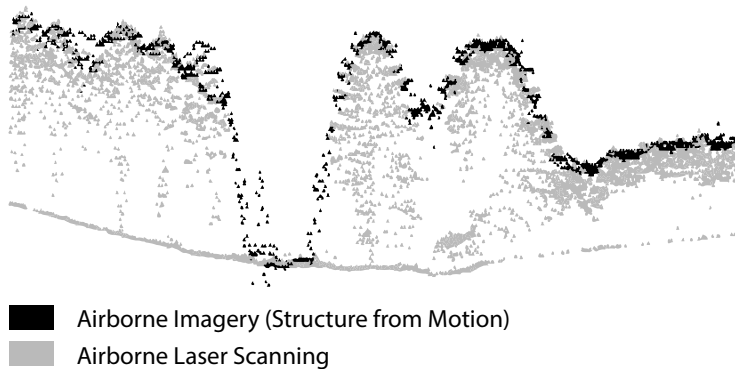


Figure 3.5: Comparison of point cloud from airborne photogrammetry and airborne laser scanning (Lisein et al., 2013).

3.3.2 Digital model of the terrain and of the surface

The most common products from airborne laser scanning are digital terrain models or digital surface models (Fig. 3.6) (Flood, 2001). Such models are in principle elevation rasters that are derived from filtered point clouds using various surface interpolation algorithms (linear interpolation, IDW, etc.). The raster resolution depends in particular on scanning density. A more detailed raster, and, in effect, capturing the surface in greater detail, requires the use of a scanning method with a higher point density per square meter. Another option of the surface representation is a triangulated irregular network (TIN).

In any case, it is necessary to use a point cloud classified as correctly as possible to obtain an accurate relief/surface model. The basic prerequisite for producing an accurate digital surface model is the availability of data classified into ground and non-ground points.

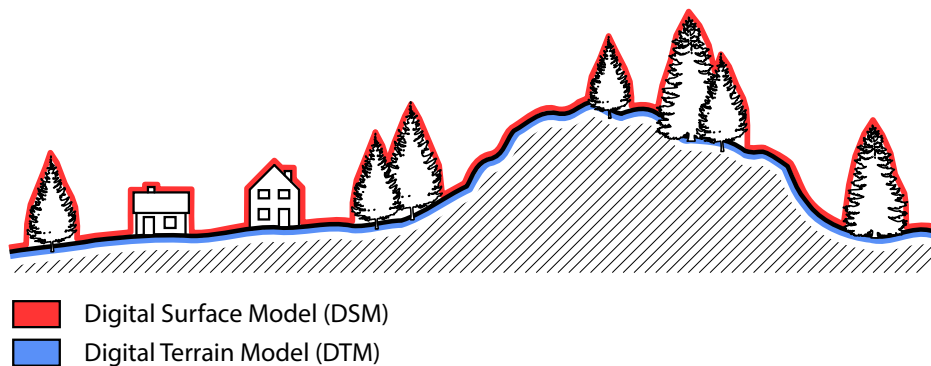


Figure 3.6: Digital surface and terrain model.

3.3.3 Canopy height model

Besides DSM and DTM, so-called normalized digital surface model (nDSM) showing differences between DSM and DTM is a commonly used product. In this way, the values of the terrain drop to zero and nDSM thus represents the objects present on top of the relief (buildings, vegetation, etc.) (Fig. 3.7). To obtain information on the vertical structure of the canopy, a DSM containing vegetation only must be created, so-called canopy height model (CHM), which is a normalized digital surface model showing the full vertical structure (Fig. 3.8) or only certain distinguishable levels of the vegetation (Lefsky et al., 2002). A CHM with a sufficient detail may be used for detection of individual trees (Pitkänen et al., 2004).

Further processing and analysis of CHMs can yield some dendrometric values. It has been however demonstrated by several studies that vegetation parameters acquired from ALS data processing are typically underestimating heights by 0.2-0.5 m (Næsset and Økland, 2002; Coops

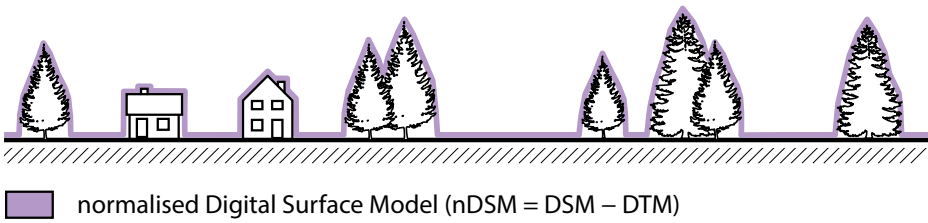


Figure 3.7: Normalised digital surface model.

et al., 2007; Heurich, 2008). A dependency of the vertical distribution of the canopy on the circular case and amount of the above-ground biomass has also been shown (Lefsky et al., 1999). The highest correlation was detected between the median square canopy height and size of the above-ground biomass. This way, it is possible to estimate the amount of biomass in forests from the tree height.

In general, the difference in elevation between the first and last return can be expected to imply the canopy height. There are however problems, especially where the small-footprint ALS is concerned. As the diameter of the beam is small, it may fail to capture the treetop. This problem does not apply to the large footprint systems where the laser beam captures the entire crown of the tree (Nelson, 1997; Dubayah and Drake, 2000).

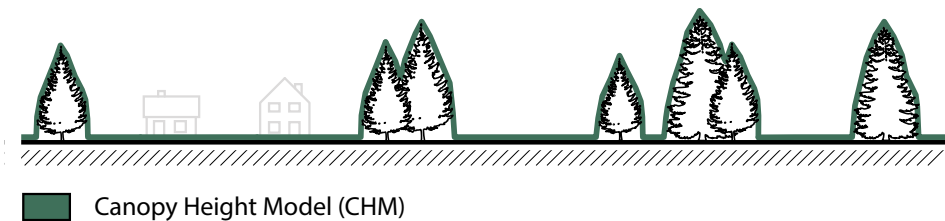


Figure 3.8: Canopy height model.

When creating CHMs, pits in raster occur. Such pits are a result of incorrect classification of the return from the ground (or lower layers of vegetation) in the middle of high vegetation points; if such points are classified as canopy, the canopy appears to suddenly drop to the

ground in the created nDSM or CHM raster. There are several specific approaches and techniques for reducing pits occurrence. A typical representative of such methods is raster smoothing (Yu et al., 2011), other advanced algorithms such as Pit-free algorithm (Khosravipour et al., 2014) or Spike-free algorithm (Khosravipour et al., 2016) have however also been developed.

3.3.4 Ecological applications and three-dimensional structure

ALS data provide a high accuracy both in the horizontal and vertical resolution, which makes them suitable for investigations of biodiversity in various extents (Weisberg et al., 2014). It is well known that the three-dimensional structure of the sites is a principal driver of the interaction of animals with their surroundings (Davies and Asner, 2014). The structure may be defined both in the vertical and horizontal dimension (Bergen et al., 2009). Among other parameters (see review by Bakx et al., 2019) CHM parameters generated from the maximum or mean canopy height are often used (Flaspohler et al., 2010; Garabedian et al., 2014; Barnes et al., 2015; Sasaki et al., 2016). Other such parameters that can be utilized include ratios of raw LiDAR points at defined vertical levels above the terrain (Ackers et al., 2015), elevation percentiles, canopy cover (Graf et al., 2009), penetrability of the canopy and relative ratios of LiDAR returns from individual vertical layers (Hill and Hinsley, 2015). The vegetation structure is however not the only factor. A significant effect on the habitat selection of individual animal species or communities may be attributed to the composition of tree species and vegetation growth pattern. LiDAR data can not provide full information on vegetation and for this reason, some studies use ALS data in combination with multispectral or hyperspectral imagery to acquire additional vegetation characteristics (Colgan et al., 2012; Asner et al., 2015).

Part II

Research

Chapter 4

Suitability, Characteristics, and Comparison of an Airship UAV with LiDAR for Middle Size Area Mapping

Bronislav Koska, Vladimír Jirka, Rudolf Urban, Tomáš Křemen, Petra Hesslerová, Jakub Jon, Jiří Pospíšil, **Michal Fogl**

Adapted from International Journal of Remote Sensing 38 (2017): 2973–2990, with permission of corresponding author (B. Koska).

Publication metrics:

14 of 30 (Q2) rank in WOS category Remote Sensing

IF (2018) 2.493; AIS (2018) 0.531

5 times cited on WOS (2019 August)

Author's contribution: 10%

Abstract

In this article, the autonomous mapping airship (AMA) equipped with LiDAR along with its basic properties is introduced. Other methods and technologies using unmanned aerial vehicles (UAVs) or conventional aircraft are then compared to the AMA, namely automatic reconstruction from photographs acquired with fixed wing UAVs and LiDAR taken from conventional aircraft. Comparison of technologies was performed at a site of a brown coal mine spoil heap. The size of the area of interest is about three square kilometres and it is covered with wind-blown vegetation (trees, grass, bush). For the purpose of accuracy analysis, we measured about 100 height check points (HCPs) using real-time kinematic Global Navigation Satellite System technology. The HCPs were equally distributed between vegetation-free ground and the terrain with low vegetation (grass). Other properties of the used methods and acquired data were also compared. The most important of these were data density, vegetation penetrability, speed of data collection, and economical aspects.

4.1 Introduction

Various suitable technologies with different properties are nowadays available for mapping of medium size areas (1–10 km²). Besides conventional selective surveying methods, we can distinguish two basic principles for data collection, namely LiDAR (also called laser scanning) and (intersection) photogrammetry. These include fixed-wing or multicopter UAVs with a camera or a conventional aircraft with LiDAR. Drones with LiDAR also exist but their practical usage is still very limited. We use a rather unusual type of drone, a model airship equipped with LiDAR, an autonomous mapping airship (AMA) – a system with some unique properties.

We try to compare various available solutions, including the experimental system AMA, for mapping of an uninhabited and difficult to access area of part of a spoil heap of about 3 km².

4.2 Technologies Used

Two main airborne data acquisition technologies, namely LiDAR and photogrammetry, using three different kinds of platforms are considered in this study. They will be described in detail in the following subsections.

4.2.1 AMA

The AMA is a mapping system with specific properties suitable for effective mapping of medium-sized areas (in the range from 1 to 10 km²). This system should be useful especially for areas that are too large for conventional selective surveying with Global Navigation Satellite System (GNSS) or total station and too small for the use of manned aircraft in terms of cost and accuracy. Accessories of the system will

allow, for example, collecting data for urban area modelling, creating thermometric georeferenced maps, and mapping of dangerous or inaccessible areas (dumps, open-pit mines). For this reason, the platform is equipped with a laser scanner, a visible spectrum (VIS) camera (one for vertical capturing or more for slope capturing), a thermal camera, and inertial navigation system INS/GPS as an exterior orientation (pose) determination unit. Especially in the field of urban mapping the airship, as a platform, should have some legislative advantages in the future as has been alleged during consultation with Civil Aviation Authority of the Czech Republic. The resulting absolute accuracy of the developed system should be better than 10 cm (standard deviation) with the random component less than five centimetres, which is based on an a priori accuracy analysis. This accuracy is lower than for conventional measurements, but on the other hand higher than the scanning system carried by a conventional aircraft. In terms of properties (accuracy, speed of data collection) our system is close to the terrestrial mobile scanning systems, without its disadvantage in the lack of availability in locations with difficult accessibility. More detailed information about the AMA project is given by [Jon et al. \(2013\)](#). We also have experience with conventional aircraft-mounted LiDAR systems ([Pavelka et al., 2010](#)) and other UAV systems ([Řezníček and Straková, 2013](#)), so we can compare their properties and specify suitable areas of use.

The selection of a platform was based on our specific requirements such as the carrying capacity in the first place, long flight time, safety (in case of failure there is no danger of straight fall as the airship stays always little bit heavier than air, 2–3 kg depending on the actual amount of petrol, it will drop smoothly to the ground without putting people's health or equipment in danger) and flight characteristics such as stability of flight in terms of vibrations and possibility of flight at low speed.

The airship ACC15X (Fig. 4.1) made by the company AirshipClub.com is 12 m long with maximum envelope diameter of 2.8 m filled with 57 m³

helium. The airship has operating speed of 30 km/h, maximum speed of 55 km/h and practical altitudinal accessibility of 1000 m (maximum legal altitudinal accessibility for any civil UAV in the Czech Republic is 300 m above terrain). Movement is provided by two AXI 5320/34 electro motors with propellers produced by MODEL MOTORS s.r.o. The whole system is powered by a petrol engine power generator that can work for about three hours with fully loaded fuel tank (volume 5 L). The petrol engine model is ZDZ 50 NG; its maximum power is 3.07 kW and was produced by ZDZ Modelmotor. The necessary equipment for the ACC15X airship also includes a helium compressor and two high-pressure cylinders (300 bars). The equipment is relatively heavy (the compressor 105 kg, one cylinder approximately 200 kg) and spacious, therefore it is usually transported on a trailer as in our case.



Figure 4.1: The autonomous mapping airship – AMA.

4.2.1.1 Measuring platform

The measuring platform is designed and optimized to run suspended from an airship. It is mounted on the muted (Teflon shaft in adjustable frictional bush) gravitational gimbal and it has modular concept which allows employing different sensors and change their number and positions. The only limitation is the total weight, which should not exceed 15 kg (the carrying capacity of the airship). Gimbal was chosen to maintain the stability of the vertical instruments' field of view.

Currently, complete equipment consists of INS and GPS combined unit (iMAR iTracer – F200), laser scanner (SICK LD-LRS1000), digital camera in the visible spectrum (Canon EOS 100D) and a professional thermometric camera (FLIR SC645). For logging data, an industrial computer Stealth LPC-125LPM is used. All these components are mounted on one platform close to each other to prevent inaccuracies due to torsion of construction. Determination of the spatial relation of all used components is necessary for accurate direct georeferencing of any acquired data, which was the main objective of the AMA project. It has been theoretically solved in the article (Koska, 2013), which is based on the work of Skaloud and Lichti (2006). The result of practical calibration was published in the work of Koska et al. (2014).

4.2.1.2 Laser scanning unit – SICK LD-LRS1000

SICK LD-LRS1000 is a rotating two-dimensional (2D) scanner developed primarily for industrial safety applications. The company SICK AG has a long tradition in laser scanner manufacturing and their products have a favourable price/performance ratio, which makes the scanners often used in mobile robotics and mapping application (Derenick et al., 2008).

The most important parameters of the scanner are listed in Table 4.1, all parameters can be found in the product technical specification sheet.

Table 4.1: Basic parameters of laser scanner SICK LD-LRS1000.

Range/reflectance	2.5–250 m/100%, 80 m/10%
Angle range	360°
Maximum measuring frequency	14,400 Hz
Rotating frequency	5–10 Hz
Standard (statistical) deviation (1σ)	25 mm
Accuracy (systematic error)	± 38 mm to 80 m, ± 63 mm over 80 m
Minimal angle resolution	0.125°
Beam diameter at output	40 mm
Laser beam divergence	2.8 mrad = 0.16°
Interfaces	RS-232/RS-422, Ethernet, CAN

4.2.1.3 Time synchronization

A synchronization board based on the Arduino platform was made for the purpose of precise time synchronization (better than 1 ms). The ‘Interface Routing’ scanner service, which enables a full control of communication for the selected pair of interfaces, is used for synchronization. A message composed of an exact GPS time is sent in regular intervals onto the second connected interface (RS-232). The scanner does not interpret the message; it only saves the time of its inner clock for the message last sign and resends the message with its time to the master interface (Ethernet).

The whole functionality of the synchronization board follows this principle: the inner clock of the synchronization board is set and kept by time pulse (PPS), and its NMEA message (of \$GPGGA type) from the GPS with accuracy is better than 1 ms. Commands on taking an image by a digital camera or a thermometric camera are sent in the selected time moments from the control computer into the synchronization board. After executing the command, the synchronization board sends a message with identification of the command with an exact GPS time of the command execution into the control computer. In regular intervals, the synchronization board also sends synchronization messages with GPS time into the laser scanner. These messages are marked by the

laser scanner with time of its inner clock and automatically resent to the control computer.

4.2.2 Photogrammetry from fixed wing UAV

Photogrammetry from UAVs is becoming a standard method for spatial data mass collection for small areas (less than 1 km²).

We have two different fixed-wing UAVs at our disposal at the moment, namely eBee from senseFly SA and a home-assembled UAV which consists of an Easy Star II airframe from Multiplex and autopilot 3DR Pixhawk B (Fig. 4.2). eBee is equipped with a digital camera Canon S110 optionally with standard visible, near infrared or red edge spectrum. Easy Star is equipped with a Nikon Coolpix A camera, which has much better imaging characteristics than the Canon S110 (see [DxOMark, 2016](#)), which is why it was used in the project.



Figure 4.2: Easy Star II (wingspan 1366 mm) with 3DR Pixhawk B autopilot in the measurement locality.

Photogrammetric processing is based on the structure from motion technology, which was probably first publicly demonstrated in the

project Photo Tourism (Snavely et al., 2006) and next on Multi View Stereo technology (see for example Furukawa and Ponce, 2009).

If precise differential phase GNSS processing for image localization is not used, as in our case, it is necessary to apply ground control points (GCPs) to achieve output accuracy in the range of centimetres.

It is shown in several works (e.g. Vorster and Strecha, 2013; Nocerino et al., 2013) that in the case of correctly performed photogrammetric projects, it is possible to achieve an accuracy of about 1 pixel of image ground surface resolution (GSR) in the horizontal components and about 1.5–2 pixels of resolution in the vertical component.

4.2.3 LiDAR from conventional aircraft

Another method used for comparison is LiDAR data acquired from a conventional aircraft. We did not order custom scanning of the site because of economical and time aspects, but we instead used ČÚZK (Czech Office for Surveying, Mapping, and Cadastre) product called DMR 5G, which is maintained for the whole area of the Czech Republic.

The ČÚZK description of the DMR 5G product on its website (cuzk.cz) is: ‘the digital terrain model of the Czech Republic of the fifth generation (DMR 5G) represents natural or by human activity modified terrain surface in a digital form as heights of discrete points in an irregular triangular network (TIN) with X , Y , H coordinates, where H means the altitude in the Baltic Vertical Datum – after adjustment with total standard error of 0.18 m of height in the bare terrain and 0.3 m in forested terrain. The model is based on the data acquired by altimetry airborne laser scanning of the territory of the Czech Republic between 2009 and 2013. DMR 5G is established to analyse terrain situation at local scale and character, for example, for land adaptations projecting, transport, and water management projects planning, local natural phenomena modelling, etc. DMR 5G is the fundamental source database

for creating contours for maps at large scales and computer visualization of altimetry in territorially oriented information systems at high level of detail⁷.

We can find more detailed information about the DMR 5G product in the official introduction documentation (Brázdil, 2012). LiteMapper 6800 mapping system by IGI GmbH is used for data collection. This system uses Riegl LMS-Q680 laser scanner. In the documentation (Brázdil, 2012), it is also declared that the lowest accuracy of about 0.21 m is obtained in the areas with low vegetation (grass). This value was determined by empirical tests. The stated reason for the result is the difficulty to automatically identify areas with low vegetation.

4.3 Measuring

All the measuring campaigns were realized in 2016 with the exception of LiDAR from a conventional aircraft with realization in 2011.

4.3.1 Locality

The study area corresponds with Hornojiřetínská spoil heap, which covers an area of about 6 km² (Fig. 4.3). It is one of the largest spoil heaps in the North Bohemian lignite basin, where more than 17 spoil heaps after coal mining with total area about 150 km² are located. Approximately half of the spoil heap was technically reclaimed whereas the other half was left to spontaneous succession. Therefore, it provides a perfect environment to study the effects of technical reclamation versus spontaneous succession on species diversity (Doleřalová et al., 2012). Many studies have been performed in this area, but they have been limited to labour intensive field surveys. Comprehensive knowledge of physical structure and composition of vegetation and terrain will allow more detail study of species–environment relationships.

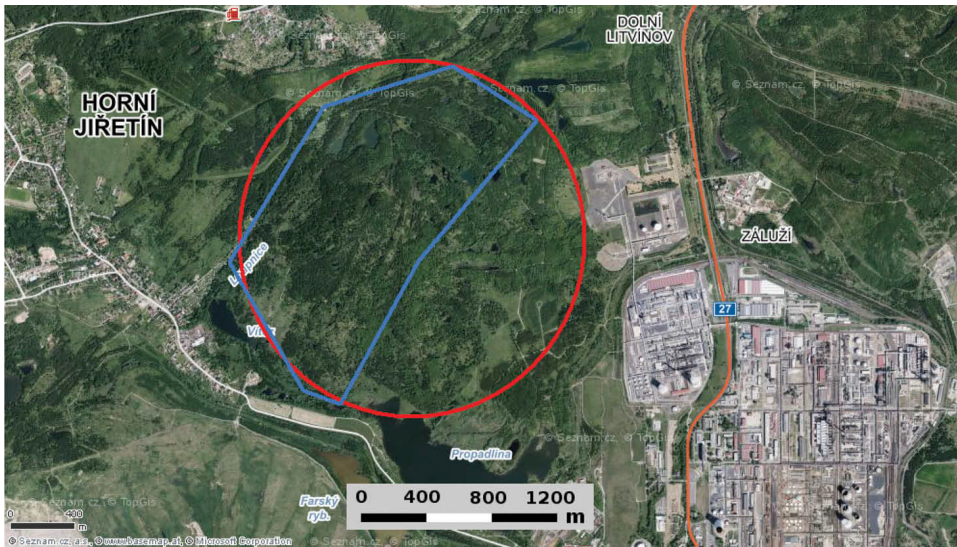


Figure 4.3: Main part of Hornojřetínská spoil heap (red line), area of measuring (blue line) [source of orthophoto: mapy.cz].

The spoil heap consists of small lakes, low vegetation with scattered shrubs, and forest areas. Only a part of Hornojřetínská spoil heap was planned as a study area (blue part in Fig. 4.3) because of the restricted airspace around an important chemical plant Záluží (visible in the right bottom part of Fig. 4.3). In reality, an even smaller parts of the intended area were measured (see Fig. 4.4) during individual campaigns for operational reasons, which are described in the following sections.

4.3.2 Notes about UAV legislation

The legislation for commercial UAV operation in the Czech Republic is issued by Civil Aviation Authority (CAA) of the Czech Republic and the basic regulation are: an operator has to complete registration of an UAV and pilot, pass practical exams, and arrange property damage insurance to obtain flight permission. In addition to this, it is necessary to fulfil some other administrative procedures and pay administrative fees to obtain so called ‘permit for aerial work’.

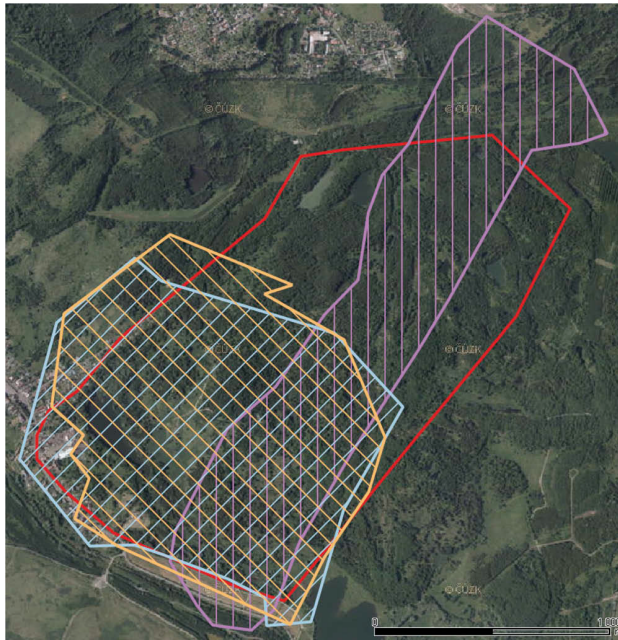


Figure 4.4: Measured areas: AMA – violet, first UAV photogrammetry – yellow, and second UAV photogrammetry – light blue (red lines bounds the area of interest).

Minimal basic traffic rules are common for both commercial and recreational operation in the Czech Republic. The maximum legal flight height above terrain for any civil UAV is 300 m (less around airports, etc.). It is prohibited to fly above inhabited areas (except for explicit permission from CAA). Visual line of sight (VLOS) must be kept at all times but the maximum VLOS distance is not specified in any legislation.

In case of a 12 m long airship and good visibility, we have experience with VLOS about 1 km (representing an area about 3 km² in an ideal situation).

4.3.3 AMA

Experimental measurement of a part of Hornojiřetínská spoil heap with the AMA system was conducted on 17 March 2016. A flying height

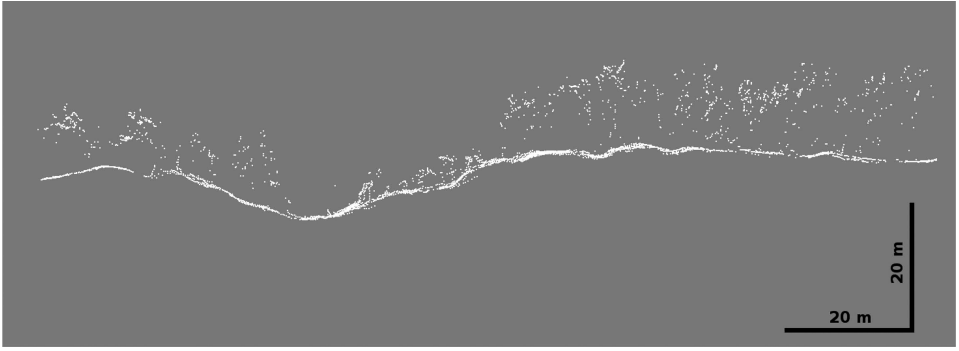


Figure 4.5: Digital surface model cross section from AMA measurement (depth of cross section about 3 m).

was set to 80–100 m above the terrain. The assumed accuracy of the measured data should be about 5–10 cm in case of correct system calibration and the data ground resolution was about 15 points m^{-2} (depending on the flight speed and flight lines density). The density and accuracy of the gathered data should be higher than for a conventional aircraft-flown LiDAR.

Because of AMA petrol engine failure, only a part of the area of interest was studied (the violet area in Fig. 4.4). The obtained data covered bare ground as well as trees (see Fig. 4.5).

The basic output of the AMA system is a digital surface model in the form of a georeferenced point cloud. Using LiDAR processing software (e.g. LAStools), we can separate the digital terrain model (ground) and other objects. The digital terrain model and digital surface model from AMA of the same part and view are shown in Fig. 4.6 and 4.7.

4.3.4 Photogrammetry from fixed wing UAV

Measurement with this technology was carried out twice. The area marked with yellow border in Fig. 4.4 was captured first on 29 April 2016, and the area marked with light blue in the same figure was measured on 1 July 2016. The main reason for the second measurement

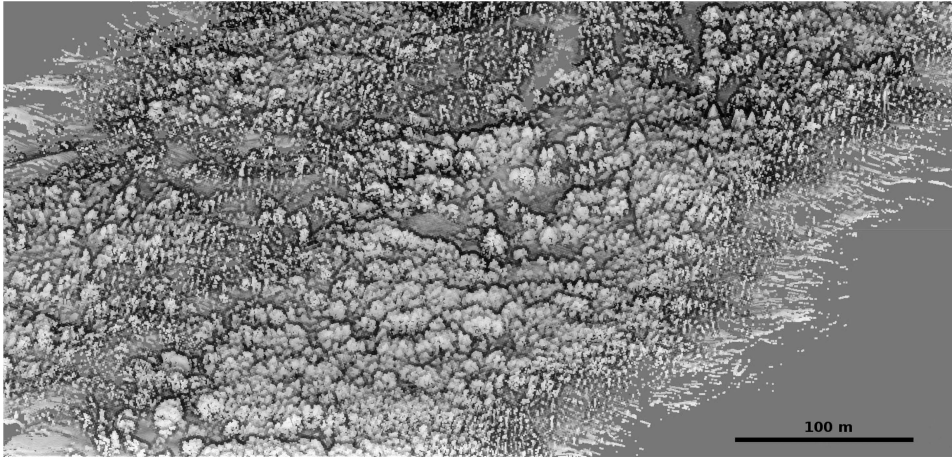


Figure 4.6: Point base rendering of spoil heap part measured by AMA with sample density about 15 point m^{-2} from an arbitrary isometric view.

was insufficient time for completing the whole area measurement on the first day. The time schedule was more realistically arranged the second time but the UAV operator could not find any suitable place for take-off and landing to measure the northeastern part of the locality.

The data was captured during four individual flights because of the limited flight endurance limit of the UAV that was used (same in both days). Ground surface resolution was set to 25 mm. The maximum possible image overlap of 80% was set for the longitudinal direction because of the wooded character of some areas and time-balanced overlap of 65% for the transverse direction. Altogether, about two thousand images were taken in each day.

Processing was carried out with the software Agisoft PhotoScan Professional version 1.2.4. Due the lack of precise differential GNSS on used UAV we had to use GCPs for image geo-location and photogrammetric project optimization. GCPs measured with real-time kinematic (RTK) GNSS method were distributed throughout the study area (for distribution of control and HCPs, see Fig. 4.8).

There were 153 GCPs divided into three categories, were geolocated using the GNSS method RTK throughout the study area (see Fig.

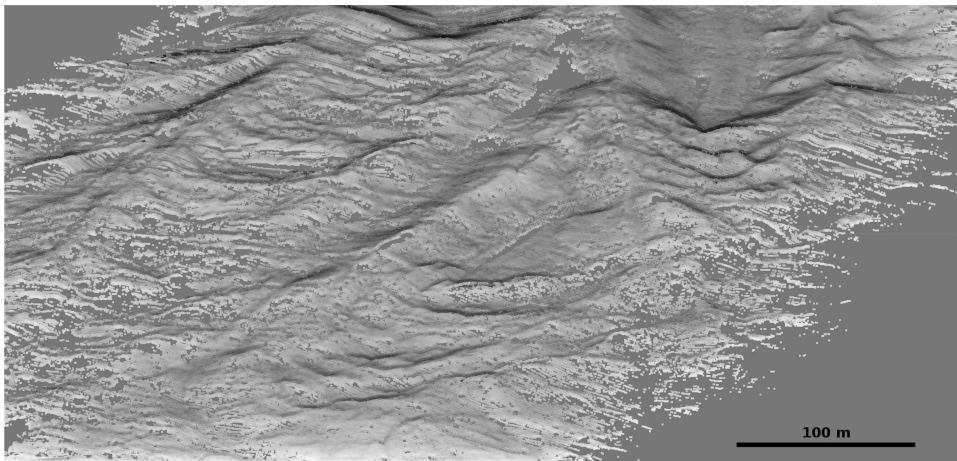


Figure 4.7: Separated ground points (digital terrain model) for the same area (view) as in Fig. 4.6.

4.8). The first category contains 56 GCPs placed on bare ground without any vegetation and marked with a sprayed red cross in reality (red points in Fig. 4.8). The second category consisted of 36 HCPs located also on vegetation-free ground (blue points in Fig. 4.8), and the last category of 61 HCPs located on the ground with low vegetation (green points in Fig. 4.8). GCPs are necessary for accurate photogrammetric solution (localization and optimization of photogrammetric project). Height check points were used only for outputs comparison and accuracy analysis of the methods used. The output in the form of dense point cloud (Fig. 4.9) was used for accuracy analysis.

In the parts with high vegetation, the bare ground was mostly not detected due to technology limitations (see for example [SPAR 3D, 2016](#)) in contrast with laser scanning technology. The only exception is broadleaf forest during plant dormancy.

4.3.5 LiDAR from conventional aircraft

Data collection in this part of the Czech Republic was carried out during 2011. The average flight height was about 1200–1400 m above

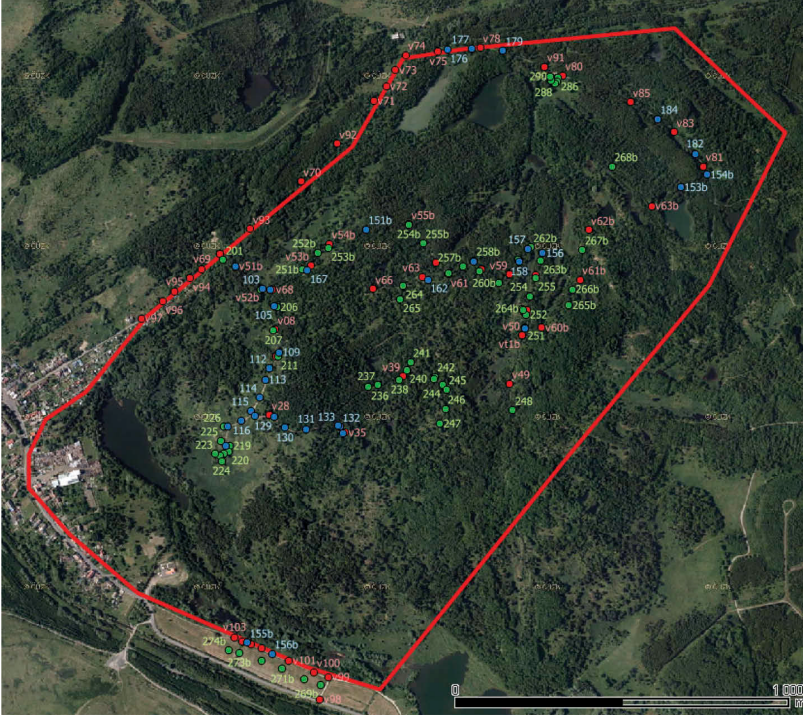


Figure 4.8: Distribution of ground control points (red), vegetation-free height check points (HCPs) (blue), and HCPs on low vegetation (green).

the terrain (Brázdil, 2012). More information about the DMR 5G products were presented in Section 4.2.3 on page 57.

4.4 Accuracy Analysis

Empirical accuracy analysis is based on height comparison between the ground point cloud and HCPs divided into two categories (see Section 4.3.4 on page 61). The height difference was computed for each HCP using formula:

$$\Delta H = H_{GNSS-RTK} - H_{PC} \quad (4.1)$$

where $H_{GNSS-RTK}$ is the height of the HCP determined with GNSS method RTK, and H_{PC} is the height interpolated from the terrain point



Figure 4.9: Visualization of dense point cloud from the first photogrammetric measurement.

cloud at the geographical position of the HCP.

Then the height standard deviation σ_H and systematic error s_H were computed for each category and method using formulas:

$$\sigma_H = \sqrt{\frac{\sum_{i=1}^n \Delta H_i^2}{n}} \quad (4.2)$$

$$s_H = \frac{\sum_{i=1}^n \Delta H_i}{n} \quad (4.3)$$

where n is the number of HCPs in the category.

The minimum and maximum height differences were also recorded. The open source software Cloud Compare was used for height interpolation from the point cloud in the position of HCP.

4.4.1 Results

Accuracy analysis results were summarized in tables for clarity. Table 4.2 shows results for vegetation-free HCPs.

Table 4.2: Accuracy analysis results for height check points (HCPs) on vegetation-free surfaces ('Phot.' stands for photogrammetry).

	AMA	Phot. 1	Phot. 2	DMR 5G
σ_H (m)	0.10	0.07	0.05	0.11
s_H (m)	-0.01	0.05	-0.02	-0.08
Maximum difference (m)	0.22	0.17	0.07	0.07
Minimum difference (m)	-0.11	-0.05	-0.12	-0.29

Height standard deviation for the AMA system is on the inferior edge of presumed accuracy. From the point of view of previous experience (Koska et al., 2014), it seems that the problem is caused by insufficient calibration of the measuring platform. The optimum calibration process described by Koska et al. (2014) could not be repeated due to new legislative restrictions for UAVs in the Czech Republic (it is not allowed to fly above populated urban areas at all) and the old calibration was disrupted during the development process. The used calibration was carried out in an unsuitable configuration from terrestrial measurements on the roof of our faculty (optimal cloverleaf pattern could not be kept).

The outputs of photogrammetric measurements are in accordance with the expectation that in case of a correctly performed photogrammetric project it is possible to achieve accuracy of about one pixel of image GSR in the horizontal components and about 1.5–2 pixels of GSR in the vertical component (Vorster and Strecha, 2013; Nocerino et al., 2013). The GSR in this case was about 25–30 mm.

The result of the DMR 5G product is surprisingly good because its provider states a significantly higher vertical standard deviation of 0.18 m for vegetation-free terrain.

Table 4.3 summarizes results for HCPs on the terrain with low vegetation (grass). Results for all technologies are naturally worse than in case of vegetation-free surfaces but the advantage of LiDAR/laser scanning lying in better penetration of low vegetation is clearly evident. We can also see much higher negative (determined terrain is mostly above GCPs)

systematic error s_H and higher maximum and minimum differences generally for all technologies than in the first case.

The AMA system had the advantage of having been carried out earlier in the vegetation season (in March) with low and weak grass.

Table 4.3: Accuracy analysis results for HCPs on the ground with low vegetation.

	AMA	Phot. 1	Phot. 2	DMR 5G
σ_H (m)	0.16	0.11	0.38	0.16
s_H (m)	-0.02	0.00	-0.32	-0.13
Maximum difference (m)	0.40	0.35	0.13	0.08
Minimum difference (m)	-0.40	-0.22	-0.85	-0.37

In the DMR 5G documentation (Brázdil, 2012), it is stated that the biggest error (standard deviation) of about 0.21 m is obtained in the areas with low vegetation (grass). The accuracy was determined by empirical tests. The stated reason for the test result is the difficulty to automatically identify areas with low vegetation for use of special filters for bare ground determination. In the case of low vegetation, it is also not possible to exploit the LiDAR multiple echoes recording properly because of the minimum necessary interval between them is of the order of metres. The standard deviation of the height is anyway slightly better than is stated in the product documentation.

We can see a significant difference between the first and second measurements in case of photogrammetry. The reason lies in the important difference in the vegetation condition between end of April (29 April) and beginning of July (1 July). Vegetation growth during these two months was significant (see Fig. 4.10). It is not possible to reach better results during full growing season with this technology.



Figure 4.10: Vegetation difference between two photogrammetry campaigns (29 April 2016 (left) and 1 July 2016 (right)).

4.5 Comparison of Other Characteristics

Besides accuracy, there are some other important characteristics of the used technologies. The most important characteristics taken into consideration are vegetation penetrability, data density, data collection speed, and economic aspects.

4.5.1 Vegetation penetrability

It is a natural and generally known fact that unlike photogrammetry, LiDAR can be used for bare ground measurements and determination even in terrain with vegetation (e.g. [SPAR 3D, 2016](#)). In the case of photogrammetry, the possibilities for ground determination in such terrain are very limited but under specific conditions they are not impossible as presented below.

It is obvious that LiDAR in contrast with photogrammetry needs only a single direct optical connection between a sensor and the measured point. This fact is clearly evident in resulting point clouds (see Fig. 4.11).

In Figure 4.11, we can see that it is possible to photogrammetrically measure bare ground in parts with broadleaf or sparse trees in mixed forest near the dormancy (29 April 2016, red and blue points) in contrast with the growing season (1 July 2016) when only the top part of tree crowns and grass was recorded (green points). It is evident that photogrammetry can be used for identification of bare ground in case of dormancy and broadleaf forests. In such a case, it can be recommended to acquire images with maximal possible overlap to ensure ‘seeing through’ leafless branches.

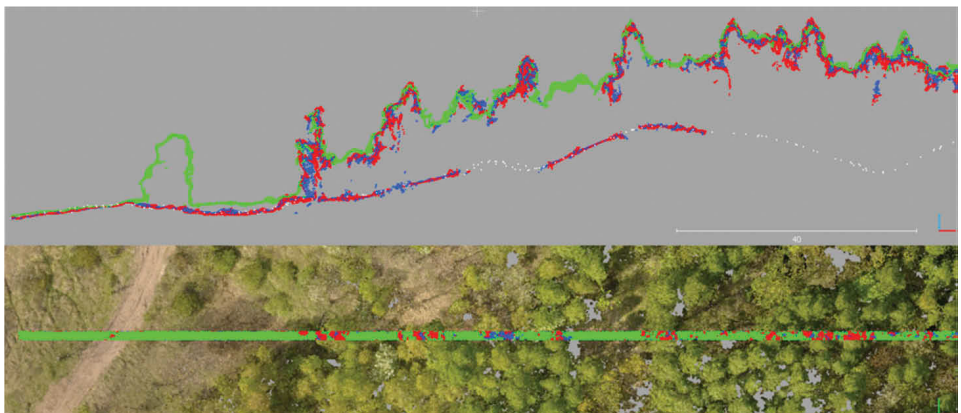


Figure 4.11: One metre thick cross section through the part with mixed forest: blue points – photogrammetry 29 April 2016, red points – photogrammetry 29 April 2016 with higher correlation resolution, green points – photogrammetry 1 July 2016, and white points – ground points from LiDAR (DMR-5G).

In Figure 4.12, we can see a cross section through a purely broadleaf forest including AMA measurement. The AMA system equipped with laser scanner with a quite narrow laser beam diameter (in comparison with LiDAR from conventional aircraft) measures mostly the top part of the tree crown and ground and occasionally also canopy, branches, and trunk.

Photogrammetry was successful in identification of bare ground during dormancy (29 April 2016, red and blue points) but in such case, trees are not captured at all. In contrast, during growing season, (1 July 2016) only the top parts of tree crowns were measured (green points).

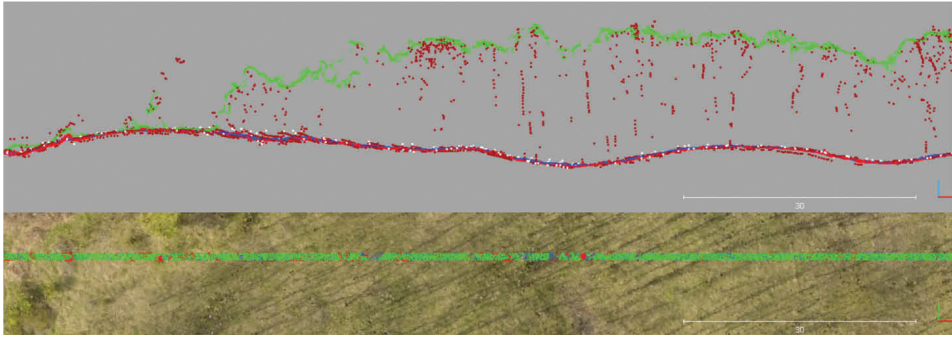


Figure 4.12: One metre thick cross section through the part with broadleaf forest: blue points – photogrammetry 29 April 2016, red points – photogrammetry 29 April 2016 with higher correlation resolution, green points – photogrammetry 1 July 2016, white points – ground points from LiDAR (DMR-5G), and brown points – AMA (17 March 2016).

At the end of this section, we can summarize that under specific conditions and in contrast with general assumptions, we can photogrammetrically measure bare ground (during dormancy) and top parts of tree crowns (during growing season) in the case of broadleaf forest.

4.5.2 Data density

Density of data recorded by the AMA system depends on the flight height above terrain, flight speed, and density of flight lines. In the case of operationally optimal project configuration, as in this experiment, it leads to an average point density of about 15 points m^{-2} and average point spacing of about 0.2 m.

In case of photogrammetry, data density depends on GSR of captured images and on settings of input image degradation for dense point cloud generation algorithms. For the average GSR of about 25 mm and the $16\times$ lower input image resolution for dense matching (medium settings in Agisoft PhotoScan), this means an average point density about 100–120 points m^{-2} and average spacing about 0.09 m.

The DMR-5G product is distributed with point density of about 0.2 points m^{-2} only, which means an average point spacing of about 1.8 m. Points are measured with higher density about of 1.6 points m^{-2} (spacing about 0.7 m) but the density drops especially in low rugged areas due to density inhomogeneity and large data volume in general.

4.5.3 Data collection speed

The time scheduled for the AMA measurement of the whole area was about three hours, but because of petrol engine failure of the AMA, only a part of locality was measured. An important disadvantage of the technology is the necessity for helium compression into high-pressure cylinders after a mission, which takes about 5 h for the airship and compressor that are used. The time needed for flight preparation is about 2 h.

The photogrammetry from the fixed wing UAV was carried out using four approximately 20 min long flights because of the flight endurance limit of the UAV used but only half of the study area was measured (see Section 4.3.4 on page 61). Two ground positions for landing and take-off had to be used so altogether with relocation and flight settings, the measurement took about 4 h. This is approximately the same time as was necessary for GNSS measurement of necessary GCPs.

It is obvious that in case of LiDAR from a conventional aircraft, the actual measurement is a matter of tens of seconds or a few minutes at maximum.

4.5.4 Economic aspects

It is very difficult to assess the economic aspects of an experimental and prototype technology such as the AMA project, but it seems that the operating costs are somewhere between those of UAV photogrammetry

and LiDAR from a conventional aircraft. It must be mentioned here that the whole necessary equipment is very spacious (high pressure cylinders and compressor are usually placed on a trailer) and it needs at least two field operators. About 1 or 2 m³ of helium loss must be also calculated to the operating costs for each helium compression into cylinders.

According to a preliminary quotation by a company providing UAV photogrammetry, the commercial price for mapping such an area (3 km²) with GSR 30 mm and with standard outputs (dense point cloud, mesh model, orthophoto) should be between 1000 and 2000 EUR depending on the distance of the area and other aspects. But in this particular case, the photogrammetric measurement of the whole area could not be done because of the inaccessibility of the northeast part for small UAVs.

Based on the information by the manager of Argus Geo System s.r.o. (a company providing LiDAR from a conventional aircraft), the price of measurement and point cloud output should be about 2000–4000 EUR depending on the distance of the study area from their airport. On the other hand, the DMR-5G product is available for the price of 23 EUR for a 2 km × 2.5 km map sheet.

4.6 Conclusion

The experimental mapping system AMA equipped with LiDAR is first introduced in this article. Other technologies and methods using UAVs or conventional aircraft are then compared with the AMA system on the basis of a practical project of medium size spoil heap mapping (about 3 km²). The most important parameter in the comparison is the accuracy of outputs but other relevant characteristics are also taken into consideration, such as vegetation penetrability, data density, data collection speed, and economic aspects.

The results of the AMA system are on the inferior edge of presumed accuracy – the vertical standard deviation is 10 cm in the case of vegetation-free surfaces and about 16 cm in case of low vegetation. From the point of view of previous experience and tests with better results, it seems that it is caused by an insufficient calibration of the measuring system. The optimal calibration process described by [Koska et al. \(2014\)](#) could not be repeated due the new legislative restrictions for UAVs in the Czech Republic (it is not allowed to fly above populated urban areas) and the previous calibration was disrupted during the development process. The calibration used was carried out in an unsuitable configuration from terrestrial measurements on the roof of our faculty (optimal cloverleaf pattern from two heights could not be kept). Also, the high frequency of failure of the carrier used – airship ACC15X from AirshipClub.com company – has proved to be a serious issue as a result of which it was not possible to measure the whole area. The ACC15X model is the first model from the producer that is powered by a petrol generator and it still has some teething problems.

The application of photogrammetry from a fixed wing UAV showed that the selected area is too large and its accessibility for this technology is especially difficult. The measurement was carried out twice with this technology and in both cases, only half of the proposed study area was measured because we could not find any suitable place for UAV landing and take-off to measure the northeast half of the study area.

The accuracy of photogrammetry outputs on the vegetation-free surfaces is in accordance with the expectation that in the case of a correctly performed photogrammetric project, it is possible to achieve an accuracy of about one pixel of image GSR in the horizontal components and about 1.5–2 pixels of GSR in the vertical component. In the case of surfaces with low vegetation, the limited ability of this technology to penetrate through the vegetation is clearly shown and the results are significantly worse especially for the vegetation season. On the other hand, under specific conditions, we can photogrammetrically measure

the bare ground (during plant dormancy) and the tops of the tree crowns (during the growing season) in case of broadleaf forests. The advantages of the technology are a high density of acquired data (data spacing up to the GSR) and lower operating/acquisition costs.

In the case of LiDAR from conventional aircraft, it seems that it achieves higher accuracy than stated in product documentation in the study area, namely 0.11 m on vegetation-free surfaces and 0.16 m on low vegetation surfaces. The main advantage of this technology is the ability to measure top surface and ground at the same time. The disadvantage of this technology is a low data density. The next evaluation depends on the product we consider. The disadvantage of the DMR-5G product can be data obsolescence (data for the site are from 2011); contrary, the significant advantage lies in acquisition costs which is only 46 EUR (two map sheets) for the entire study area. In case of an individual order of conventional aircraft LiDAR scanning, the data would be up to date but the acquisition costs would be at least twice as high as for the most expensive of remaining technologies (AMA).

Various technologies with different properties exist at present for mapping of medium sized areas (1–10 km²), which is why a lot of aspects must be considered to make the right decision about which one to use. Some of the most important aspects based on practical project were hopefully outlined in this article.

Chapter 5

Assessment of LiDAR Ground Filtering Algorithms for Determining Ground Surface of Non-natural Terrain Overgrown with Forest and Steppe Vegetation

Vítězslav Moudrý, Petr Klápště, **Michal Fogl**, Rudolf Urban, Kateřina Gdulová, Vojtěch Barták

Manuscript submitted to Measurement, with permission of corresponding author (Vítězslav Moudrý).

Publication metrics:

23 of 88 (Q2) rank in WOS category Engineering, Multidisciplinary
IF (2018) 2.791; AIS (2018) 0.483

Author's contribution: 30%

Abstract

Light detection and ranging has seen numerous applications across multiple environmental disciplines. Regardless of the application, an inevitable step of the point cloud processing is a ground filtering. Our objectives were to evaluate the performance of six software solutions and to assess the effect of vegetation and terrain on filtering accuracy. The point clouds filtering and vertical accuracy were evaluated qualitatively, quantitatively and by comparison with a GNSS survey. All tested algorithms achieved good results but their performance was affected by the terrain slope and vegetation cover. Algorithms performed better in forests than in steppes with a high density of low vegetation. The performance of all algorithms decreased with slopes over 15° . LAStools provided overall well-balanced results in all environments. Recently proposed algorithm implemented in PDAL has shown promising results, particularly in forests. We suggest that software developers should provide users with suggestions of optimal parameters for individual environments.

5.1 Introduction

Creating an accurate representation of the Earth surface has been a fundamental goal of researchers in many environmental disciplines (Moore et al., 1991). The most widely used representations of the Earth's surface are the Digital Surface Models (DSMs) and Digital Terrain Models (DTMs). DSMs represent the Earth surface including vegetation, buildings and other natural or man-made objects and can be used, for example, for viewshed analyses (Klouček et al., 2015; Lagner et al., 2018) or solar potential estimates (Fogl and Moudrý, 2016). In contrast, DTMs provide a bare earth representation of terrain topography and is frequently used in environmental studies. For instance, in the fields of hydrology (Sangireddy et al., 2016), species distribution modelling (Bazzichetto et al., 2018; Moudrý et al., 2018), digital soil mapping (Penížek et al., 2016; Baltensweiler et al., 2017), or yield prediction (Kumhálová and Moudrý, 2014).

The ways of acquisition of accurate information on the 3D structure of the environment have greatly expanded over the past two decades. In particular, laser altimetry, commonly referred to as light detection and ranging (LiDAR) or airborne laser scanning (ALS) has revolutionized the quality of 3D representation of the environment and has become the primary method for acquisition of accurate terrain information (Wehr and Lohr, 1999). LiDAR pulses can penetrate through gaps in vegetation canopies and register multiple returns representing both above ground objects and terrain. The point clouds generated in this way hence contain reflections from various features (e.g. ground, vegetation, buildings). The acquisition costs of LiDAR data per unit area have decreased considerably over the last two decades and the use of LiDAR is therefore on the rise, especially for large scale projects (e.g. Johansen et al., 2010). Furthermore, ALS data are increasingly available and provided free of charge through government agencies in many countries (e.g. Denmark, Poland, Estonia, Finland, Slovenia),

which in turn leads to a greater use of the data in many disciplines such as forestry (Chen et al., 2017), hydrology (Yang et al., 2014), geomorphology (Chalupa et al., 2018), and ecology (Davies and Asner, 2014). Regardless of the application and a final product needed, an inevitable and the most critical step of the point cloud processing is the ground filtering (i.e., the process when points that represent bare ground are separated from non-ground points representing objects above the bare ground such as trees). The correct filtering (sometimes called classification) of ground points is essential to the subsequent creation of DSMs, DTMs or other derived products (Jakubowski et al., 2013; Hawryło et al., 2017). The quality of the ground filtering also affects the scale of the derived products, which is important for many applications (e.g. Yang et al., 2014; Lecours et al., 2017; Šímová et al., 2019). The point cloud filtering is therefore, besides being a crucial component of any LiDAR dedicated software, also available in some more complex geographic information systems (GIS) software solutions such as ArcGIS (ESRI, 2014).

Many algorithms for ground filtering of ALS data have been designed (e.g. Meng et al., 2009; Susaki, 2012; Rashidi and Rastiveis, 2017), usually developed with some specific environment in mind (e.g. forests, steppes; or urban areas; Shan and Aparajithan, 2005; Tinkham et al., 2011; Maguya et al., 2014) and as each environment poses specific challenges, the efficiency of the algorithms varies across environments. While a dense forest canopy tends to block LiDAR pulses and therefore to introduce gaps in the data, low vegetation can confound ground filtering algorithms and be misclassified as a ground surface. Ground filtering can be also challenging in regions with a complex topography (Leitold et al., 2015).

The first comparison of ground filtering algorithms was performed by Sithole and Vosselman (2004). More recently, Meng et al. (2010) reviewed critical issues of ground filtering algorithms and criteria for their selection. With the increasing availability of ALS data and conse-

quent implementations of ground filtering algorithms in various software solutions, the attention focused on the performance of individual algorithms has increased (Gonçalves and Pereira, 2010; Sulaiman et al., 2010; Tinkham et al., 2011; Julge et al., 2014; Korzeniowska et al., 2014; Montealegre et al., 2015; Polat and Uysal, 2015; Silva et al., 2018).

An overwhelming number of choices of the algorithms and their implementations in various software solutions can easily leave an inexperienced practitioner daunted. On the other hand, most software products implement only a single algorithm, which can lead users to select a solution that is readily available but sub-optimal for a particular environment. Furthermore, filtering methods usually require parameter tuning and manual editing to achieve the best results (e.g. Wan et al., 2018). Some software solutions allow advanced parameter settings, thus giving the users an option to influence the results while on the other hand posing higher demands on their experience. In contrast, other software solutions try to be as simple as possible and require minimal number of input parameters or allow only a few predefined options. Another aspect that can influence the selection of algorithms can be a lacking algorithm documentation and high software costs. Some algorithms implemented in commonly used software are at least partly described in the documentation. However, many ground points filtering algorithms are considered proprietary knowledge and as such, they represent a grey- or black-box solution.

With the ongoing development of new algorithms (Pingel et al., 2013; Zhang et al., 2016) and their implementation in both LiDAR-dedicated and complex GIS software, evaluation of the performance of these algorithms in a variety of terrains and vegetation conditions is needed. Therefore, in this study, we evaluated the performance of six ground filtering algorithms contained in five frequently used software solutions. In addition to algorithms evaluated by prior studies, we also assessed relatively recent algorithms that have never been compared to others so far (see Appendix 1 for overview of existing comparative studies).

In particular, we: (1) evaluated the filtering error; (2) assessed the accuracy of generated DTMs using field measurements as reference data; and (3) assessed the effect of vegetation and terrain characteristics on the performance of the individual algorithms in a complex non-natural terrain (i.e., a spoil dump) overgrown with forest, steppe and grass vegetation.

5.2 Material and Methods

5.2.1 Study area

The study area is located at Hornojiretinska spoil dump (north-west Bohemia, Czech Republic, 50°34'N, 13°34'E) that covers an area of approximately 450 ha. The spoil heap served as a deposit of the overburden from brown coal mining. The spoil dump has never been technically reclaimed and the terrain morphology thus remained rugged, with areas of steep slopes resulting from heaping and consequently developing heterogeneous vegetation (e.g. Frouz et al., 2018). To be able to cover the entire study area with reference GNSS measurements (see below), we limited the study area to a fraction of the dump – 30 hectares representative of different conditions on the spoil dump (Fig. 5.1). In general, the terrain in the study area changes especially in the south-north direction, from a flat area outside of the spoil heap to slopes and the rugged terrain of the actual spoil heap (Fig. 5.1). The vegetation includes grass, aquatic vegetation, steppes and forests. Five areas with different vegetation and terrain character were manually vectorised over an orthophoto, combining the orthophoto with our knowledge of the area (Fig. 5.1, Tab. 5.1). Area I is outside the actual spoil heap and is dominated by low grass with only a few scattered trees. The terrain is flat with ditches alongside the gravel roads. Areas II and III are dominated by low vegetation, especially bush grass *Calamagrostis epigejos* and tall oat grass *Arrhenatherum elatius*, with

dense shrubs and scattered trees such as elder *Sambucus*, rosehip *Rosa*, common snowberry *Symphoricarpos albus*, birch *Betula*, or hawthorn *Crataegus*. Area II also includes several terrain depressions that are overgrown with common reed *Phragmites australis* and common cattail *Typha latifolia*. Area IV is a forest dominated by willow (*Salix spp.*) and alder (*Alnus spp.*) while Area V is a forest dominated by birch *Betula pendula*. All Areas (except Area I) have undulated terrain with steep slopes, small scale valleys and ridges (Fig. 5.1, Tab. 5.1).

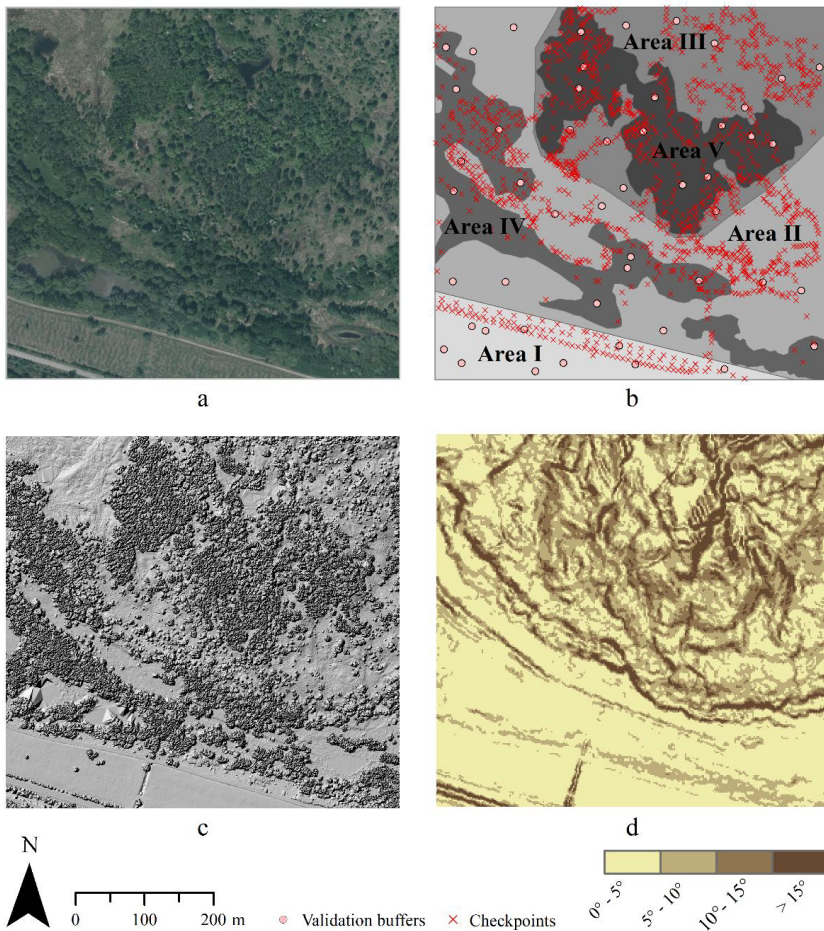


Figure 5.1: Details of the study area. Orthophoto (a); Five areas with different character of vegetation and terrain including the location of validation buffers and checkpoints (b); Hillshaded model (c); Slope (d).

5.2.2 LiDAR and Reference data acquisition

5.2.2.1 ALS data acquisition

A Riegl full-waveform laser scanner (LMS-Q780) was used for the ALS data acquisition over the study area. The data were acquired by the Flying Laboratory of Imaging Spectroscopy (FLIS) in May 2017. The aircraft flight altitude was 1030 m above the ground level with a ground speed of 110 knots. The scanner is based on a rotating mirror and scans in parallel lines with a field of view of 60°, the wavelength is 1064 nm. The point density of the resulting point cloud was 7.7 points per square meter. ALS data were processed using a proprietary software of the CAS Global Change Research Institute (CzechGlobe), referenced to the European Terrestrial Reference System, Universal Transverse Mercator projection (ETRS UTM33N), and provided with elevations as ellipsoidal heights.

5.2.2.2 Manual classification of point clouds and survey of checkpoints

To properly assess classification success, reference data are necessary. We randomly generated 50 point locations (10 point locations in each of the Areas I-V); all points within a 5 m distance (hereafter buffers) from those locations were selected as test points and manually classified as ground and nonground. That resulted in 14,102 non-ground and 16,683 ground points used for the validation, respectively.

Compared to pre-existing studies (e.g. [Montealegre et al., 2015](#)), the areas manually classified in our study for assessment of the filtering performance are relatively large; this on the one hand improves the overall validity of the study, it however on the other hand also increases the risk of manual filtering errors that can still be present in our evaluation dataset. Therefore, we also evaluated the vertical accuracy

of DTMs using independent data obtained through a RTK GNSS survey. The RTK GNSS survey was conducted during the early spring under leaf-off conditions in 2017 and 2018 using Leica GPS1200 system. In total, 1439 checkpoints distributed throughout the study area (Tab. 5.1, Fig. 5.1) were used. All check points were measured in ETRS89 with ellipsoidal heights and projected to UTM33N.

Table 5.1: General characteristics of the study area.

	Area	Num. of	Slope [°]	Height [m]	Maximum
	[ha]	checkpoints	Mean \pm S.D.	Mean \pm S.D.	height [m]
Area I <i>grass</i>	3.3	107	2.6 \pm 3.6	5.9 \pm 3.0	18.1
Area II <i>shrub</i>	10.9	437	4.8 \pm 4.1	6.9 \pm 4.0	24.2
Area III <i>shrub</i>	6.5	395	8.9 \pm 5.4	5.8 \pm 3.2	19.4
Area IV <i>forest</i>	5.2	170	5.7 \pm 4.8	10.3 \pm 4.3	23.8
Area V <i>forest</i>	5.0	330	9.6 \pm 4.6	9.8 \pm 3.6	21.5
	Canopy	Dens. of ground	Density of	Density of	Density of
	cover [%]	& low veg. [%]	shrubs [%]	low trees [%]	high trees [%]
		(< 0.3 m)	(0.3–3 m)	(3–15 m)	(> 15 m)
Area I <i>grass</i>	5.8	92.3	2.7	4.8	0.1
Area II <i>shrub</i>	22.8	72.7	8.3	18.0	0.9
Area III <i>shrub</i>	31.6	64.5	11.4	23.9	0.2
Area IV <i>forest</i>	70.4	29.1	6.5	54.9	9.5
Area V <i>forest</i>	60.2	40.5	3.1	52.8	3.7

Maximum, mean and standard deviations of height are calculated from a pit free Canopy Height Model. Other characteristics are calculated directly from LiDAR point cloud. Canopy cover is calculated as the number of first returns above breast height (1.37 m) divided by the number of all first returns. Densities of ground, shrubs and trees are derived as numbers of returns in each height interval divided by a total number of returns. Slope is represented by a mean value \pm standard deviation.

5.2.3 Ground points classification algorithms

In this study, we compared six algorithms implemented in two open source and three commercial software products that have been increasingly used for ground point classification (Tab. 5.2). One of the currently most popular software solutions for point cloud processing

is Rapidlasso LAStools (rapidlasso.com), which has a unique position among the tested programs – it is a commercial software but the limitations of its free version are kept to minimum. Open source programs CloudCompare (danielgm.net/cc) and PDAL (pdal.io) have also become quite popular. Of the commercial software, we tested the ground classification algorithms implemented in the widely used programs ArcGIS (esri.com) and Trimble Realworks (geospatial.trimble.com). In each software, we started from default settings and through expert tuning of the parameters (based on our experience with the tested algorithms and our knowledge of the terrain and vegetation in the study area) progressed to the best achievable results for each individual algorithm.

Table 5.2: List of evaluated software solutions, algorithms and their parameters fine-tuned in this study.

Software	Algorithm	Author	Number of evaluated settings	Parameters
CloudCompare	CSF	Zhang et al., 2016	12	Predefined options: <i>Steep slope, Relief, Flat</i> ; Cloth res. Slope processing: <i>enabled/disabled</i>
LAStools	PTIN	Isenburg, 2018	38	Step, Spike, Offset
ArcGIS	ARC	Esri, CA, USA	3	Predefined options: <i>Aggressive, Standard, Conservative</i>
PDAL	PMF	Zhang et al., 2003	30	Initial distance, Max distance, Max window size, Slope
PDAL	SMRF	Pingel et al., 2013	36	Scalar, Slope, Threshold, Window
RealWorks	RW	Trimble, CA, USA	1	-

CSF - Cloth Simulation Filter; *PTIN* - Progressive Triangulated Irregular Network; *PMF* - Progressive Morphological Filter; *SMRF* - Simple Morphological Filter; Note that *ARC* and *RW* are only abbreviations used for black-box algorithms implemented in *ArcGIS*, and *RealWorks*, respectively. While other abbreviations are commonly used.

Rapidlasso LAStools (rapidlasso.com/lastools) use a progressive triangulated irregular network (PTIN) densification algorithm (Axelsson, 2000). This algorithm identifies the ground points with respect to the

distance between each point and a generated triangulated irregular network of lowest points. CloudCompare (danielgm.net/cc) uses a newly proposed algorithm based on the cloth simulation filter (CSF; Zhang et al., 2016). In this technique, the original point cloud is at first rotated by 180 degrees and a simulated cloth is subsequently “dropped” on the inverted surface, creating a simulated surface. In PDAL (pdal.io), there are two different algorithms to choose from; a Progressive Morphological Filter (PMF) (Zhang et al., 2003) and a Simple Morphological Filter (SMRF) (Pingel et al., 2013). Both of them use mathematical morphology operations such as erosion and dilation to remove non-ground objects (Haralick et al., 1987; Zhang et al., 2003). Both filters iteratively change the size of a moving window to successfully remove objects of different size. The algorithms implemented in ArcGIS (hereafter ARC) and Trimble Realworks (hereafter RW) are grey-box algorithms with default settings only.

5.2.4 Quantitative and Qualitative validation

The classified point clouds were compared with manually classified reference data to quantify the performance of individual classification methods. We calculated the Type I error (omission error), representing the percentage of ground points that are incorrectly classified as non-ground as:

$$Type\ I\ error = \frac{b}{a + b} \quad (5.1)$$

where a is the number of correctly classified ground points and b is the number of ground points misclassified as non-ground points.

Type II error representing non-ground points incorrectly classified as ground points was calculated as:

$$Type\ II\ error = \frac{c}{c + d} \quad (5.2)$$

where c represents the number of non-ground points misclassified as ground points and d stands for the number of correctly classified non-ground points.

In addition, we calculated the success rate, i.e., the ratio between the number of correctly classified points and the total number of points.

$$Success\ rate = \frac{a + d}{e} \quad (5.3)$$

where e stands for total number of all points.

In addition, ground classified points were used to generate DTMs with a cell size of 0.5 m. We used a bin-average method calculating the elevation for each cell by assigning the average value of all points within that cell. Areas containing no ground points were triangulated across and linearly interpolated to determine their cell values. We used several accuracy measures to assess the vertical accuracy of DTMs. The GNSS survey, representing the most accurate data, was used as the reference dataset (true elevation) to evaluate the DTMs. We first calculated vertical differences among the 1439 surveyed point elevations and the corresponding DTMs. Those differences were subsequently used to calculate the mean error (ME) and root mean square error (RMSE). We also calculated the normalized absolute deviation (NMAD), which is a robust metric less sensitive to the presence of outliers (see [Höhle and Höhle, 2009](#)).

It is a common approach in existing studies to compare algorithms based on results obtained using parameters that resulted in the highest filtering accuracy ([Korzeniowska et al., 2014](#); [Montealegre et al., 2015](#)). Parameter tuning, however, is greatly dependent on the user's experience and the parameters are not always optimally tuned (e.g. [Wan et al., 2018](#)). In our study, we calculated above mentioned quantitative metrics for all evaluated parametrizations to assess whether the algorithms tend to cause Type I or Type II error regardless of a parameters set.

In other words, the “within algorithm variability” based on different parametrizations was evaluated.

In addition to the above, we selected the best ground filtering setting for each algorithm and performed both qualitative and quantitative “between algorithms” comparison. The qualitative assessment consisted of a visual examination and comparison of a shaded relief of the generated DTMs. To study the effect of the character of the environment (i.e. the combined effect of vegetation and terrain), the assessment was performed separately for each area (I-V, Fig. 5.1). These areas differ mainly in vegetation character (i.e. grass, shrub, forest), however, they also differ in terrain complexity (Tab. 5.1). Therefore, the effect of the terrain on the filtering algorithms was also evaluated using the terrain slope calculated from the national DTM of the Czech Republic (see [Moudrý et al. \(2019\)](#) for more details about this dataset) and divided into four categories (0° - 5° , 5° - 10° , 10° - 15° and $>15^\circ$). We tested for the differences in the Type I error, Type II error, and Success rate between areas (I - V) and classification algorithms using linear mixed models, with an identifier of the 50 randomly distributed buffers as random effect. We thus fitted three different models (one for each error measure as a response variable) with algorithm and area as predictors, including their interaction. Similarly, we tested whether the elevation difference measured in the 1439 check points differed between areas and algorithms, again using a linear mixed model with interactions. Statistical analysis was performed using the R statistical software ([R Core Team, 2018](#)), the models were fitted using lme4 package for R ([Bates et al., 2015](#)), and statistical significance of the model fixed effects was evaluated using Wald chi-square tests (function Anova in the package car for R ([Fox and Weisberg, 2011](#))).

5.3 Results

5.3.1 Selection of best parameters

In total, 120 classifications were performed (Tab. 5.2). Type I and Type II errors, and hence the RMSE, vary even within a single algorithm depending on the settings. However, all algorithms achieved relatively good results in terms of RMSE, no matter whether fine-tuning was needed or whether software allowed only a few predefined options (Fig. 5.2). A general trend of individual algorithms can be observed regardless of particular settings of the parameters (Fig. 5.3). SMRF, CSF and RW successfully identified most of the ground points. However, they often classified non-ground points as ground (i.e. have lower Type I error than Type II error). In contrast, ARC, PTIN, and PMF showed a lower tendency to classify non-ground points as ground, but not all ground points were successfully identified (i.e. have lower Type II error than Type I error).

5.3.2 Quantitative assessment: Vertical accuracy, Type I and Type II errors

In the following sections, point clouds acquired with parameters achieving the best results for the individual algorithms will be compared. The optimal sets of parameters in this respect was a set that resulted in a terrain model with the minimum number of visually evident errors (evaluated using shaded relief) and the lowest RMSE in combination with the highest success rate for each algorithm. Where similar RMSEs and success rates were obtained, parameters resulting in a lower Type II error were selected. The summary of optimal combinations of parameters for our study area and their validation metrics are presented in the Tab. 5.3. The RMSE ranged from 0.15 m to 0.21 m. PTIN yielded

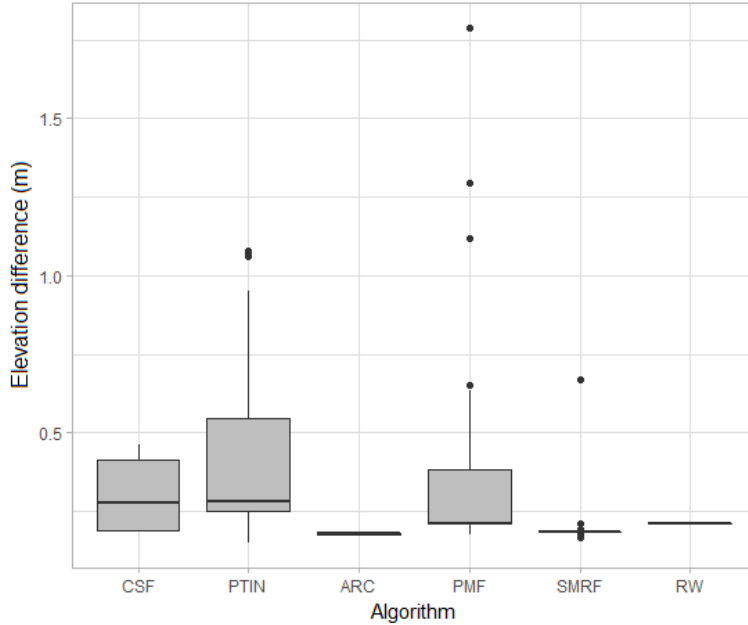


Figure 5.2: Performance of individual ground filtering algorithms throughout calculations using different settings of optional parameters. The central horizontal line in the box marks the median. The boxes show interquartile range (25th to 75th percentile) and the whiskers show 1.5 times the interquartile range.

the best result with the RMSE of 0.15 m, followed by SMRF (0.17 m), ARC (0.18 m), PMF (0.18 m), CSF (0.19 m), and Trimble (0.21 m; Tab. 5.3, Fig. 5.4). The success rate of point clouds filtered with the optimal parameters for each algorithm ranged from 79.2% to 90.8%. Success rates of all software solutions (with the exception of ARC) were higher than 85%. CSF yielded the highest success rate (90.8%) closely followed by RW (90.6%), both however have a notably high Type II error (>15%). On the other hand, ARC yielded the lowest success rate (79.2%), particularly due to the highest Type I error of all algorithms (32.4%). The Type II error ranged from 0.5% to 19.2%. The lowest Type II error was observed for PTIN (<1%) while the highest for CSF (19.2%) and RW (15.3%). The lowest Type I error, on the other hand, was obtained by the CSF (<1%).

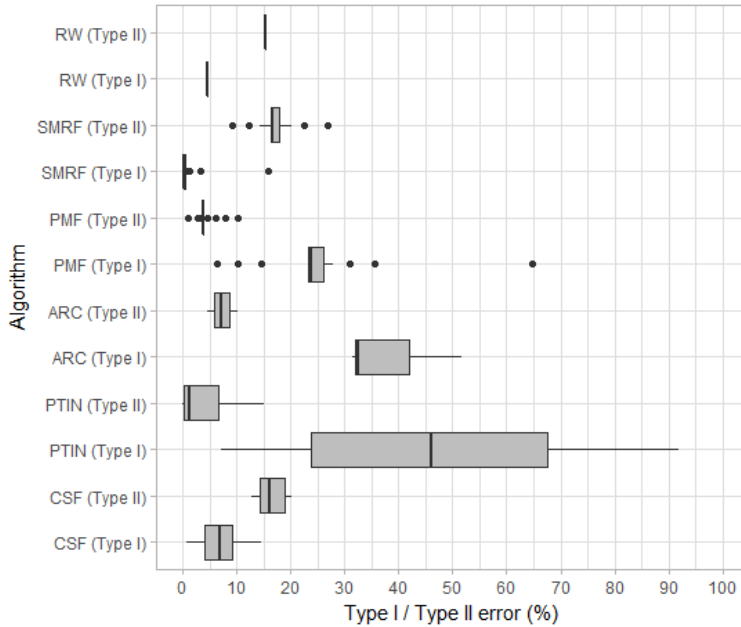


Figure 5.3: Comparison of algorithms' tendency to yield Type I and Type II error. Note that the use of CSF, SMRF and RW tends to cause Type I error while PTIN, ARC and PMF tend to Type II error. The boxes show interquartile range (25th to 75th percentile) and the whiskers show 1.5 times the interquartile range.

5.3.3 Effect of vegetation and terrain

In our study area, we identified three problematic circumstances under which classification algorithms were likely to fail: (i) sharp ridge/steep slope; (ii) very dense vegetation and (iii) vegetation on slopes or in ditches. The most notable deterioration of the classification results caused by dense vegetation and vegetation on steep slopes was observed for PMF and CSF algorithms (Fig. 5.4b, e). The terrain derived from both PMF and CSF filters showed obvious erroneous peaks throughout the study area that were caused by the vegetation and present even in the area with prevailing grass vegetation (some shrubs and dense vegetation in ditches were misclassified as ground; Fig. 5.4b, e). RW filter tended to eliminate ground points excessively and result in omission of many terrain features such as ditches and steep slopes in

densely vegetated areas (Fig. 5.4g). PTIN, ARC and SMRF preserved the terrain relatively well; however, they eliminated ground points and partly omission some of the steep slopes and they did not remove the very dense vegetation (Fig. 5.4c, d, f). It should be however noted that at places (Fig. 5.4), the very dense vegetation formed an impenetrable surface and only very few LiDAR pulses penetrated it; in other words, in such places, almost no ground points were present in the raw data. Where this was the case, any failures were more due to the problematic character of the data itself than due to a problem with the algorithm. For some algorithms, we were able to filter out even the dense vegetation during a manual fine-tuning of the algorithms, it was however only at the cost of failure at the ridges, the convex shape of which was then not preserved (results not presented here).

Table 5.3: Best results achieved by evaluated algorithms.

Algorithms	RMSE	ME	NMAD	Type I	Type II	Success	Parameters
	[m]	[m]	[m]	error	error	rate	
				[%]	[%]	[%]	
CSF	0.19	0.13	0.13	0.9	19.2	90.8	
	General parameters setting: <i>Flat</i> ; Slope processing: <i>enabled</i> ; Cloth resolution: <i>0.2</i>						
PTIN	0.15	0.10	0.11	18.6	0.5	89.7	
	Predefined: <i>Nature</i>						
ARC	0.18	0.12	0.13	32.4	7.1	79.2	
	Ground detection method: <i>Standard</i>						
PMF	0.18	0.08	0.11	23.3	3.9	85.6	
	Exponential: <i>true</i> ; Initial distance: <i>0.15</i> ; Max distance: <i>2.5</i> ; Max window size: <i>10</i> ; Slope: <i>1</i>						
SMRF	0.17	0.11	0.12	15.7	9.1	87.3	
	Scalar: <i>1.25</i> ; Slope: <i>0.15</i> , Threshold: <i>0.05</i> ; Window: <i>18</i>						
RW	0.21	0.13	0.13	4.5	15.3	90.6	-

CSF - Cloth Simulation Filter; PTIN - Progressive Triangulated Irregular Network; PMF - Progressive Morphological Filter; SMRF - Simple Morphological Filter; Note that ARC and RW are only abbreviations used for black-box algorithms implemented in ArcGIS, and RealWorks, respectively. While other abbreviations are commonly used.

The results indicate a contrasting performance of the algorithms in the five areas of different environment character (Tab. 5.4, Tab. 5.5).

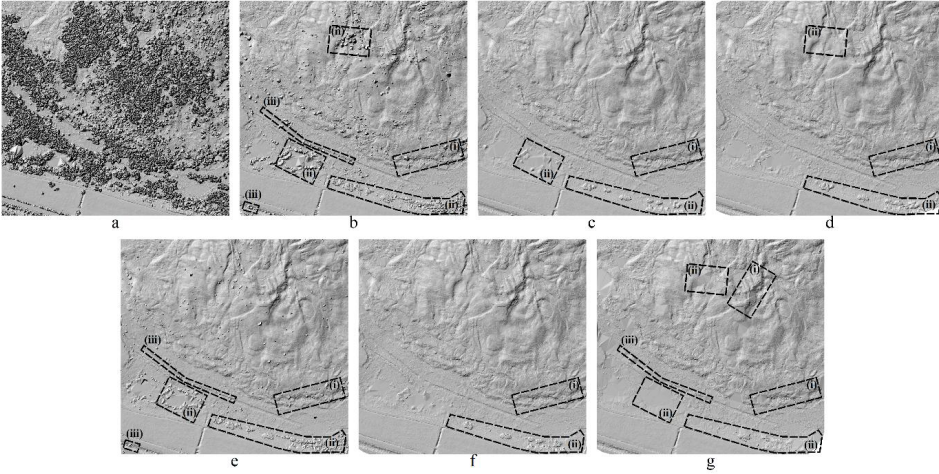


Figure 5.4: Hillshaded surface models generated from unfiltered point cloud (a) and point clouds filtered using CSF (b), PTIN (c), ARC (d), PMF (e), SMRF (f), RW (g) algorithm. Note the problematic area - right bottom corner - of very dense vegetation that formed an impenetrable surface and only very few LiDAR pulses penetrated it.

The effects of the area, algorithm and their interaction on elevation difference, Success rate, Type I and Type II error were statistically significant (Tab. 5.6, see Appendix 2 and 3 for boxplots). In areas dominated by shrub vegetation (Areas II and III), the RMSE ranged from 0.17 m to 0.23 m (Area II) and from 0.16 m to 0.21 m (Area III). PTIN, PMF and SMRF yielded the best results with $RMSE \leq 0.20$ m in both areas (see Appendix 4 for box plots of vertical differences). In addition, PTIN and PMF yielded the lowest Type II error. The average success rate ranged from 72.1% to 86.9% and from 76.4% to 89.7% for Area II and Area III, respectively. CSF and RW often misclassified non-ground points as ground and have therefore the highest Type II error in the shrub vegetation of all evaluated algorithms. All algorithms performed better in the forested areas than in the shrub vegetation, which is likely caused by the fact that in forests, there is a relatively lower representation of low vegetation (see Tab. 5.1) bearing a profound effect on misclassification, especially in combination with steep slopes. In forests, RMSE ranged from 0.16 m to 0.33 m and from 0.12 m to

0.22 m for Area IV and Area V, respectively (see Appendix 4 for box plots of vertical differences). All algorithms yielded average success rates greater than 90% except for ARC. The best results in forested areas were yielded by PTIN and SMRF. Finally, PMF and PTIN algorithms were the most suitable options in the areas dominated by grass vegetation with respect to classification accuracy (see range of success rate in Tab. 5.5) but PMF was not able to remove all vegetation in ditches (Fig. 5.4e). The increasing slope of the terrain resulted in deterioration of the terrain accuracy with the most evident decrease on steep slopes (greater than 15°; Tab. 5.7). The most accurate and consistent results with respect to the terrain slope was obtained by PTIN and SMRF. PMF also provided very good results but a significant drop in accuracy was detected even at intermediate slopes (10°-15°).

5.4 Discussion

In this study, we evaluated the performance of six ground filtering algorithms. In principle, two error types can occur while filtering ground points of LiDAR data. The first error type is the failure to identify true ground points, classifying them as non-ground objects (omission error), the other type is incorrect classification of non-ground points as bare earth (commission error) (e.g. [Sithole and Vosselman, 2004](#); [Korzeniowska et al., 2014](#); [Montealegre et al., 2015](#)). Ideally, one would compare all points to calculate the omission and commission error. However, this is impractical due to a large number of points recorded. Therefore, an approach using randomly sampled points is usually used (e.g. [Montealegre et al., 2015](#)) and was also used in our study.

Our results show that some algorithms tend to Type I error while others towards Type II error and they do so regardless of the parameter setting and vegetation character (which does not necessarily apply to other

areas not tested in our study, especially to urban environment). [Sithole and Vosselman \(2004\)](#) raised the question whether or not filtering algorithms should be fine-tuned towards the reduction of Type I errors, even if this is at the expense of an increase in Type II errors as Type II errors are considered conspicuous and therefore easy to remove by manual editing. Some algorithms in our study tended to cause Type I error (PTIN, ARC and PMF) while others tended more to the Type II error (CSF, SMRF and RW). In contrast, [Sithole and Vosselman \(2004\)](#) found that most algorithms produced Type I errors than Type II errors. There is always a trade-off between resulting Type I and Type II errors, all the more due to the fact that usually, one of those two types of error is considered more serious than the other, depending on the application of the filtered data. For some applications, Type I error is considered less costly and not a serious handicap due to further point cloud processing, such as applications that do not require DTMs with sub-meter resolution (e.g. applications in forestry at plot and larger scales; e.g. [Frazer et al., 2011](#)). It can be assumed that gaps caused by misclassified ground points are filled by interpolation and hence do not create an issue. On the other hand, hydraulic modelling would require very accurate DTMs and such gaps would be a serious drawback (e.g. [French, 2003](#)).

Our results show obvious differences between the performances of ground filtering algorithms in areas with different vegetation cover (i.e. grass, shrub, forest) and terrain complexity (i.e. slope). In general, all filters performed similarly well in the area of low complexity characterized by grass vegetation and flat terrain. However, with increasing terrain complexity and vegetation density, error rates caused by the filters increased. This corroborates findings of previous studies that also highlighted that vegetation and terrain character have a serious effect on the success of filtering algorithms (e.g. [Tinkham et al., 2011](#); [Korzeniowska et al., 2014](#); [Montealegre et al., 2015](#)). In particular, sites with low vegetation and shrubs were problematic for all algorithms and

resulted in a higher Type II error than forested areas. Parts of the vegetation were incorrectly classified as ground points due to similarities in the distribution of points (i.e. their slope and elevation differences). In particular, CSF, ARC, SMRF and RW tended to misclassify non-ground objects (e.g. low shrubs) as ground, thus having a high Type II error. On the other hand, the performance of PTIN and PMF was relatively good even in the shrub vegetation with relatively low Type II error and RMSE approximately 0.17 m; PMF however showed obvious erroneous peaks or bumps on the shaded relief map. For all algorithms, the tendency to cause Type I or Type II error was consistent across the vegetation types. The only exception was RW with a high tendency to Type I error in forests while to Type II error in shrubs (Tab. 5.5). This can be attributed to the fact that Realworks is primarily designed for Terrestrial laser scanning (TLS), and although it has also been successfully used for photogrammetric point clouds (Kršák et al., 2016), it is not well suited for ALS data. The increased slope also negatively affected the algorithms' performance. Most of the evaluated algorithms showed relatively good results for slopes up to 15°; with slopes over 15°, however, the performance of all algorithms decreased rapidly. The algorithm showing the lowest vulnerability by slope was PTIN, which corroborates results by Montealegre et al. (2015).

It should be noted that in this study, we concentrated mostly on the quantitative measures of the algorithm performances, although visual qualitative evaluation of generated DTMs was also performed. A more complex qualitative validation (for example, through the number of properly preserved terrain features) would however require a larger study area (Sithole and Vosselman, 2004; Montealegre et al., 2015). This would however be incompatible with our effort to cover whole area with GNSS measurements.

Existing studies followed two different approaches in terms of datasets used. While some studies (e.g. Sithole and Vosselman, 2004; Meng et al., 2009; Pingel et al., 2013; Zhang et al., 2016) used datasets

prepared solely for such purposes by the International Society for Photogrammetry and Remote Sensing (ISPRS), others used their own datasets (Korzeniowska et al., 2014; Montealegre et al., 2015; Stereńczak et al., 2016). The ISPRS data consist of several LiDAR datasets with varying degree of vegetation, terrain character and density and the nature of man-made structures (e.g. buildings, bridges). The undisputed advantage of the use of the same input data in all experiments and a consequent creation of a large database of results lies in a better comparability of results among individual studies. It is particularly beneficial when a new algorithm is developed and an assessment of its performance, together with its comparison with existing algorithms, is needed (e.g. Pingel et al., 2013). On the other hand, many studies prefer to test existing algorithms with their own data, particularly due to the fact that landscapes are often very specific in their terrain, presence of manmade objects and vegetation character and such individual approach is therefore necessary (e.g. Stereńczak et al., 2016). Such studies can be motivated by the need of accurate DTMs for specific purposes (e.g. application in forestry; Montealegre et al., 2015) and bring therefore additional benefits for the particular purposes, such as expanding our understanding of behaviour of filtering algorithms in different environments. Similarly, our study was motivated by a project that required accurate terrain models for analysis of post-mining sites, the character of which is very specific with respect to both terrain and vegetation (e.g. Moudrý et al., 2019).

Most existing comparative studies used collections of different algorithms (e.g. Sithole and Vosselman, 2004) or focused on the implementation of multiple algorithms into an open source software (e.g. Montealegre et al., 2015). Few authors evaluated also algorithms implemented to commercial software (e.g. Korzeniowska et al., 2014) as it is expensive and thus available only for large companies or research centres. We evaluated algorithms implemented in both commercial and open source software; however, evaluation of proprietary algorithms in commercial

software is complicated due to the unavailability of their description. For example, ESRI answered to our query on the algorithm implemented in ArcGIS: “The classification method used by the Classify LAS Ground tool is a comprehensive proprietary solution that does not fit in the given classes of algorithms, and no information has been published regarding the technique which is used”. This complicates the use of such software for ground classification. As we have shown, the algorithm performances vary among environmental conditions and users need to know whether a particular algorithm (or some of the predefined settings) is suitable for a particular environment (e.g. forest, shrubs) (Sithole and Vosselman, 2004; Montealegre et al., 2015). Moreover, fine-tuning is usually necessary for proper ground classification in different environments and algorithms implemented in commercial software often only allow predefined options (but see Wan et al. (2018) for automated tuning of ground filtering algorithms). However, such “black box” algorithms do not necessarily produce worse results and despite the high Type I error, the algorithm implemented in ArcGIS performed quite well, particularly in forest areas. However, its high initial costs are a serious drawback.

5.5 Conclusions

All tested ground filtering algorithms achieved relatively good results but their performance is notably affected by the terrain slope and vegetation cover. With increasing slope, the performance of the algorithms tends to deteriorate with a noticeable drop at terrain slope over 15°. Algorithms performed better in forests than in steppes with a high density of low vegetation. In our study area, PTIN implemented in LAsTools provided the best overall results, although some other algorithms performed better in specific environments. For example, the recently proposed SMRF algorithm has shown promising results in the forests.

The list of algorithms used in this study is not comprehensive and we are aware that other algorithms are available. We concentrated on popular open source software and recently developed algorithms that have not been previously tested (e.g. SMRF, CSF). Of the commercial software, we used solutions available to us. Such bias is almost inevitable and also obvious in prior studies in which authors usually evaluated algorithms that are easily available or those which the authors have experience with (see Appendix 1 for overview of existing comparative studies).

It is evident from our results and from prior studies that to achieve the optimal filtering performance, the selection of the algorithms and parameter settings should be guided by a specific landscape type. Such principle is for example implemented in LAStools, which allows users to select a set of parameters for a particular landscape (e.g. nature or town). It is worth mentioning that results for PTIN algorithm with such predefined settings implemented in LAStools are the best of all software tested, which only confirms the value of that approach. Until more automated approaches for parameters estimation will be developed, we can suggest this approach also to other software developers.

Table 5.4: Comparison of six algorithms in five areas of different vegetation structure (LiDAR DTM and GNSS differences).

Area	Algorithm	Number of checkpoints	RMSE [m]	ME [m]	NMAD [m]
Area I (grass)	CSF	107	0.04	-0.01	0.04
	PTIN		0.05	-0.02	0.04
	ARC		0.04	-0.01	0.04
	PMF		0.05	-0.02	0.04
	SMRF		0.05	-0.02	0.04
	RW		0.04	-0.01	0.04
Area II (shrub)	CSF	437	0.23	0.20	0.12
	PTIN		0.18	0.15	0.11
	ARC		0.21	0.18	0.11
	PMF		0.17	0.14	0.10
	SMRF		0.20	0.16	0.10
	RW		0.22	0.19	0.11
Area III (shrub)	CSF	395	0.19	0.14	0.12
	PTIN		0.17	0.11	0.11
	ARC		0.18	0.13	0.11
	PMF		0.16	0.08	0.10
	SMRF		0.18	0.11	0.11
	RW		0.21	0.13	0.12
Area IV (forest)	CSF	170	0.18	0.13	0.11
	PTIN		0.17	0.10	0.11
	ARC		0.18	0.13	0.12
	PMF		0.16	0.09	0.11
	SMRF		0.18	0.11	0.11
	RW		0.33	0.16	0.15
Area V (forest)	CSF	330	0.13	0.07	0.10
	PTIN		0.12	0.06	0.10
	ARC		0.13	0.07	0.10
	PMF		0.22	0.04	0.10
	SMRF		0.13	0.07	0.10
	RW		0.14	0.07	0.11

CSF - Cloth Simulation Filter; PTIN - Progressive Triangulated Irregular Network; PMF - Progressive Morphological Filter; SMRF - Simple Morphological Filter; Note that ARC and RW are only abbreviations used for black-box algorithms implemented in ArcGIS, and RealWorks, respectively. While other abbreviations are commonly used.

Table 5.5: Comparison of six algorithms in five areas of different vegetation structure (classification error).

Area	Algo.	Type I error			Type II error			Success rate		
		Mean \pm S.D.	Min	Max	Mean \pm S.D.	Min	Max	Min	Max	
Area I (grass)	CSF	0.5 \pm 1.04	0	3.1	21.5 \pm 37.38	0	87.5	93.3 \pm 18.16	41.8	100
	PTIN	16.8 \pm 11.65	5.1	34.6	2.4 \pm 5.29	0	11.8	84.2 \pm 10.66	65.4	96.6
	ARC	26.7 \pm 4.96	16.6	32	4.6 \pm 6.5	0	15.7	76.4 \pm 4.76	69.3	83.4
	PMF	10.4 \pm 10.02	0	29.4	3.5 \pm 4.86	0	11.8	91.4 \pm 7.86	79.5	100
	SMRF	19.2 \pm 9.11	10.4	39.1	7.1 \pm 9.18	0	21.7	81.5 \pm 8.63	60.9	89.7
	RW	0.7 \pm 1.11	0	3.1	17.7 \pm 31.06	0	72.7	94.3 \pm 15.18	51.3	100
Area II (shrub)	CSF	3 \pm 4.71	0	13.3	51.1 \pm 40.3	0	99.3	82.4 \pm 18.47	44.6	100
	PTIN	24.8 \pm 12.19	2.7	46.7	0 \pm 0.11	0	0.3	86.9 \pm 9.27	74.8	98.3
	ARC	38.3 \pm 6.14	27.6	48.6	20.5 \pm 18.16	0	54.2	72.1 \pm 12.98	55.4	97.8
	PMF	31.3 \pm 15.57	6.7	52	7.4 \pm 8.66	0	23.2	77.5 \pm 13.03	61.2	99.6
	SMRF	26.1 \pm 16.62	3.6	53.3	19.9 \pm 22.09	0	69.9	80.6 \pm 9.72	65.5	97.1
	RW	22 \pm 41.23	0	100	34 \pm 29.28	0	95	85.6 \pm 10.72	61.3	98
Area III (shrub)	CSF	0.7 \pm 0.82	0	2.3	28.9 \pm 29.31	1.1	100	87.3 \pm 11.69	66	99
	PTIN	15.5 \pm 14.04	1.4	39.7	0 \pm 0	0	0	89.7 \pm 12.85	61.5	99.5
	ARC	36.4 \pm 3.2	31	41.9	11.1 \pm 15.57	0	52.3	76.4 \pm 9.03	61.9	89.4
	PMF	34.9 \pm 9.28	22.6	49.5	5.4 \pm 7.22	0	24.1	79.5 \pm 9.07	61.4	88.1
	SMRF	9.8 \pm 3.86	4.5	16.8	13.4 \pm 17.2	0	58	88.5 \pm 5.52	79.3	96.6
	RW	6.4 \pm 9.12	0	29.9	21.2 \pm 28.61	0	96	88.2 \pm 8.65	77.2	97.8
Area IV (forest)	CSF	0.9 \pm 1.83	0	5.7	4.2 \pm 5.15	0	15.4	96.7 \pm 3.61	90.8	100
	PTIN	22.8 \pm 20.34	3.7	67.5	0 \pm 0	0	0	93.9 \pm 6.29	79.5	99.4
	ARC	38.8 \pm 7.78	27.2	53.8	1.2 \pm 2.27	0	7	89.6 \pm 4.76	77.9	94.4
	PMF	21.7 \pm 13.19	3.4	41.4	1 \pm 1.22	0	3.9	93.4 \pm 4.77	82.7	97.8
	SMRF	16.9 \pm 12.6	2.6	45.5	1.7 \pm 2.95	0	9.2	94.9 \pm 2.06	91.8	97.3
	RW	33.9 \pm 33.1	2.3	100	2.5 \pm 4.05	0	12.7	91.6 \pm 5.39	82.4	98.6
Area V (forest)	CSF	0.1 \pm 0.16	0	0	7.8 \pm 6.9	0	22	95.4 \pm 3.98	87	100
	PTIN	7 \pm 8.44	0	23.5	0 \pm 0	0	0	96.8 \pm 4.26	88.2	100
	ARC	28.6 \pm 4.3	20.6	34.4	4.2 \pm 4.48	0	11.8	85.6 \pm 4.33	80.3	92.6
	PMF	16.4 \pm 4.36	7.4	22.4	4.1 \pm 4.12	0	11.3	90.8 \pm 3	85.6	95.7
	SMRF	3.2 \pm 2.68	1.2	9.7	6.1 \pm 6.21	0	18.8	95 \pm 3.68	87.5	99.2
	RW	2.3 \pm 3.74	0.	12.1	7.2 \pm 7.26	0	22	95 \pm 3.98	87.2	100

The maximum, minimum, mean and standard deviation of error are calculated from 10 buffers in each of the Areas I-V.

Table 5.6: Significance of the effect of algorithm, area, and their interaction on Type I error, Type II error, Success rate, and elevation difference.

Fixed effect	Type I error			Type II error		
	χ^2 stat.	DF	P	χ^2 stat.	DF	P
Algorithm	197.757	5	$< 10^{-16}$	126.184	5	$< 10^{-16}$
Area	32.324	4	$1.6 \cdot 10^{-6}$	15.361	4	0.0040
Interaction	62.182	20	$3.3 \cdot 10^{-6}$	81.233	20	$2.4 \cdot 10^{-9}$

	Success rate			Elevation difference		
	χ^2 stat.	DF	P	χ^2 stat.	DF	P
Algorithm	67.897	5	$2.8 \cdot 10^{-13}$	463.049	5	$< 10^{-16}$
Area	35.892	4	$3.0 \cdot 10^{-7}$	317.745	4	$< 10^{-16}$
Interaction	37.038	20	0.0116	80.946	20	$2.7 \cdot 10^{-9}$

Table 5.7: The effect of the terrain slope on the filter accuracy. Evaluated by RMSE calculated for four slope categories.

Algorithm	Slope			
	0° - 5°	5° - 10°	10° - 15°	> 15°
CSF	0.17	0.18	0.19	0.24
PTIN	0.14	0.15	0.17	0.22
ARC	0.16	0.17	0.19	0.24
PMF	0.13	0.14	0.27	0.22
SMRF	0.15	0.16	0.18	0.23
RW	0.19	0.21	0.23	0.27
Num. of checkpoints	557	506	245	131

Chapter 6

Comparison of Leaf-off and Leaf-on Combined UAV Imagery and Airborne LiDAR for Assessment of a Post-mining Site Terrain and Vegetation Structure: Prospects for Monitoring Hazards and Restora- tion Success

Vítězslav Moudrý, Kateřina Gdulová, **Michal Fogl**, Petr Klápště,
Rudolf Urban, Jan Komárek, Lucie Moudrá, Martin Štroner, Vojtěch
Barták, Milič Solský

*Adapted from Applied Geography 104 (2019): 32–41, with permission
of corresponding author (V. Moudrý).*

Publication metrics:

15 of 83 (Q1) rank in WOS category Geography

IF (2018) 3.068; AIS (2018) 0.858

4 times cited on WOS (2019 August)

Author's contribution: 25%

Abstract

Mining is an important human activity that significantly affects the landscape character, particularly through excavation of spoil material and its deposition on spoil banks. The information on terrain or vegetation cover of spoil banks is often required for two different reasons: (i) to monitor and prevent adverse effect of hazards associated with unstable terrain; and (ii) to assess restoration success. Traditionally used in situ methods for monitoring surface displacement or restoration success are restricted in terms of spatial and temporal coverage. Therefore, in this study, we assessed the value of photogrammetrically and Light Detection and Ranging (LiDAR) derived point clouds for characterizing a post-mining site. We acquired images under leaf-off and leaf-on conditions and showed that point densities of point clouds acquired photogrammetrically under leaf-off conditions exceeded densities of those acquired under leaf-on conditions and uniformly covered ground of the entire study area (an average density of 288 points per m^2). In addition, the accuracy of the digital terrain model (DTM; 1 m resolution) derived from images acquired under leaf-off conditions was comparable to the LiDAR-derived DTM (RMSE of 0.19 m and 0.12 m, respectively). While LiDAR-derived DTM accuracies were consistent across vegetation categories (RMSE 0.12–0.14 m), accuracy of image-based DTMs declined in the following order: forest (RMSE 0.15 m), steppes (RMSE 0.21 m), and aquatic vegetation (RMSE 0.36 m). We suggest the leaf-off UAV imagery as a viable alternative for building DTMs that can be utilized for assessment of risks associated with instability of spoil banks terrain. In addition, we also suggest that a combination of acquisitions under leaf-off and leaf-on conditions have a potential to replace expensive airborne LiDAR surveys for applications requiring information on vegetation cover or vegetation height.

6.1 Introduction

Mining is an important human activity with strong social, environmental, and economic impacts (Lechner et al., 2017). It significantly affects landscape character, including ecological stability (Hendrychovia and Kabrna, 2016; Popelkova and Mulkova, 2018), aesthetic value (Svobodova et al., 2012), and morphology (Tarolli and Sofia, 2016; Brown et al., 2017). Open-pit mining and associated extensive disturbances, especially within the coal mining industry, significantly influence large areas. This involves formation of large pits as well as deposition of the excavated spoil material on spoil banks.

Mining is in general associated with geomorphic processes such as erosion, subsidence, landslides and runoff (Tarolli and Sofia, 2016). This is particularly true for spoil banks that are for various reasons (e.g. slope inclination, composition of waste material, subterranean combustion), especially prone to erosion (Haigh and Gentcheva-Kostadinova, 2002; Hancock et al., 2008; Nyssen and Vermeersch, 2010), terrain subsidence (Bell and Donnelly, 2006; Dulas, 2016; Sedlak et al., 2018), and landslides (Steiakakis et al., 2009; Cho and Song, 2014; Bednarczyk, 2017; Wasowski et al., 2018). To be able to study these processes or even to identify instability problems and to prevent potential adverse effects of such events (or at least minimize their impact), the knowledge of spoil banks terrain and vegetation cover is essential. Besides, spoil banks have been shown, curiously enough, to become important biodiversity refuges (e.g. Harabiš et al., 2013). Hence, information on the terrain and vegetation cover of spoil banks is not only needed for studying geomorphic processes but is also useful for assessment of their conservation value (Doležalova et al., 2012) and for understanding factors affecting the successional trajectory (Frouz et al., 2018) or restoration success (Vymazal and Sklenicka, 2012; Wortley et al., 2013).

To efficiently manage spoil banks, namely for detection and quantification of terrain changes (e.g. Xiang et al., 2018) or terrain stability

analyses (e.g. [Close et al., 2016](#); [Stephenne et al., 2014](#); [Zalesky and Capova, 2017](#)), repeated topographic surveys and information on vegetation cover are required. The traditional techniques used to monitor spoil banks terrain such as total station and GNSS surveys are expensive and restricted in terms of spatial and temporal coverage (e.g. [Zalesky et al., 2008](#); [Hogarth et al., 2017](#)). Similarly, terrain topography and vegetation cover used by restoration ecologists are usually determined by spatially limited and simple categorical variables due to the labour intensive field collection of data (e.g. [Šálek, 2012](#); [Harabiš et al., 2013](#); [Vojar et al., 2016](#)). A great benefit of remote sensing over more traditional techniques lies in its ability to provide continuous information over a large area. However, references to the use of remotely sensed data for monitoring or restoration success assessment of post-mining sites are scarce ([Weżyk et al., 2015](#); [Cordell et al., 2017](#); [Koska et al., 2017](#); [Ćmielewski et al., 2018](#)).

Remote sensing methods commonly used to collect data for generation of digital terrain models (DTMs) and derivation of vegetation cover variables include terrestrial and airborne light detection and ranging (LiDAR; [Wehr and Lohr, 1999](#)) and, more recently, structure from motion (SfM) and multi-view stereo (MVS) photogrammetry workflows ([Fonstad et al., 2013](#); [Smith et al., 2016](#)). Although airborne laser scanning (ALS) data are increasingly available, sometimes even free of charge (in some European countries, for example, they are available through government agencies; e.g. [Fogl and Moudrý, 2016](#); [Langhammer et al., 2018](#)), the coverage is still lacking in many countries (e.g. [Hofierka et al., 2018](#)) and high acquisition costs limit a wider use of the data when repeated measurements are needed. In contrast, photogrammetric methods offer low-cost alternatives for repeated measurements, especially so in combination with unmanned aerial vehicles (UAVs), which makes such a combination a potentially valuable and practically applicable tool for monitoring of terrain and vegetation cover changes (e.g. [van Iersel et al., 2018](#); [Xiang et al., 2018](#)).

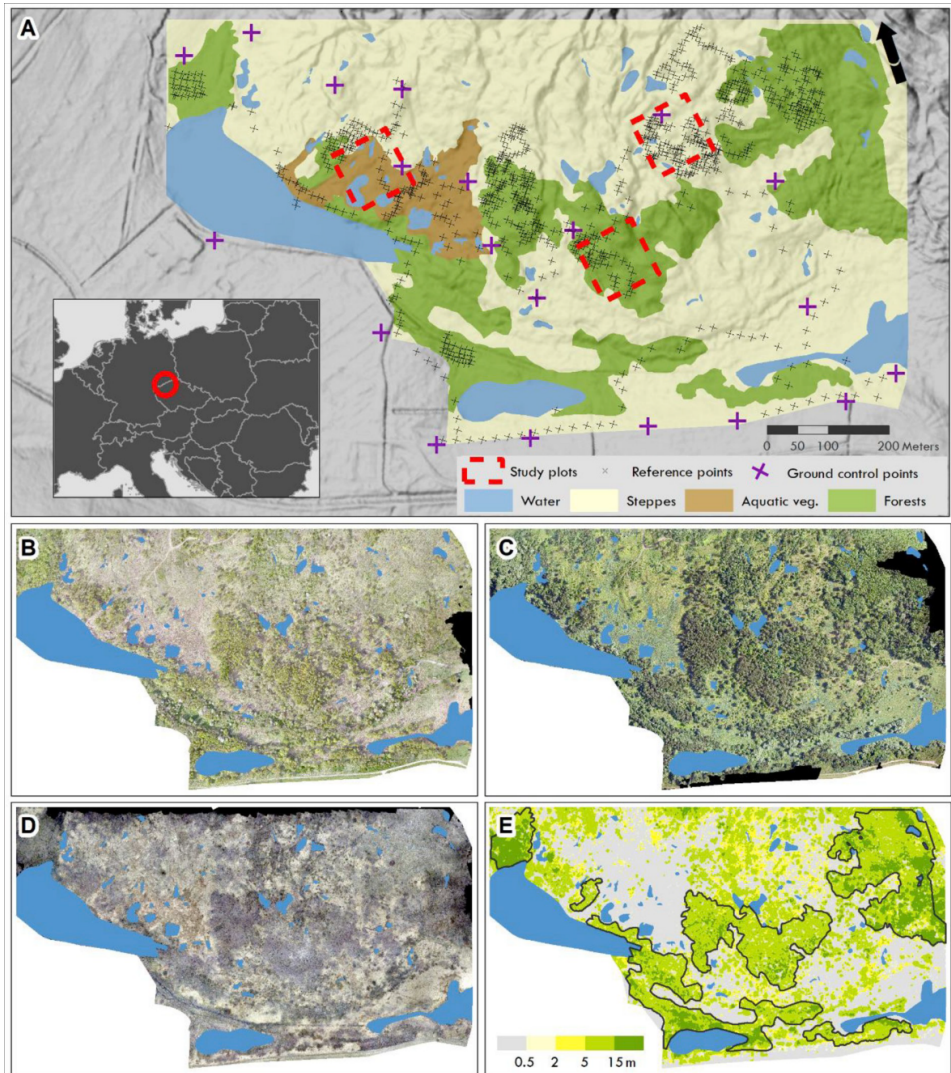


Figure 6.1: Study Area. (A) Hill-shaded terrain and location of the study area in the southern part of the Hornojřetínská spoil heap in the Most basin (north-west Bohemia, Czech Republic, $50^{\circ}34'N$, $13^{\circ}34'E$); (B) Spring orthophotomap; (C) Summer orthophotomap; (D) Winter orthophotomap; (E) Canopy height model. The study plots were used for visual comparison of DTMs, see Fig. 6.4.

The DTM generation is however affected by vegetation cover and the prospects to acquire accurate DTMs under dense vegetation canopies are limited. Spoil banks are usually covered by heterogeneous vegetation, which further complicates the use of photogrammetric methods.

Negative effects of vegetation on building of DTMs have been reported for various types of environment and vegetation cover. Forested areas are among the most challenging environments and failure to record a single ground point in such areas is not uncommon. For this reason, recent studies on the use of photogrammetric methods in forests mostly focus on partially open canopies. For example, [Kachamba et al. \(2016\)](#) derived a DTM from UAV imagery in order to estimate biomass at miombo woodlands. [Jensen and Mathews \(2016\)](#) showed that in a woodland ecosystem in Texas, SfM DTM provided a suitable representation of the bare ground under a vegetation cover (compared to LiDAR-derived DTM). More recently, [Tomaščík et al. \(2017\)](#) assessed the quality of a DTM under temperate broadleaf and mixed forests derived from UAV imagery with different level of canopy openness.

The obvious advantage of LiDAR is the ability of the pulses to penetrate through gaps in vegetation canopies and registering multiple returns representing both canopy and terrain. Many studies concentrated on the accuracy of LiDAR-derived DTMs in dense forest environments that might be difficult to penetrate even for LiDAR pulses, such as tropical forests (e.g. [Clark et al., 2004](#)) or temperate coniferous forest (e.g. [Reutebuch et al., 2003](#)). Only few studies, however, concentrated recently on temperate deciduous forests, which are among the principal canopies in our study. For example, [Aryal et al. \(2017\)](#) evaluated a DTM accuracy in temperate forests of Bavarian forests national park, [Balenović et al. \(2018\)](#) in an oak forest in Central Croatia, and [Simpson et al. \(2017\)](#) in mixed deciduous woodland in northeast England.

In the case of deciduous forest stands, a promising strategy to generate accurate DTM is to use images acquired under leaf-off conditions – an approach that has been only scarcely tested for photogrammetric methods ([Dandois and Ellis, 2013](#); [Ni et al., 2015](#); [DeWitt et al., 2017](#)) but commonly used for ALS data acquisition (e.g. [Hodgson et al., 2005](#)). Bare ground is clearly visible on the leaf-off imagery and the DTM accuracy similar to that derived over non-vegetated surfaces can

be therefore expected; however, leaf-off imagery may include complex shadowing and branch patterns and the quality (and extent) of the terrain visibility strongly depends on the density of forest stands.

The general aim of this study was to assess the value of photogrammetrically and LiDAR-derived data for characterizing a post-mining site. We acquired ALS data during summer (leaf-on period) and UAVborne imagery during different seasons (summer, spring, winter) and we (1) assessed the character of the generated point clouds with emphasis on the ability to capture bare earth and compared results yielded by both methods; (2) assessed whether the accuracy of SfM-derived DTMs can be improved by acquisition of images under leaf-off conditions and hence potentially used in combination with leaf-on conditions to estimate vegetation cover characteristics; and (3) evaluated the influence of vegetation cover (aquatic vegetation, steppes, and forests) on the DTM quality.

6.2 Materials and Methods

6.2.1 Study area

The present study was conducted on an area of 61 ha located in the southern part of the Hornojiřetínská spoil heap in the Most basin (northwest Bohemia, Czech Republic, 50°34′N, 13°34′E, Fig. 6.1). The spoil heap's elevation ranges from 220 m to 280 m above sea level. Due to plans to mine the underlying coal seam in the future, this part of the Hornojiřetínská spoil heap has never been technically reclaimed. The terrain morphology has remained rugged as a result of heaping that has formed a typical undulated terrain and consequently heterogeneous vegetation (e.g. Doleřalová et al., 2012; Frouz et al., 2018). The vegetation is in a late succession stage 35–50 years after heaping and consists of aquatic vegetation in terrain depressions (e.g. *Phragmites australis*

and *Typha latifolia*), steppes (low vegetation, especially *Calamagrostis epigejos* and *Arrhenatherum elatius* with scattered shrubs and trees, for example *Sambucus*, *Rosa*, *Betula*, *Crataegus*), and forests. Three forest types are present in our study area; homogenous plantations of even-aged growth of European ash (*Fraxinus excelsior*; eastern part of the study area), spontaneously grown forest dominated by Birch (*Betula pendula*; central part of the study area), and mature forests of Willow (*Salix spp.*) and Alder (*Alnus spp.*) (western part of the study area; Tab. 6.1, Fig. 6.1).

6.2.2 ALS and UAV image data collection

Airborne LiDAR data was collected over the study area in May 2017 using a remote sensing platform FLIS (The Flying Laboratory of Imaging Spectroscopy) (Hanuš et al., 2016). Although the system is equipped with a Riegl LMS-Q780 full-waveform laser scanner, we used only discrete return data. The scanner has a rotating polygon mirror and scans in parallel lines. The scan field of view is 60° and the wavelength is 1064 nm. Flights for data collection were conducted at 1030 m above ground with a velocity of 110 knots (ground speed) and with 55% flight line side overlap, which provided the average density of 7.7 points per square meter.

A home-assembled UAV consisting of an Easy Star II airframe by Multiplex and 3DR Pixhawk autopilot equipped with a Nikon Coolpix A camera (28 mm prime lens with f/2.8) was used for the series of flights (in different phenological conditions) over the study area. Hereafter, we refer to these three flights as Winter (11 March 2017 – leaf-off), Spring (29 April 2016 – partly leaf-on), and Summer (1 July 2016 – leaf-on) flights. Parallel flight lines were set to acquire an image overlap of 85% and sidelap of 65%. Approximately 1000 images were taken during each survey from an average flight altitude of 100 m above ground level,

resulting in a 3 cm ground sampling distance. The camera settings were manually set to ISO 400 and shutter speed priority 1/1250 s.

Table 6.1: General characteristics of the study area. Maximum, mean and standard deviation of height are calculated from a LiDAR derived pit free Canopy Height Model (LiDAR data were collected in May). Other characteristics are calculated directly from LiDAR classified point cloud. Canopy cover is calculated as the number of first returns above breast height (1.37 m) divided by the number of all first returns. Density of ground, shrubs and trees are number of returns in each height interval divided by total number of returns.

Vegetation type	Area	Canopy	Height [m]		
	[ha]	cover [%]	Max.	Mean	Std. dev.
Aquatic	3.4	4	16.5	0.5	94.4
Steppe	38.5	25	27.1	3.6	69.4
Forest	19.0	63	29.4	11.5	37.5

Vegetation type	Density [%]			
	Ground and low vegetation	Shrubs	Low trees	High trees
	(< 0.3 m)	(0.3–3 m)	(3–15 m)	(> 15 m)
Aquatic	94.4	2.5	3.0	0.0
Steppe	69.4	7.7	22.1	0.8
Forest	37.5	4.4	47.2	10.9

6.2.3 Ground control points and verification data survey

Prior to UAV flights, 20 ground control points in the form of white square fibreboard targets (40×40 cm) with black round centre (15 cm in diameter) were distributed over the study area. The coordinates of the ground control points were surveyed using a Trimble GeoXR 6000 handheld differential GPS with a pole-mounted Zephyr 2 external antenna in the dual-frequency differential real-time kinematic (RTK) mode. It was connected to the CZEPOS permanent GNSS network and provided 2–4 cm horizontal and vertical relative accuracies.

The RTK GNSS survey was conducted in the study area on 28 March 2017 (leaf-off period) to locate reference points for DTMs evaluation using a Leica GPS1200 system. In order to quantitatively assess the effect of different vegetation canopies on DTMs' accuracy, the information about vegetation canopy (i.e., aquatic vegetation, steppes, and forest) was recorded for each surveyed point. Because collection of GNSS data under tall canopies was challenging even during the leaf-off period, a conventional, total-station survey was used in forested areas. All reference points were transformed into the Datum of Uniform Trigonometric Cadastral Network (S-JTSK; EPSG: 5514) and Baltic Vertical Datum - After Adjustment (Bpv; EPSG: 5705) coordinate systems. In total, 796 reference points were collected for this study (55 in aquatic vegetation, 311 in steppes, and 430 points in forests).

6.2.4 Point clouds processing and DTM generation

The LiDAR point cloud was processed using a proprietary software by Global Change Research Institute CAS, referenced to the local Datum of Uniform Trigonometric Cadastral Network and Baltic Vertical Datum – After Adjustment. The LiDAR point cloud was further processed using LAStools (lastools.org). LASnoise and LASground tools of the LAStools software were used to determine ground points. We tested several settings for LASground and visually assessed the resulting DTMs using hill-shaded terrain and the success of ground points identification in the most troublesome areas. Our final setting was as follows: step 4, bulge 1, spike 2.3, offset 0.1, and stddev 10.

The UAV-acquired images, along with positional data measured by the onboard GPS during the flight, were loaded into Agisoft Photoscan Professional version 1.2.4 (agisoft.ru) and used to generate a 3D point cloud. Agisoft Photoscan follows a common SfM–MVS workflow ([Smith et al., 2016](#)). First, the alignment algorithm iteratively refined external

and internal camera orientations and camera locations through a least squares method and generated a sparse point cloud. The alignment process was completed with the accuracy parameter set to ‘high’ and the pair pre-selection parameter to ‘disabled’. The accuracy setting ensured the use of the original image resolution while the ‘disabled’ setting of the pair pre-selection ensured the best image matching. The limit was set to 20,000 for key points (indicating the maximum number of points sampled within each image) and to 5,000 for tie points (the number of points used for image matching). Dense point clouds were built using a dense multi-view 3D reconstruction algorithm with a high reconstruction quality and mild depth filtering. Point clouds were georeferenced using ground control points in the same horizontal and vertical datum as LiDAR and exported into the LAS format (hereafter we refer to these point clouds as SfM_{SPRING}, SfM_{SUMMER}, and SfM_{WINTER}). Points representing the ground surface were identified using LAS Ground tool of the ArcGIS 10.4.1 software (ESRI, Redlands, CA, USA).

The identified ground points were used to create DTMs with a cell size of 1 m (hereafter, we refer to these point clouds as DTM_{SPRING}, DTM_{SUMMER}, DTM_{WINTER}, and DTM_{LIDAR}). We used a bin-average method, which calculates the elevation for each cell by assigning the average value of all points within that cell. Areas containing no ground points (voids, see below) were triangulated and linearly interpolated to determine their cell values. Water areas were manually vectorized over a winter orthophoto and removed from the analysis.

6.2.5 Comparison of LiDAR and SfM point clouds

Both LiDAR and SfM point clouds were compared by quantifying the overall point density, density of identified ground points, and percentage of ground points in relation to all points. Subsequently, point clouds were overlaid with a 1×1 m grid and the number of grid cells containing no ground points was calculated (termed the “void fraction”). The void

fraction represents areas that had to be interpolated in order to create a DTM. We also visually compared the point clouds with orthophoto maps for the three seasons (spring, summer, and winter) and through all assessed types of canopy (i.e. aquatic vegetation, steppes, and forest).

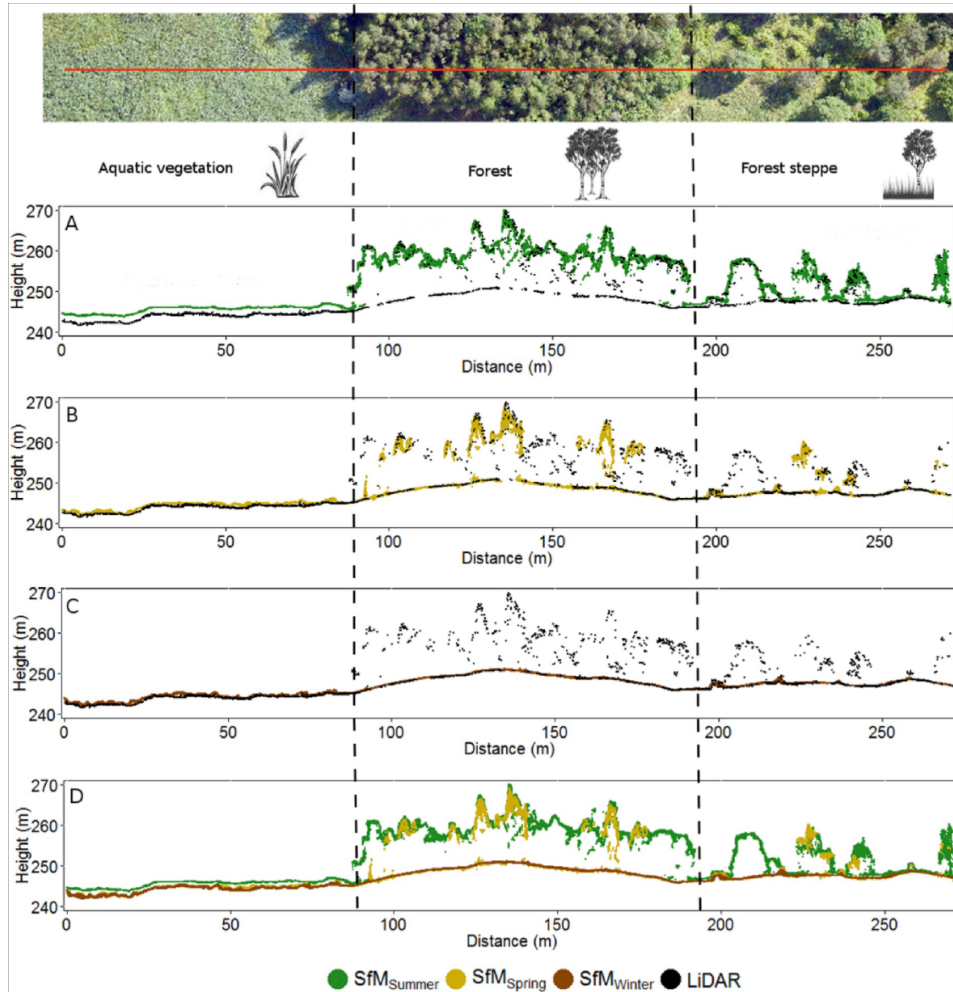


Figure 6.2: Structure of four point clouds (winter, spring, summer, and LiDAR) over three different environments (aquatic vegetation, forest, and forest steppe). Comparison of LiDAR and summer point cloud (A) demonstrates the known fact that dense vegetation prevents SfM ground detection. However, spring (B) and especially winter (C) point clouds show a good potential for detecting ground even under forest stands. The combination of all three SfM point clouds (D) allows the identification of both ground and vegetation canopy. The profile is 1 m wide.

6.2.6 DTM accuracy assessment

We used six accuracy measures to assess the vertical accuracy of DTMs generated from data collected using the SfM and LiDAR surveying techniques (i.e. maximum, minimum, mean, skewness, RMSE, NMAD). The GNSS survey, representing the most accurate data, was used as the reference dataset (true elevation) to evaluate the DTMs. We first calculated vertical differences among the 796 surveyed point elevations and the corresponding DTM_{SPRING} , DTM_{SUMMER} , DTM_{WINTER} , and DTM_{LIDAR} grid cell elevations. Descriptive statistics (i.e. maximum, minimum, and mean) were calculated for vertical differences. To evaluate the success of ground identification and vegetation removal, we calculated the Bowley’s coefficient of skewness. We also used the differences to calculate root mean square error (RMSE). We assessed the deviation from the normal distribution using histograms and Q-Q-plots (see Supplementary Materials Figs. S1–S4). As we detected a highly non-normal distribution (fat-tailed), we also calculated normalized absolute deviation (NMAD), a robust metric that is less sensitive to the presence of outliers (see [Höhle and Höhle, 2009](#)).

6.2.7 Analysis of vegetation cover effect on DTM accuracy

Inaccuracy in the generated DTMs results partially from an interpolation of cells containing no ground points. Therefore, to compare solely the accuracy of the two methods (and not of the interpolation algorithm), we identified cells containing ground points from both SfM and LiDAR surveys and performed a pairwise combination between DTM_{WINTER} and DTM_{LIDAR} using cell-by-cell subtraction. Being the best of all available SfM point clouds, only the winter point cloud was used for this evaluation as a representative of SfM models (Tab. 6.2; Fig. 6.2). Furthermore, we visually compared the results with respect

to prevailing vegetation type (aquatic vegetation, forest steppe, and forests) over the study area. To quantitatively evaluate the impact of vegetation on DTM accuracy for each vegetation type, we calculated the same descriptive statistics as mentioned above for individual vegetation categories (which had been recorded for all reference points during the field surveys).

Table 6.2: Summary of point cloud characteristics for the SfM and LiDAR datasets. Point density is shown as Mean \pm Standard deviation. Voids fraction is the percentage of cells (1×1 m resolution) not containing any ground point.

Dataset	Total points	Point density (points/sq. m)	Ground points
SfM _{WINTER}	196,103,451	333 \pm 57	167,631,147
SfM _{SPRING}	83,358,151	139 \pm 74	31,383,865
SfM _{SUMMER}	78,098,227	135 \pm 77	18,241,318
LiDAR	4,667,778	7.7 \pm 3.3	2,696,995

Dataset	Ground point density (points/sq. m)	Percent ground (%)	Void fraction (%)
SfM _{WINTER}	288 \pm 83	85.5	0.6
SfM _{SPRING}	61 \pm 30	37.6	15.8
SfM _{SUMMER}	56 \pm 27	23.4	45.1
LiDAR	5.3 \pm 3.0	57.8	15.6

6.3 Results

6.3.1 Comparison of point clouds

Point cloud characteristics varied substantially for the acquired datasets (Tab. 6.2; Fig. 6.2). Point densities acquired with SfM significantly exceeded densities of the LiDAR point cloud. Of the 196,103,451 SfM_{WINTER} points (i.e., under optimal conditions for terrain measurements), 85.5% were classified as ground points. In contrast, both SfM_{SPRING} and SfM_{SUMMER} (i.e., suboptimal conditions) resulted in

just 83,358,151 and 78,098,227 points, respectively, of which 37.6% and 23.4% were classified as ground points. Accordingly, when overlaid with a 1×1 m resolution grid, the number of cells containing no ground points was the highest for leaf-on conditions. For both total points and ground points, the identified point densities for individual flights differed significantly. The most evident difference was observed for the forest environment, for which no ground points were identified through the summer flight (Tab. 6.2; Fig. 6.3).

The density of photogrammetrically derived point clouds is much greater than that of the LiDAR point clouds but that greater point density does not necessarily indicate a greater accuracy. The reason is that only LiDAR can penetrate through the gaps in vegetation canopies and capture underlying canopy layers or ground elevation. It is evident that with the point density used in our study, there are many gaps in LiDAR ground coverage (Fig. 6.3G). By comparison, the density of ground points in the SfM_{WINTER} point cloud (Fig. 6.3E) is much higher. This is quantitatively shown in the percentage of void cells (“void fraction”) (Tab. 6.2). On the other hand, although the percentages of void cells are similar for LiDAR and SfM_{SPRING} point clouds, LiDAR ground points are more evenly distributed. Furthermore, the point density of SfM_{WINTER} was considerably greater (333 points per square meter) than those of SfM_{SPRING} and SfM_{SUMMER} (with fewer than 140 points per square meter).

6.3.2 Combination of point clouds acquired under leaf-on and leaf-off conditions

SfM_{SUMMER} (leaf-on conditions) recorded elevation for the top surface, which in this case means vegetation canopy (Fig. 6.2A). By comparison, SfM_{SPRING} (partly leaf-off conditions) and SfM_{WINTER} (leaf-off conditions) point clouds were able to capture ground elevation, albeit

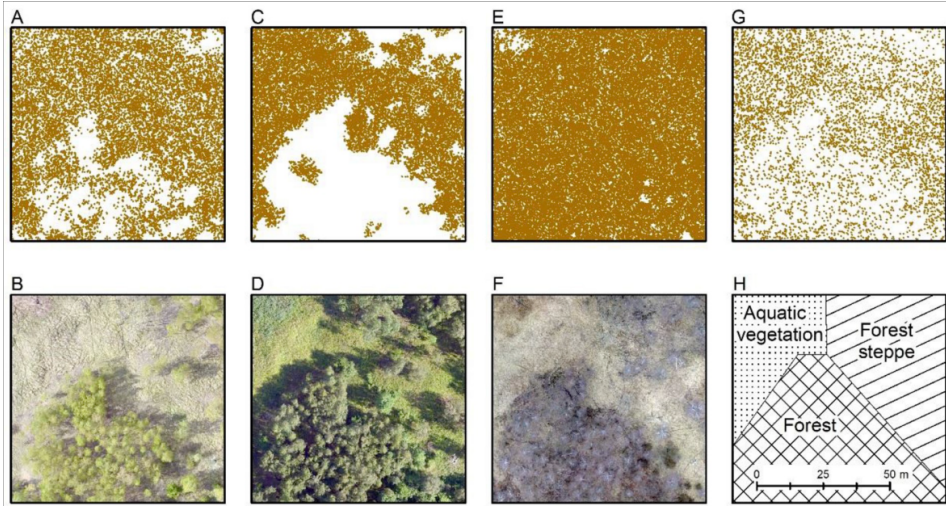


Figure 6.3: Visual comparison of ground point densities. All figures are from the same location. (A) Spring SfM point cloud and (B) orthophoto; (C) summer SfM point cloud and (D) orthophoto; (E) winter SfM point cloud and (F) orthophoto; (G) LiDAR point cloud; (H) approximate distribution of the three types of vegetation under study in the displayed area. No ground points were identified in the summer (leaf-on period) under the forest vegetation (C) while the ground is perfectly identified in the winter survey (E). Although ground points are identified in aquatic vegetation and forest steppes in summer (C), these may capture low vegetation (e.g. reed, grass) and do not accurately represent bare ground. See also Fig. 6.2.

with varying degrees of success in various studied environments (i.e. aquatic vegetation, forest steppe, and forest; Fig. 6.2B and C). Given the differences in the point clouds acquired in the different phenological phases, a combination of SfM_{SPRING} , SfM_{SUMMER} , and SfM_{WINTER} point clouds allowed us to record both vegetation canopy and ground elevation and resembled the structure of the LiDAR point cloud (Fig. 6.2D).

6.3.3 Comparison of DTMs

With RMSE of 0.19 m and of 0.12 m, respectively, DTM_{WINTER} and DTM_{LIDAR} achieved very similar results (Tab. 6.3). DTM_{WINTER} had a higher maximum and minimum error than DTM_{LIDAR} and exhibited

a slight positive skew. This higher frequency of positive errors suggests a persistent presence of above-ground features even in winter (see vegetation category comparison). In contrast, $\text{DTM}_{\text{SPRING}}$ and in particular $\text{DTM}_{\text{SUMMER}}$ achieved poorer results. $\text{DTM}_{\text{SUMMER}}$ had the highest mean error of 0.83 m and RMSE of 1.71 m. $\text{DTM}_{\text{SPRING}}$ had a mean error of 0.07 m and RMSE of 0.46 m (see Tab. 6.3).

6.3.4 The effect of the vegetation on DTMs accuracy

A high maximum positive error in $\text{DTM}_{\text{SUMMER}}$ indicates an existence of artefacts resulting from an unsuccessful filtering of the tree foliage. These have been successfully avoided in $\text{DTM}_{\text{SPRING}}$ and $\text{DTM}_{\text{WINTER}}$ due to the smaller amount of tree foliage (or absent foliage in case of $\text{DTM}_{\text{WINTER}}$) during data acquisition (Fig. 6.3B and F). A low minimum negative error is however present in $\text{DTM}_{\text{SPRING}}$ and $\text{DTM}_{\text{SUMMER}}$ indicating that some areas are below the ground. This is due to the inability to capture the undulated terrain over void areas without ground points that had to be interpolated. In addition to these void areas, low vegetation is often identified as terrain in summer and the $\text{DTM}_{\text{SUMMER}}$ therefore showed a positive error skew. Both $\text{DTM}_{\text{WINTER}}$ and $\text{DTM}_{\text{LIDAR}}$ tend to overestimate the terrain elevation in all vegetation categories (Tab. 6.4). While the quality of $\text{DTM}_{\text{LIDAR}}$ is relatively consistent across vegetation categories, $\text{DTM}_{\text{WINTER}}$ shows variable accuracy. Both methods achieved the best accuracy in forests (Fig. 6.4).

6.4 Discussion

The negative effect of the vegetation on DTM quality and overestimation of bare earth due to the inconsistent ability of passive methods

Table 6.3: Results of DTMs error analysis. Comparison of each DTM with 796 GNSS-gathered validation points. Bowley coefficient of skewness is used. NMAD is a normalized absolute deviation – a robust metric less sensitive to the presence of outliers than RMSE.

DTM	Maximum (m)	Minimum (m)	Mean (m)
DTM _{SPRING}	1.43	-6.23	0.07
DTM _{SUMMER}	12.88	-4.26	0.83
DTM _{WINTER}	1.39	-1.25	0.09
DTM _{LIDAR}	0.56	-0.48	0.05
DTM	Skewness (m)	RMSE (m)	NMAD (m)
DTM _{SPRING}	-0.002	0.46	0.15
DTM _{SUMMER}	0.21	1.71	0.58
DTM _{WINTER}	0.12	0.19	0.13
DTM _{LIDAR}	0.002	0.12	0.10

to penetrate vegetation canopies is a common observation (Dandois and Ellis, 2013; Tonkin et al., 2014; Lovitt et al., 2017). Both methods achieved best accuracy in forests, which is not surprising if we consider the vertical vegetation structure. The density of the most problematic, i.e., shrub, vegetation in forests is low (Fig. 6.4H, Tab. 6.1) while it is considerably higher in forest steppes (Fig. 6.4E). Although an effective use of UAVs in combination with photogrammetry in ecosystems dominated by shrub vegetation has been demonstrated by Cunliffe et al. (2016), the quality of acquired DTMs depends on the character of the vegetation and terrain. In our study area, the accuracy of DTMs in steppes was better for DTM_{LIDAR} (with RMSE of 0.12 m) but DTM_{WINTER} also achieved a very good result (with RMSE of 0.21 m). DTM_{WINTER} error was skewed slightly positively. Positive elevation errors can be attributed to the effect of short vegetation, which is often misclassified as ground by the filtering algorithms due to the small height difference between the vegetation and terrain (Meng et al., 2010). Another reason for such errors may lie in the presence of very dense shrubs that form an impenetrable flat area and resemble terrain (e.g. *Symphoricarpos albus*). Besides, for photogrammetrically derived

point clouds, we performed no manual processing of the data acquired under leaf-off conditions while both datasets acquired under leaf-on conditions required further manual processing as the tops of the dense canopies had been identified as ground. Distinguishing ground points from dense vegetation is particularly complicated for photogrammetric point clouds due to the very high densities, but its influence is only local and should be evident and easy to remove by manual evaluation.

LiDAR ground height estimation is particularly problematic for aquatic vegetation due to the weak laser backscatter caused by water absorption. As most LiDAR systems operate in the infrared region (like the one adopted in this study), free water surfaces and saturated soils dampen the returning signal (Hopkinson et al., 2005). As photogrammetry methods are based on images from passive sensors, acquired point clouds do not suffer from this issue and they may be better suited for DTMs acquisition (Kalacska et al., 2017). Aquatic vegetation stands however often persist during the winter, and our results show a large difference of RMSE 0.36 m versus 0.14 m between DTM_{WINTER} and DTM_{LIDAR} , respectively, for aquatic vegetation. DTM_{WINTER} error shows a positive skew due to stands of dry aquatic vegetation (e.g. *Typha latifolia* and *Phragmites australis*). These create dense vegetation stands completely obscuring the bare earth and making its detection impossible. On the other hand, the soil in the area of aquatic vegetation is not constantly saturated (and was not at the time of LiDAR acquisition) and LiDAR was therefore able to detect the bare earth. This is also evident from the cell-by-cell comparison of DTM_{WINTER} and DTM_{LIDAR} (Fig. 6.4). DTM_{WINTER} overestimated the bare earth in areas of aquatic vegetation compared to DTM_{LIDAR} . Recently, Lovitt et al. (2017) compared the performance of photogrammetric and LiDAR point clouds for characterizing terrain under peatland vegetation. In contrast to our study, they found photogrammetric point clouds to perform better than LiDAR point clouds in characterizing terrain under peatland vegetation. This difference is likely caused by differences

in the vegetation type within the study areas as the authors also reported significant decline in accuracy for the most densely vegetated areas (RMSE of 0.42 m, which is similar to our results). Luo et al. (2015) reported RMSE of 0.15 m for a LiDAR-derived DTM under short wetland vegetation, which is consistent with our result (RMSE of 0.14 m).

Table 6.4: Results of DTMs error analysis for SfM winter and LiDAR in three environments. Comparison of each DTM with 796 GNSS gathered validation points.

DTM	Mean (m)	Skewness (m)	RMSE (m)	NMAD (m)
<i>Aquatic vegetation</i>				
DTM _{WINTER}	0.32	0.21	0.36	0.12
DTM _{LiDAR}	0.07	0.03	0.14	0.11
<i>Steppes</i>				
DTM _{WINTER}	0.08	0.25	0.21	0.12
DTM _{LiDAR}	0.07	-0.06	0.12	0.09
<i>Forests</i>				
DTM _{WINTER}	0.06	-0.02	0.15	0.11
DTM _{LiDAR}	0.04	-0.003	0.12	0.11

Besides the evaluation of the digital terrain models, we also investigated the possibility of replacing costly LiDAR data with a combination of SfM data acquired from leaf-off and leaf-on imagery. Our results suggest that at least for some applications (e.g. calculation of vegetation structure characteristics often used to measure restoration success; Wortley et al., 2013; Shackelford et al., 2018), such a substitution may be possible. This is a significant improvement as studies usually relied on DTMs acquired from external sources, such as ALS (Lisein et al., 2013; Hawryło et al., 2017) or close-range terrestrial photogrammetry (Mikita et al., 2016). However, it is important to note that photogrammetric point clouds are inherently different from LiDAR point clouds, lacking detail in the lower canopy. In addition, the point density can be affected, for example, by flight parameters, camera settings, and environmental conditions such as foliage movement in the wind (Jensen and Mathews, 2016; Moudrý

et al., 2019). Consequently, the densities of point clouds combined from different acquisition periods could be unpredictably biased and their use likely limited to deriving simple variables (e.g. canopy height and canopy cover). It is however fair to point out that many of the above mentioned problems can also affect LiDAR data (e.g. Coops et al., 2007; Roussel et al., 2017).

Our results have shown that DTMs derived from UAV-borne images acquired during leaf-off period are comparable with a LiDAR-derived point cloud in a forest and only slightly poorer in forest steppes and in aquatic vegetation. This is consistent with recent findings by DeWitt et al. (2017) that satellite images acquired under leaf-off conditions can be used successfully to mitigate the effect of above-ground vegetation and to acquire DTMs of similar accuracy to that of LiDAR-derived DTMs. Similarly, Dandois and Ellis (2013) showed an improvement in a DTM generated under leaf-off conditions of a temperate deciduous forest; the benefit in their study was however not as significant as our results (they reported RMSEs from 0.73 m to 2.72 m). This is likely due to the differences in structure of the forests and thus of acquired point clouds. The species composition on the three deciduous forest plots (250×250 m) in their study was different (mainly American beech *Fagus grandifolia*, oak *Quercus spp.*, hickory *Carya spp.*, and tulip-poplar *Liriodendron tulipifera*) and the canopy was higher (mean canopy height between 20 m and 37 m; maximum height up to 42 m). In contrast with Dandois and Ellis(2013; see Figs. 2 and 7 in their paper) high vegetation was only residually present in our point clouds (Fig. 6.2). Besides, they used a hexacopter and flew only 40 m above the peak canopy height (our flying altitude was almost double that above the canopy). Given the differences in accuracy between our results and those acquired by Dandois and Ellis (2013), additional investigations covering a range of various forest stands are needed to investigate the accuracy, precision, and resolution of photogrammetrically derived DTMs under deciduous forests. In addition, although our results

indicate that natural conditions in winter appear promising, it must be noted that the operation of UAVs is restricted to specific conditions that must be met to acquire accurate terrain information. Meeting such conditions in winter may be problematic because of snow, wind, and relatively short duration of proper light conditions.

6.5 Conclusion

This work evaluated the quality of LiDAR and UAV-borne digital terrain models of a spoil bank that could be possibly used for various safety, remediation or ecological research purposes. We generated DTMs from images acquired under leaf-on and leaf-off conditions in three different environments (aquatic vegetation, steppe, and forest). Bare ground was identified using ground classification methods and then binned or interpolated over void areas to create DTMs at 1 m resolution. The point cloud derived from images acquired under leaf-off conditions was of the highest density. Vegetation artefacts were more successfully removed by the filtering procedure for leaf-off point clouds than for leaf-on point clouds and the identified ground points covered almost the entire study area. The accuracy of DTMs generated from leaf-off point cloud differed among the three environments. Overall accuracy was close to that of LiDAR-derived DTMs, with the best agreement in forests and the worst in the environment with aquatic vegetation. We suggest that accuracy of both methods is sufficient to monitor spoil banks terrain and provide information complementary to that acquired by more traditional methods. However, careful consideration must be given to site conditions at the time of image acquisition because the accuracy of methods is highly dependent on the vertical vegetation structure. While airborne LiDAR is suitable for monitoring ground instability problems and mitigation measures for all seasons and vegetation structures, UAV imagebased photogrammetry can be used successfully in steppes and deciduous forest stands only under leaf-off

conditions. The greatest advantage of the methodology described in this paper is that leaf-off images allow accurate detection of ground surface and, therefore, DTMs that can easily be compared to any subsequent DTMs derived from photos taken at a later date; such a comparison could detect any potential terrain changes. In addition, the combination of UAV imagery from leaf-off and leaf-on periods can be potentially used to calculate vegetation structure characteristics for studying a susceptibility of slope failure or restoration success assessment. Further research should quantitatively assess the sensitivity of images acquired under leaf-off conditions to the various structures seen in deciduous forest stands.

Appendix A. Supplementary data

Supplementary data to this article can be found online at <https://doi.org/10.1016/j.apgeog.2019.02.002>.

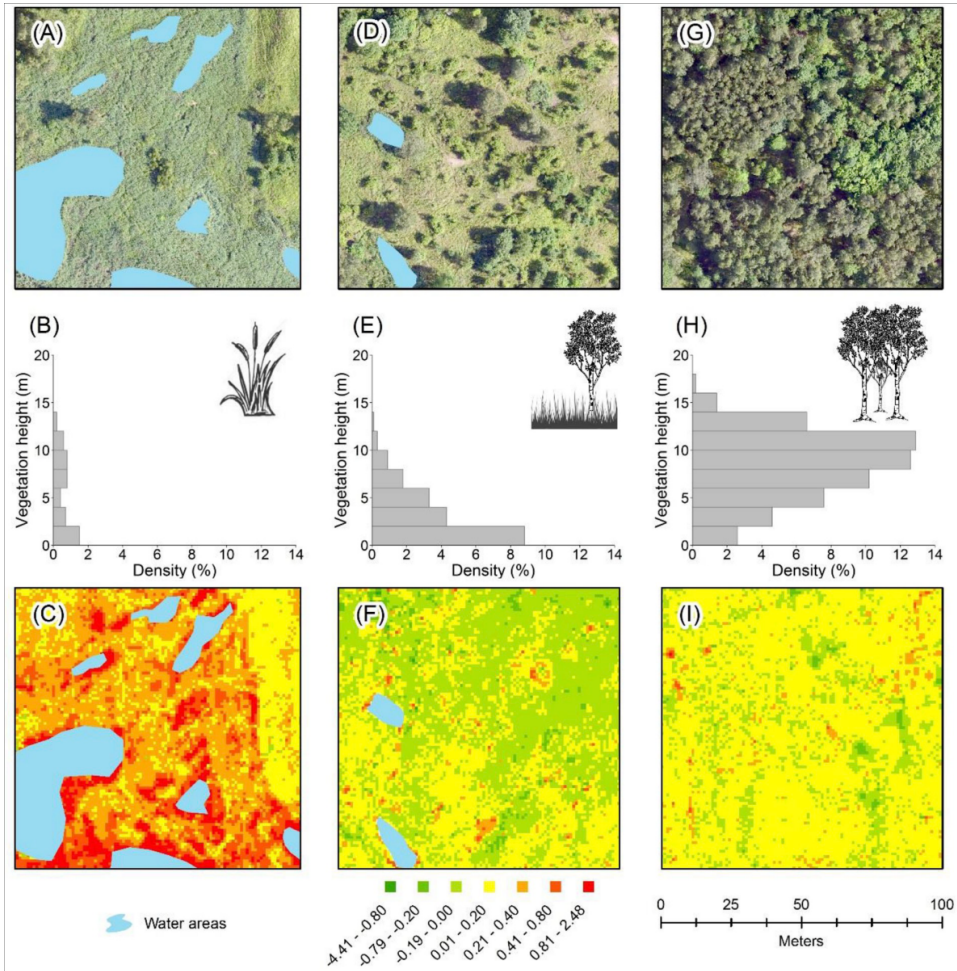


Figure 6.4: Orthophoto images of 1 ha plots inside study area at three different environments. (A) aquatic vegetation; (D) forest steppe; (G) forest. The above-ground height distribution of LiDAR returns (B, E, H), and a raster surface of vertical difference ($DTM_{WINTER} - DTM_{LIDAR}$) at 1 m resolution (C, F, I). The colour scale indicates the differences between DTM_{WINTER} and DTM_{LIDAR} , see legend. Red colour shows areas of overestimation and green colour areas of underestimation of DTM_{WINTER} compared to DTM_{LIDAR} . Note that overestimation occurs mainly in areas of aquatic vegetation around water areas. Density is calculated as number of returns in each bin (here 2 m) divided by the total number of returns. See Fig. 6.1 for location of the plots.

Chapter 7

Influence of Vegetation Canopies on Solar Potential in Urban Environments

Michal Fogl, Vítězslav Moudrý

Adapted from Applied Geography 66 (2016): 73–80

Publication metrics:

15 of 83 (Q1) rank in WOS category Geography

IF (2018) 3.068; AIS (2018) 0.858

12 times cited on WOS (2019 August)

Author's contribution: 60%

Abstract

Solar energy is clearly a promising option among the many available sources of renewable energy, and its market has seen outstanding growth. Careful evaluation to determine suitable locations for photovoltaic installations is needed, however, as their efficiency is highly dependent on exposure to sun. Especially in urban environments, quantifying the shadows cast by other buildings and vegetation canopies may be essential. In the present study, we used light detection and ranging (LiDAR) data and geographic information systems (GIS) to assess the influence of shading vegetation on solar irradiation estimates in five European towns. The fraction of annual solar irradiation lost to shading by existing vegetation ranged between 3% and 11%. The fraction lost was higher in winter and lower in summer. Due to greater incoming solar radiation in summer, however, more than 50% of annual loss was accounted for in summer. We suggest that at the broad scale of whole cities the influence of vegetation on rooftop solar potential estimates is negligible (especially in densely populated areas). Analyses which do not consider vegetation because of data availability nevertheless provide valuable insight into localities' solar potential.

7.1 Introduction

Use of energy from renewable sources is an important objective of the European Union's energy policy (see [Calvert et al., 2013](#) for review of progress in renewable energy mapping). According to EU Directive 2009/28/EC, the adoption of which established a common framework for production and promotion of energy from renewable sources, the EU should achieve a 20% share from renewable energy sources in total electricity consumption by 2020. Among many available sources of renewable energy, solar energy is clearly a promising option and its market has seen outstanding growth in recent years ([Devabhaktuni et al., 2013](#)). In some countries, however, incentives for employing photovoltaic (PV) installations has led to a situation wherein they consist predominantly of large ground-mounted facilities located on agricultural land, also referred to as solar farms ([Gallay et al., 2015](#)). Solar farms are often a preferred solution among investors due to their high economic returns, but their negative impacts are typically not considered. Solar farms jeopardize wide agricultural terrains and compete for limited land with other renewable energy sources, such as bioenergy feedstock systems ([Calvert and Mabee, 2015](#)). An adequate alternative to solar farms may be PV installations on rooftops in urban environments (e.g. [Santos et al., 2014](#)), and these, too, have been promoted by recent changes in support schemes for PV installations in some countries ([Hofierka et al., 2014](#)). Moreover, solar potential has been proposed as important design parameter in urban planning (e.g. [Kanters and Horvat, 2012](#)).

The estimation of rooftop solar potential in urban environments has been of considerable interest in recent years. At a very broad scale, the solar potential of building-integrated photovoltaics in EU member states is estimated to be more than 22% of expected European 2030 annual electricity demand ([Defaix et al., 2012](#)). Urban environments present challenges, however, due to the complex urban morphology. As

more homeowners and businesses investigate the feasibility of rooftop PV installations, there is growing demand for data and tools enabling more accurate prediction of incident solar radiation.

Such tools have long been implemented in the most frequently used GIS software: *r.sun* (Hofierka and Šúri, 2002) in GRASS and Solar Analyst (Fu and Rich, 1999) in ArcGIS. However, only with increasing availability of spatial data of adequate quality and extent, such as light detection and ranging (LiDAR) data, have these tools inevitably become common in the successful development of photovoltaic systems in urban environments. For example, solar potential has been estimated for the city of Bardejov in Slovakia (Hofierka and Kaňuk, 2009), a small parish in the city of Lisbon (Santos et al., 2014), and downtown San Francisco (Li et al., 2015). Moreover, many cities across the world have developed their own solar maps to support the decision-making process and identify locations suitable for PV installations. These typically consist of a user-friendly web-based interface that visually provides information about solar irradiation and instructs users about the costs and benefits of PV installations. To examine a list of existing solar maps, see Kanters et al. (2014) and Freitas et al. (2015). Given the complexity of factors influencing incident solar radiation, the most important factor in urban environments relates to shadowing effects. For example, Sarralde et al. (2015) have explored the relationship between urban morphology and the potential to harvest solar energy and found as much as a 9% increase in rooftop solar potential when the urban form is optimized.

In seeking suitable locations for photovoltaic installations, it is essential to quantify the shadows cast by other buildings and vegetation canopies. Vegetation is an important component of the urban environment, and it has a multiplicity of functions: reducing air and noise pollution, mitigating the urban heat island effect, and beautifying the urban environment (Smardon, 1988). However, it is also a source of shadow which may limit incident solar radiation. Moreover, it is often considered

only simplistically or even excluded from solar radiation modelling (Freitas et al., 2015). That is due mainly to a lack of appropriate data in developing countries (e.g. Araya-Muñoz et al., 2014). Only two studies to date have directly addressed the influence of vegetation shading on rooftop solar potential.

It is difficult to draw conclusions from these studies, because their results differ significantly. Levinson et al. (2009) found annual solar irradiation loss due to vegetation of as much as 8%, and Tooke et al. (2011) reported even 38%. Moreover, Tooke et al. (2011) limited their study to typical days (solstices and equinoxes) for reasons of computational efficiency and Levinson et al. (2009) derived shapes of tree canopies manually from orthophotos, which is a laborious and time-consuming process for larger areas. In the present study, we assess the importance of including vegetation data into models and evaluate its impact on monthly rooftop solar irradiation estimates while utilizing all the advantages of LiDAR data. Whereas previous studies have concentrated their efforts on parts of larger cities, mostly because of data availability, we rather selected four small European towns to encompass different urban morphologies.

7.2 Methodology

7.2.1 Study area

The study encompassed five small European towns (Fig. 7.1) located in the Czech Republic (Pec pod Sněžkou), Denmark (Kalvehave), Finland (Pellesmäki), Slovenia (Lukavci), and the Netherlands (Macharen). The locations differ in latitude, topography, and morphology. Those in the Czech Republic, Finland are representative of cities with sparse buildings, whereas those in the Netherlands, Denmark and Slovenia are representative of more developed cities with dense housing (Tab. 7.1). All study areas were cropped to be within a rectangle of 1 km², which

represents majority of towns' built-up areas and only distant buildings were removed from the analyses. Appendix A in the Supplementary Material shows maps of the study areas (Fig. A.1 – A.5). The workflow depicted in Fig. 7.2 was used to evaluate rooftop solar potential and estimate the influence upon it of shadowing vegetation.

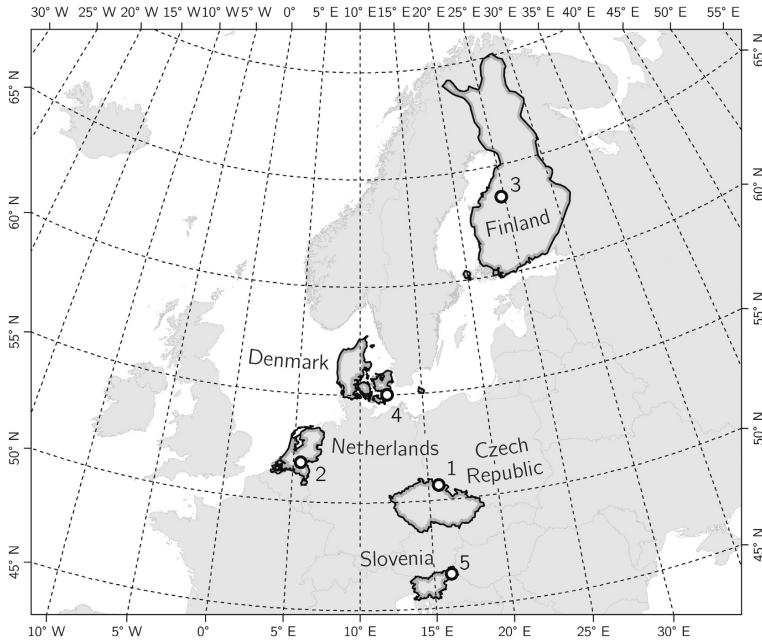


Figure 7.1: Locations of study areas within Europe.

7.2.2 LiDAR data

LiDAR is an active remote sensing device that consists of three components: a laser scanner, which emits and receives laser pulses; an inertial measurement unit (IMU), which detects changes in pitch, roll, and yaw; and the Global Positioning System (GPS). By recording the exact location of the sensor and the time it takes for each laser pulse to return, a detailed three-dimensional dataset stored as a point cloud is produced over a given area (Wehr and Lohr, 1999). LiDAR provides a highly accurate, fast, and easy way to collect data, and many state governments have collected high-resolution aerial LiDAR data for

various purposes. Some of them have made this data freely available so that everyone can benefit from their advantages. In this study, we used airborne LiDAR datasets which are freely available (Tab. 7.2).

7.2.3 LiDAR-derived footprint and DSM

A building’s footprint and digital surface model (DSM) are required for modelling rooftop solar irradiation. While many previous studies have had to compile heterogeneous sources of spatial data, which may have led to serious drawbacks with respect to data accuracy (Agugiario et al., 2012), we grasped the comprehensiveness of LiDAR and used it as a single reliable source. See study by Martín et al. (2015) for a review of existing studies that applied LiDAR data to assess solar potential in urban environments.

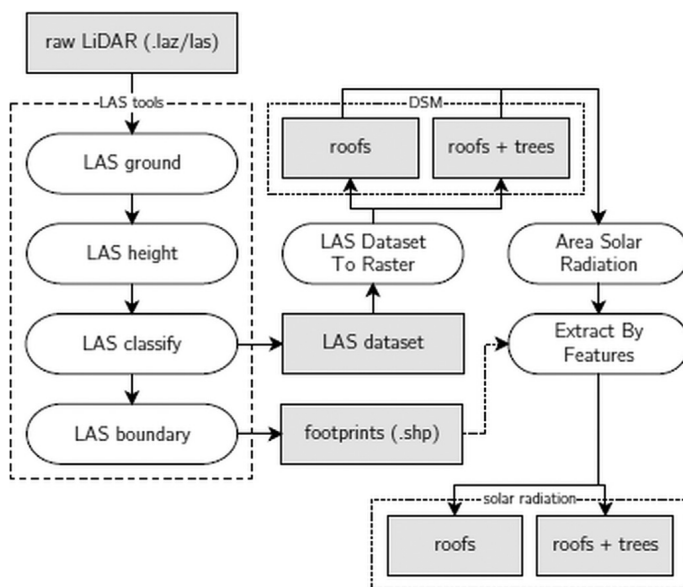


Figure 7.2: Workflow to calculate rooftop solar potential and estimate the influence of shading vegetation.

We used LAsTools to detect buildings and vegetation from LiDAR data (LAsTools, 2014). First, point clouds were classified into ground and non-ground returns (lasground) and the height of each return above

the ground was computed (`lasheight`). Second, discrimination was made between returns representing buildings versus vegetation (`lasclassify`). It is still challenging to accurately separate buildings from vegetation, however, and particularly when branches of trees are close to buildings' roofs. Thus, all point clouds were manually post-processed (`edited`) and errors corrected.

To model potential solar irradiation, building footprints should represent most accurately the outlines of the building roofs. There exist several approaches for acquiring building footprints. These can be acquired from cadastre data (Esclapés et al., 2014), manually digitized from high resolution orthophotos (Hofierka and Kaňuk, 2009), or derived directly from LiDAR (Tooke et al., 2011). Manual digitization is a laborious process and cadastre data often suffer from inaccuracies (Agugiaro et al., 2012). Direct generation of building footprints from classified LiDAR data, as done in this study, is a straightforward method. Boundary polygons that enclose all points representing a particular roof were created using `LAStools` (`lasboundary`) and then simplified by 'Simplify Polygon' and then 'Simplify Building' tool in ArcGIS 10.2 (ESRI, 2014).

DSMs are 2.5D representations of the Earth's surface including all objects on the ground (e.g. buildings, vegetation). The term 2.5D refers to a model that is embedded in three dimensions (3D), but is not able to represent all 3D shapes, such as caves and overhangs. This is a major drawback when calculating incident solar radiation. In order to determine the effect of vegetation canopies on the amount of incident radiation, we created two DSMs: (1) vegetation included, and (2) vegetation excluded. Both DSMs were derived from LiDAR at a spatial resolution of 0.5 m. The first raster, which represents the actual situation with vegetation, was created using the complete LiDAR point cloud. The second represents a hypothetical situation without the vegetation, and for its creation points classified as vegetation were excluded. We used simple conversion whereby the maximum elevation value of points found within a cell is assigned to the cell.

Table 7.1: Summary of study areas and their morphological characteristics.

<i>General characteristics</i>					
Country	CR	NL	FI	DK	SLO
Location	Pec pod Sněžkou	Macharen	Pellesmäki	Kalvehave	Lukavci
Latitude	50.70	51.80	62.76	55.00	46.54
Longitude	15.73	5.54	27.56	12.16	16.15
Population	630	615	516	617	662
<i>Vertical & horizontal distribution of buildings</i>					
Max. building height [m]	53.0	45.8	9.7	43.8	16.4
Avg. distance between buildings (nearest neighbour from centroid) [m]	37.7	16.4	31.6	15.7	24.2
Avg. building height [m]	7.5 ± 4.8	4.9 ± 2.1	4.3 ± 1.3	3.9 ± 1.6	4.9 ± 2.1
<i>Building geometry</i>					
Avg. building volume [m ³]	3097	1222	900	711	2987
Avg. building perimeter [m]	71.8	52.4	49.6	46.7	79.5
<i>Building density</i>					
Number of buildings	136	355	142	625	169
Plot ratio (total roof area divided by total area of neighbourhood)	0.039	0.056	0.022	0.074	0.053
Site coverage (share of total roof area) [%]	3.93	5.58	2.20	7.40	5.30
Total roof area [m ²]	39,260	55,758	21,656	74,229	52,635
Total area of location [km ²]	1.00	1.00	1.00	1.00	1.00
<i>Vertical & horizontal distribution of vegetation</i>					
Total vegetation area [m ²]	60,293	38,847	43,970	72,828	40,911
Max. vegetation height [m]	37.5	27.5	28.4	41.8	31.0
Avg. vegetation height [m]	12.0 ± 7.1	6.8 ± 3.7	9.6 ± 6.1	6.3 ± 3.8	7.6 ± 6.2

Maximum and average vegetation heights are calculated within a 30 m buffer distance to buildings.

7.2.4 Estimating the incident solar irradiation

According to Izquierdo et al. (2008), solar potential may be characterized in three hierarchical classes: (i) physical potential is the total amount of energy received from the Sun, (ii) geographical potential is

restricted to those locations where this energy can be captured, and (iii) technical potential takes into account the technical characteristics of the equipment used to transform the resource into electrical energy. Since our goal is to assess the influence of vegetation on incoming solar radiation, we focused, similarly as in previous studies (Levinson et al., 2009; Tooke et al., 2011), on the physical solar potential of the rooftops. For methods of assessing technical solar potential, see, for example, Santos et al. (2014).

To estimate monthly incident solar radiation, we used the upward-looking hemispherical viewshed algorithm developed by Fu and Rich (1999), which forms the backbone of the ArcGIS Area Solar Radiation tool (ESRI, 2014) and was more recently described briefly by Kodysh et al. (2013). We ran the model separately for each month and for both DSMs (with and without vegetation canopies). Monthly values of incident solar radiation were clipped to the building footprints and losses due to vegetation canopies were calculated by subtracting the corresponding DSMs from one another. To calculate the study areas' annual solar potential, 12 raster layers representing rooftop solar potential were summed and summarized over all roofs.

Table 7.2: LiDAR data characteristics.

Country (Year)	LiDAR dataset – available	Resolution [points·m ²]
CR (2012)	Provided by Krkonoše Mountains National Park Administration	5
NL (2011)	AHN2 (www.ahn.nl)	9
FI (2010)	MML Laserkeilaukset (tiedostopalvelu.maanmittauslaitos.fi/tp/kartta?)	0.5
DK (2014)	Danmarks Højdemodel (download.kortforsyningen.dk)	4.5
SLO (2014)	evode.arso.gov.si/indexd022.html?q=node/12	5.0

Viewsheds (angular distribution of sky obstruction) were calculated by searching in specified directions around each cell. In accordance

with our goal to estimate the shadowing effect caused by obstructing trees, we set a relatively high value of 104 calculation directions. Other topographical parameters, such as slope, aspect, latitude, and longitude, were automatically extracted from the DSM. For the estimation of incoming diffuse solar radiation (skymap), we assumed uniform sky when radiation was the same from all sky directions. Monthly values for transmissivity were obtained from the Langley Research Center Atmospheric Science Data Center (eosweb.larc.nasa.gov/sse) and diffuse proportion was taken from PVGIS (re.jrc.ec.europa.eu/pvgis) (see tables B.1 and B.2 in the Supplementary Material, Appendix B). The sky size for the viewshed, skymap, and sunmap grids was set to 350×350 . These grids are upward-looking, hemispherical raster representations of the sky. The sunmap specifies apparent position of the sun as it varies through time (day and season). The day and hour interval for estimating the sunmap (amount of direct solar radiation) were left default 14 and 0.5, respectively (see [Kodysh et al., 2013](#) for further details).

The analyses were executed on a personal workstation with CPU Intel Core i5-4670 3.8 GHz, RAM 16 GB 1600 MHz, and GPU GeForce GTX 660 2 GB and resulted in 384 raster layers. The time required for estimating annual solar irradiation was approximately 34 h for each location.

7.3 Results

7.3.1 Annual solar potential and losses due to vegetation

Annual solar irradiation estimates differed between the two scenarios (i.e., DSMs derived with and without vegetation). As expected, the results show that average direct and diffuse solar irradiation modelled for

building rooftops are substantially reduced when vegetation is included in the input DSM. The results differed among study areas, however. The reduction in mean annual sum of global (direct and diffuse) solar irradiation was slightly greater for the sparsely populated cities of Pec pod Sněžkou and Pellesmäki and lower for Macharen, Kalvehave and Lukavci with dense housing. The estimated mean yearly sums of direct and diffuse solar irradiation for the building rooftops in the study areas are shown in Tab. 7.3.

7.3.2 Monthly changes in solar potential lost

Monthly solar irradiation estimates show an obvious annual cycle for all study areas, with lowest values occurring in December and then gradual increase to a peak in June. While the lost diffuse solar irradiation remained constant throughout the year, the loss in direct solar irradiation changed significantly – with higher values occurring in summer jointly with increasing solar irradiation. Incoming solar radiation lost due to vegetation was negligible in winter (up to $1 \text{ kWh m}^{-2} \text{ month}^{-1}$) and higher in summer (up to $16 \text{ kWh m}^{-2} \text{ month}^{-1}$). More than 50% of annual energy loss was accounted for in the summer months in Lukavci, and this was seen to increase with latitude to as much as 69% for Pellesmäki (see Fig. 7.3).

The fraction of solar radiation lost exhibits the opposite course during the year, however. Inasmuch as direct radiation decreases and shadow length increases with lower solar altitude, the reduction was greatest for winter months, when the sun has a low altitude and shadows are longest (Fig. 7.3). The fraction of monthly global solar irradiation lost to shading by existing vegetation was in the range of 5–11% for Pec pod Sněžkou (CZ), 3–7% for Macharen (NL), 9–20% for Pellesmäki (FIN), 5–9% for Kalvehave (DK), and 3–6% for Lukavci (SLO).

Table 7.3: Annual solar irradiation on rooftops (physical potential) in study areas and lost due to vegetation canopies.

Location	Global irradiation [kWh/m ²]	Direct irradiation [kWh/m ²]	Diffuse irradiation [kWh/m ²]
Pec pod			
Sněžkou	1043	469	575
Macharen	887	414	473
Pellesmäki	791	384	407
Kalvehave	879	445	434
Lukavci	2131	1110	1021
Location	Global irradiation lost [%]	Direct irradiation lost [%]	Diffuse irradiation lost [%]
Pec pod			
Sněžkou	5.83	3.84	7.45
Macharen	4.12	3.06	5.06
Pellesmäki	10.9	9.36	12.35
Kalvehave	5.58	4.15	7.05
Lukavci	3.45	2.31	4.69

Incoming solar irradiation values are maximum possible values without existing vegetation. Percent represent decrease caused by existing vegetation.

7.3.3 Comparison of estimated solar irradiation rasters

The differences in solar irradiance estimates for particular cells ranged approximately between 0 and 1500 kWh m⁻² year⁻¹. For most of the cells, however, differences were relatively low (less than 50 kWh m⁻² year⁻¹), especially, for densely build-up towns (Tab. 7.4). Erroneous values lower than zero usually appeared at roof edges or elements such as chimneys or dormers.

7.4 Discussion

Many cities across the world encourage the use of solar energy technologies in urban environments by providing web-based solar maps

(Kanters et al., 2014). However, successful deployment of photovoltaic installations in urban environments requires accurate data representing terrain, vegetation, and building structures in order to estimate the spatial distribution of photovoltaic potential in sufficient detail (Redweik et al., 2013; Santos et al., 2014).

Our results corroborate previous studies and confirm that shadows from vegetation may play an important role in determining the solar irradiation received by the roofs of buildings in urban areas. The average reduction in global solar irradiation was nevertheless surprisingly lower than we had expected in light of the results of another study at similar latitudes. Tooke et al. (2011) had estimated that trees on average reduce incoming solar irradiation by 38% for the district of North Vancouver (49°15'N). They had calculated solar irradiation only for single days represented by the summer solstice, winter solstice, and equinox. Given the seasonal variance in incoming solar radiation at higher latitudes, this may possibly have caused significant overestimation. Results similar to those of our study were obtained by Levinson et al. (2009), who found annual insolation losses of up to 8% caused by vegetation shading and predicted losses of as much as 14% after 30 years of vegetation growth in four California cities (32°N–39°N).

7.4.1 Temporal changes in shadowing effects

Our results have shown obvious seasonal changes in solar energy loss due to vegetation. It is important to note that the fraction of solar irradiation intercepted by vegetation is actually higher during winter months due to low solar altitude and thus long shadows cast by trees. From an annual perspective, the major energy losses (more than 50%) were determined in summer, due to the higher incoming solar radiation in that season (Fig. 7.3). Unfortunately, there is greater energy consumption in winter due to low temperatures and thus increased demand for heating. At lower latitudes, however, the highest energy

consumption is in summer due to demand for cooling (Levinson et al., 2009). In such areas, the shadowing effect of vegetation is also considered in reducing energy demand in buildings (Balogun et al., 2014). We suggest that the two effects should be considered equally when planting trees. Traditionally, photovoltaics have been installed with a view to maximum yearly energy production. According to Sánchez and Izard (2015), however, solar panels could alternatively be mounted in non-optimal orientations with potential benefit. These areas would produce lower amounts of energy, but their hourly production profiles could be shifted away from noon, thus enabling them to better match demand. This possibility may enable the proper balance in placing solar panels and trees to optimize buildings' energy consumption and production (Tooke et al., 2011; Kodysh et al., 2013). Moreover, consideration for the temporal mismatch in peak solar energy availability and electricity demand has recently become of considerable interest (e.g. Mavromatidis et al., 2015; Ramirez Camargo et al., 2015). Nevertheless, the negative effect of shadowing vegetation has yet to be studied jointly with electricity demand during the day. Given the usual peak electricity demand in early evenings, it is possible that when the temporal aspect is taken into account the negative influence of shadowing vegetation would increase.

7.4.2 Solar radiation models based on 2.5D

In the study by Tooke et al. (2011), vegetation overhanging roofs was most often classified as trees rather than buildings and available roof area was thus underestimated. Compared to their study, we slightly improved the methodology. Our method does not suffer from this bias, because, unlike Tooke et al. (2011), we classified buildings and vegetation in a three-dimensional LiDAR point cloud. We estimated solar radiation in 2.5D, however, and thus considered rooftops under overhanging parts of trees as completely shadowed. Aggregation of a

three-dimensional point cloud into a 2.5D raster inevitably results in a loss of information.

Furthermore, the simplistic modelling approach used in our study represents vegetation as a solid shadow-caster and neglects light passing through the canopies. In particular, seasonal loss of foliage from deciduous trees in winter may significantly decrease the amount of radiation intercepted by vegetation (Levinson et al., 2009; Tooke et al., 2011). Even though more appropriate algorithms exist that consider light passing through canopies (Tooke et al., 2012) or an environment's 3D character (Jochem et al., 2009), tools based on 2.5D raster data are still preferred due to their easy availability and less time-consuming and more user-friendly nature. See, for example, study by Boz et al. (2015) for a new method for locating suitable areas for PV systems. Moreover, most novel algorithms are currently inaccessible or not readily usable for those without specialized software or knowledge. It will take time for this to change, and for the time being 2.5D numerical radiation algorithms coupled with GIS will still be valuable tools enabling researchers to take into consideration most of the important factors influencing incoming solar radiation. Of course, not only algorithms (Zhang et al., 2015) but also input data influence the quality of estimated solar irradiation. Meanwhile, modelling uncertainties such as resolution (Ruiz-Arias et al., 2009; Zink et al., 2015), different input data (Agugiaro et al., 2012) and influence of positional error (Biljecki et al., 2015) have received very little attention in the existing literature. Potential source of error, in our study, is DSM quality, its resolution and edge effects that can lead to inaccurate slopes and aspects. Although we used highly accurate LiDAR data, small objects such as dormers and chimneys are difficult to identify and higher resolution DSMs are required (Zink et al., 2015).

7.5 Conclusion

In their comprehensive review, Freitas et al. (2015) recently noted that effort is needed to develop appropriate algorithms that enable modelling light passing through vegetation canopies. Although we agree with their suggestion, our study has shown that, at least on the broad scale of whole cities, the influence of vegetation on rooftop solar potential is not so influential as previously suggested (Tooke et al., 2011). We suggest that for decisions that need to know power potential over large areas (e.g. for planning purposes) vegetation canopies can be excluded from models. This is encouraging in view of the growing number of studies from the developing world where solar energy can solve electricity shortage problems (e.g. Gautam et al., 2015) and where studies often lack appropriate data to include vegetation canopies into their models (e.g. Araya-Muñoz et al., 2014). In our opinion, such data do provide valuable insight into a location's solar potential, but this is most likely very location-dependent and researchers should proceed with caution inasmuch as including such data leads to an unknown overestimate of solar potential. Finally, at a local scale, when an individual building's roof and areas of that roof suitable for PV installation come into consideration (e.g., web-based solar maps), then vegetation should always be included into any analysis.

Appendix A. Supplementary data

Supplementary data related to this article can be found at <http://dx.doi.org/10.1016/j.apgeog.2015.11.011>.

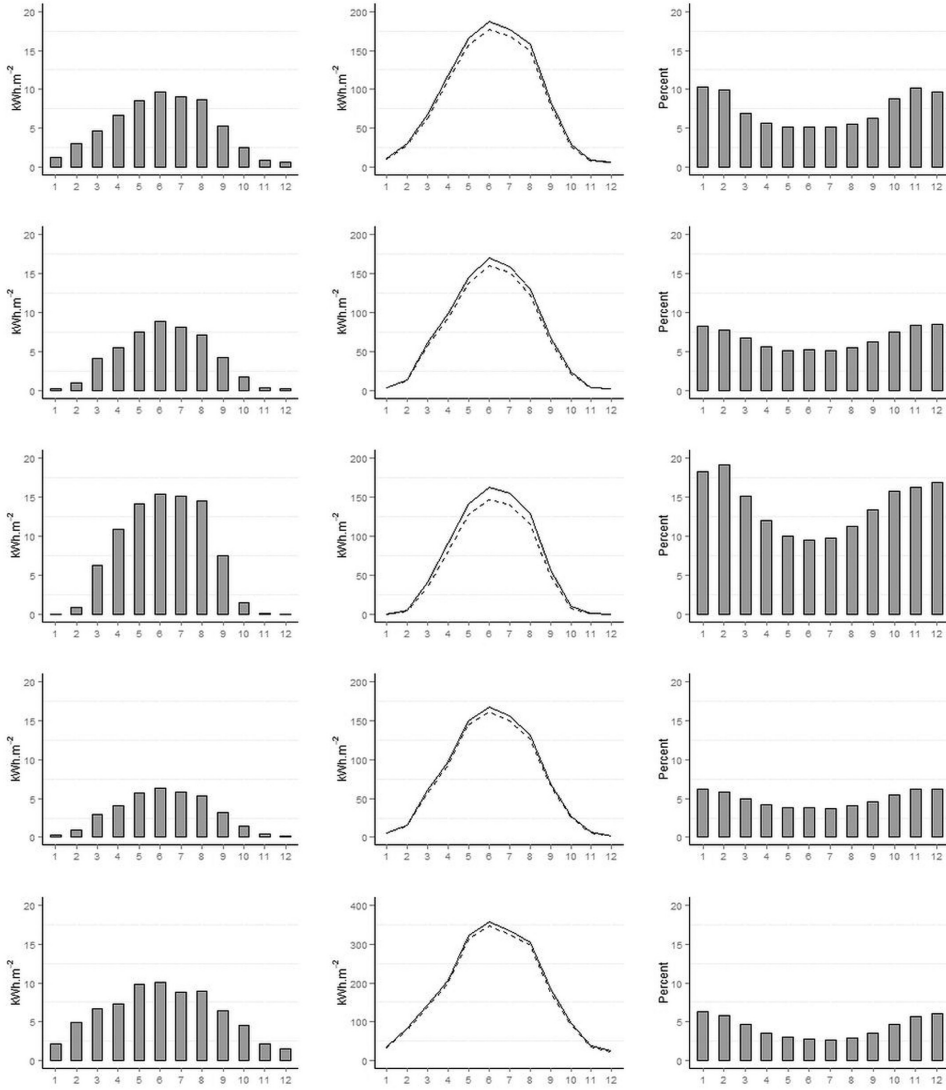


Figure 7.3: Estimates of monthly solar irradiation on rooftops and lost due to vegetation canopies. Rows represent different cities (from top to bottom: Pec pod Sněžkou, Macharen, Pellesmäki, Kalvehave, Lukavci). The left column shows solar irradiance lost due to vegetation in absolute values [$\text{kWh m}^{-2} \text{ month}^{-1}$]. The middle column shows estimates of monthly solar irradiance where the solid line represents the situation without vegetation and the dashed line that with existing vegetation. The right column shows the fraction of solar irradiance [%] lost due to vegetation canopies from monthly irradiance estimates. Note that the fraction lost is highest in winter months (right column), when the actual energy loss is relatively low (left column).

Table 7.4: Comparison of estimated solar irradiation rasters. Difference in global annual solar irradiation estimates based on models with and without vegetation.

Interval [kWh m ⁻² year ⁻¹]	Czech Republic (Pec pod Snezkou)		Denmark (Kalvehave)		Finland (Pellesmäki)	
	Num. of cells	Relative freq. [%]	Num. of cells	Relative freq. [%]	Num. of cells	Relative freq. [%]
< 0	596	0.38	3356	1.13	522	0.60
0–50	97824	62.31	226093	76.11	41781	48.21
50–100	28787	18.34	30688	10.33	19554	22.56
100–150	13492	8.59	12454	4.19	9688	11.18
150–200	7799	4.97	6885	2.32	5610	6.47
200–250	3680	2.34	4290	1.44	3424	3.95
250–300	1930	1.23	2843	0.96	2080	2.40
300–350	1037	0.66	2152	0.72	1196	1.38
350–400	774	0.49	1642	0.55	946	1.09
400–450	454	0.29	1239	0.42	698	0.81
450–500	231	0.15	1092	0.37	389	0.45
> 500	382	0.24	4327	1.46	776	0.90

Interval [kWh m ⁻² year ⁻¹]	Netherland (Macharen)		Slovenia (Lukavci)	
	Num. of cells	Relative freq. [%]	Num. of cells	Relative freq. [%]
< 0	3629	1.63	1975	0.94
0–50	181535	81.39	174596	82.92
50–100	17152	7.69	17409	8.27
100–150	7419	3.33	6203	2.95
150–200	4067	1.82	3074	1.56
200–250	2262	1.01	1823	0.87
250–300	1526	0.68	1269	0.60
300–350	1096	0.49	870	0.41
350–400	837	0.38	570	0.27
400–450	633	0.28	477	0.23
450–500	559	0.25	371	0.18
> 500	2332	1.05	1929	0.92

Interval values represent increase in annual solar irradiation for particular cells when existing vegetation is excluded. Note that the cell resolution is 0.5 m.

Chapter 8

Discussion and Summary

The presented dissertation thesis consists of one submitted and three published research studies focused on the topic of the use of laser scanning data in the field of environmental research, especially where vertical vegetation structure is concerned. The studies presented in the previous chapters deal with topics related to the entire scope of airborne laser scanning, from the data acquisition through the fundamental data processing, up to the applications. Namely, the titles of the studies are as follows: **Study I:** Suitability, characteristics, and comparison of an airship UAV with LiDAR for middle size area mapping; **Study II:** Assessment of LiDAR ground filtering algorithms for determining ground surface of non-natural terrain overgrown with forest and steppe vegetation; **Study III:** Comparison of leaf-off and leaf-on combined UAV imagery and airborne LiDAR for assessment of a post-mining site terrain and vegetation structure: Prospects for monitoring hazards and restoration success and **Study IV:** Influence of vegetation canopies on solar potential in urban environments. The following part of the dissertation thesis includes comments on the individual research topics, conclusions and summary of the thesis as well as suggestions for the future research in this field. As the full discussion and conclusions form a part of the published papers detailed in Chapters 4-7, the following chapter will only summarize the findings and provide author's comments on the individual research topic and the discussion on how the aims of dissertation were met.

8.1 Conventional Platforms versus UAVs for LiDAR Data Collection

“How to acquire LiDAR data?”

The use of UAVs as carriers for airborne laser scanning instead of conventional aircraft is a current research topic, which can be demonstrated by the high number of published scientific studies (e.g. Nagai et al., 2009; Lin et al., 2011; Wallace et al., 2012; Tulldahl and Larsson, 2014; Wallace et al., 2014; Khan et al., 2017; Guo et al., 2017; Liu et al., 2018). From the economic point of view, it is a landscape mapping method with a great potential for many fields of application. Conventional ALS scanning is still unavailable for many applications due to its high costs and researchers thus often have to rely on existing LiDAR datasets that are often not entirely suitable for the particular purpose from the perspective of point density, mapping accuracy or other characteristics even where such data are available. At many locations, however, no LiDAR data are available or are outdated and do not correspond with the current reality anymore. Besides being cost-effective for many applications, another advantage of UAVs is the creation of very high-density point clouds.

In **Study I**, the use of a very unorthodox UAV was examined, namely an autonomous airship (AMA) instead of the more commonly used multicopter. It is however not the first autonomous airship use in the field of laser scanning, see Pan et al. (2015). The LiDAR system for use on an airship was originally developed at the Czech University of Technology primarily for laser scanning in the field of geodesy for civil engineering; **Study I** was its first application in the field of environmental research. An industrial laser scanning unit was used instead of a commercial LiDAR system customized for UAV. At present, some specialized types of lightweight LiDAR systems (e.g. RIEGL, 2019;

Velodyne, 2019) have come to the market; it might be therefore expected that such systems will become increasingly available in the coming years.

Study I is also the only one utilizing AMA UAV as a carrier of a home-assembled LiDAR system. This obviously comes with certain risks, especially when comparing an experimental or home-assembled mapping carrier with a well-established commercial UAV, especially from the perspective of the possibility of any failure during data collection or with optimization and calibration of the entire system. Unfortunately, both these risks manifested themselves during the data collection. The maximum accuracy of the UAV AMA system was thus characterized by the vertical height standard deviation of approx. 10-16 cm and the maximum point cloud density of 15 points/m², although the preliminary mapping tests indicated a better accuracy (Koska et al., 2014). This was most likely caused by the unfortunate fact that calibration of the LiDAR system could not have been properly completed due to changes in UAV legislation because the UAV flights over inhabited areas (which included the test site) were banned. In all, three mapping flights were performed, however the data were successfully acquired during the last one only. Moreover, during the last mapping the airship engine failed and as a result, the airship went out of control and crashed. This incident resulted in irreparability of the system and, in effect, prevented the use of the AMA UAV for mapping of the full area. We therefore had to acquire ALS data with conventional aircraft in the end for use in **Studies II** and **III**.

Conventional ALS is a widely used technique and point clouds derived in this way form a basis for most existing studies. ALS data collection is typically not performed by researchers themselves but the data is either purchased from general purpose scanning or, if need be, ALS is custom ordered from the providers of this service. Especially where larger areas are concerned, this represents basically the only viable option, although such custom ALS is very costly. In **Studies II** and **III**, ALS data acquisition was ordered and performed using a commercially

available LiDAR system, namely Riegl LMS-Q780. This LiDAR system provides full waveform data, however we only used discrete return measurements for **Studies II** and **III**. This therefore offers further research opportunities. The average of the resulting point cloud was 8 points/m².

Purchase of existing ALS data is obviously a less costly option than that of custom ALS data acquisition. There are even freely available datasets that are often provided by national authorities. It is however necessary to point out that such datasets are not always suitable for the purposes of the research; they are usually not up to date and do not come with the data density, detail level and accuracy needed for some studies. In **Study I**, we used a national dataset of the Czech Republic that can be purchased. In **Study IV**, we used several freely available LiDAR datasets of various densities and accuracies.

8.2 Comparison of UAV Imagery and ALS for Evaluation of DTM and Vegetation Structure

“Is LiDAR so good for 3D mapping?”

In the previous chapter, we discussed platforms for collection of LiDAR data with emphasis on UAV platforms. UAVs are however nowadays very popular for imagery acquisition by optical cameras. As mentioned before, ALS is a very costly method of data collection and UAV LiDAR systems are not widely used, in view of which the UAV imagery appears to be a perfect alternative to ALS. ALS still retains one significant advantage over methods extracting vertical information from optical imagery – it can provide a relatively detailed structure of the terrain (even under a canopy) and vegetation, which is difficult to acquire from

optical imagery. It is however not always possible to acquire LiDAR data and when this is true, photogrammetry/computer vision methods in combination with UAV imagery come into play. SfM/MVS data processing results in a data structure similar to that of LiDAR data, i.e., a point cloud. The greatest difference lies in the method of extraction of the individual points – while it is a direct measurement of individual points in LiDAR, the SfM/MVS point clouds are acquired indirectly after a reconstruction of a 3D scenery from photos. Data processing of both types of point clouds is however performed in a similar way. The most common final products acquired from such point clouds then include DSMs or, in case of LiDAR, also DTMs, information about vegetation heights (canopy height model) or about vegetation structure. To a limited degree and under the right circumstances (e.g. if imagery is acquired in the leaf-off period in deciduous forests), even SfM/MVS methods may yield usable DTM and CHM; in comparison to LiDAR, however, the vertical structure of vegetation cannot be captured.

In **Study I** and **Study III**, we compared data from laser scanning (ALS, AMA) with fixed wing UAV imagery. Imaging was performed using a home assembled UAV equipped with a compact digital camera. In all, three mapping flights have been performed (winter, spring, summer). Results of the comparison confirmed that UAV imagery yields the best results on a bare, vegetation-free terrain (Tonkin et al., 2014; Lovitt et al., 2017). At sites with the vegetation occurrence, an aforementioned problem with permeability of the vegetation arose. However, it was still possible to capture terrain where the canopy was not continuous. In addition, even where the vegetation was dense, it was possible to capture terrain when using proper timing (see Tomaščík et al., 2017). The best results of terrain capture were thus achieved during the winter imaging (in the leaf-off period); this however also led to a major failure in capturing the tree heights. This problem was nevertheless resolved by combining the imagery from the leaf-on and leaf-off period as the full vegetation canopy was completely captured

during the leaf-on period. Such a combination of two image acquisitions at different time points therefore provides a potential substitution for ALS scanning. In **Study III**, we demonstrated that although the highest vertical accuracy was achieved as expected by ALS, winter UAV imagery achieved comparable accuracies, especially in the deciduous forest stands. When comparing ALS and UAV suitability, it is however obvious that to be able to replace ALS with SfM imagery, at least two flight missions must be performed to capture the vegetation structure. In winter, there is also a risk of snow cover confounding the results.

8.3 Filtering Algorithms for Processing Laser Scanning Data

“What to do with the raw LiDAR data?”

LiDAR data, or rather point cloud processing in general, is an important step in creating final products (DTM, DSM, CHM, . . .). A fundamental part of processing of the point clouds is the ground points filtering as a way of determining ground points (and, hence, the terrain), laying out a basis for further ALS data processing. The used algorithms depend largely on the type of the mapped landscape as each type of surface has its specifics. As the landscape is typically quite complex and consists of mixed landscape types, it is not possible to use a universally applicable method of ground points filtering yielding satisfactory results. There is a multitude of filtering algorithms utilizing different approaches for specific types of ground structures (Meng et al., 2009; Susaki, 2012; Rashidi and Rastiveis, 2017). Most filtering algorithms have various settings options. A common user however often has no way of finding his/her way through the settings and to choose the perfect filtering method and its optimal parameters. A typical example of a landscape type where identification of ground points is very important are forests.

As LiDAR data are frequently used for obtaining understory topography, which is then in turn used for creating DTMs and, in effect, CHMs, which are especially used in forestry, the choice of the filtering method is crucial.

In **Study II**, LiDAR filtering algorithms implemented in various programs were compared. Emphasis was laid on open source solutions; however, commercial “*black box*” algorithms were also included in the study. It is usually quite difficult to understand the way the proprietary “*black box algorithms*” operate as well as to categorize the filtering methods as the software producers often offer no information about the used algorithm (e.g. ArcGIS Classify LAS Ground tool by ESRI). Many black box solutions offer no possibility of customizing predefined settings, either. The accuracy of the ground filtering is then predominantly dependent on the character of the terrain and the vegetation, which has been reported in several studies (see e.g. [Korzeniowska et al., 2014](#); [Montealegre et al., 2015](#)). The use of such algorithms is especially problematic where low vegetation is present. At such sites, a confused point structure including noise and returns from both the ground and low vegetation with small vertical differences appears. Our results indicated that the best filtering algorithm was the one implemented in LiDAR processing software LAsTools. This algorithm was subsequently used for filtering in **Study III** and **Study IV**.

After choosing the optimum filtering parameters and acquisition of a point cloud classified into ground and non-ground points, DTM is typically the first created model. If we wanted to acquire more information about the point cloud, an additional data processing step would have to be performed, namely automatic classification, especially if man-made structures are present in the area of interest. This is the only way we can make sure that the man-made objects are not going to be considered as vegetation and that we will be able to filter them

out if need be. Such algorithm was utilized in **Study IV** where the area of interest was urbanized.

A so far untested approach to ground filtering or classification is the use of ensemble modelling, which uses several filtering algorithms and then assigns weights to individual points depending on the number of algorithms that have classified the point in the same way. Such a method could be instrumental in automatic processing of point clouds in problematic areas.

8.4 Application of Laser Scanning Data in Urban Environments

“Why and how to use LiDAR data?”

ALS data are presently extensively used. The biggest advantage is the high level of detail, be it in an environment completely without buildings as in **Studies I, II, III** where spoil banks constituted the area of interest, or be it urban environment as in **Study IV**. In the urban environment, however, ground filtering only is not a sufficient processing method and an overall data classification has to be performed. In the **Study IV**, ALS data were used for rooftop solar potential estimates, which is lately a widely used method utilized in particular for creating so-called solar cadastres or solar maps.

From the perspective of LiDAR data processing, it is however necessary to point out that in the urban environment, we usually encounter a higher rate of unusual objects and features than when mapping natural landscapes with vegetation, such as in **Studies I, II, III**. Urban environment is usually very complex with a high degree of representation of artificial structures including street or park vegetation, above-ground phone or power lines, lampposts, large industrial objects, chimneys, retaining walls, bridges and buildings with roofs of many shapes. The

correct classification or filtering in such an area is quite challenging. In particular, the fundamental filtering, i.e., determining ground points, is sometimes quite difficult.

To determine the solar potential, it was necessary to know the topography of the roof. The current classification algorithms are at present capable to detect without any major problems clusters of points forming a planar surface, which is frequently used for roof detection. In particular, detection of roofs from LiDAR data is one of the most common tasks in the urban environment (Tarsha-Kurdi et al., 2008; Jochem et al., 2009; Tooke et al., 2011). Nevertheless, the assumption of the flatness of the surface fails in case of specific and, in particular, historic buildings (churches, castles, towers, etc.). It is true that for estimating solar potential, such buildings are mostly irrelevant as mounting photovoltaic panels on such buildings is mostly out of question.

In **Study IV**, we found that the effect of vegetation on the solar potential estimates is at the relatively large scale of cities negligible; at the local level, however, shadows of surrounding vegetation could represent problems. Nevertheless, even analyses disregarding vegetation can in the urban environment provide a valuable solar estimate of a site.

8.5 Conclusions

In the theoretical and methodical parts of the thesis, we described various options of the use of LiDAR for studying the environment and the methods of its application. This thesis includes research on data processing, UAV experiments or LiDAR comparison with other methods of RS. The principal pros and cons of individual investigated methods can be found in the discussion and conclusions of each individual study or in the summary chapter above. Still, here are some of the most important points:

- Mapping accuracy using AMA LiDAR UAV system was on the inferior side of the expected accuracy, which was most likely caused by insufficient calibration of the system. The use of LiDAR UAV is obviously a promising method, a suitable carrier/platform must be however used. The airship demonstrated its negative properties such as inferior manoeuvrability and, unfortunately, a high rate of failure of the used propulsion system, which in effect prevented the measurement of the entire area of interest. Even application of fixed wing UAV imagery showed that the selected area of interest was too large for this platform and data had to be acquired in several flight missions. From the perspective of accuracy, data derived from UAV imagery show the accuracy similar to those of LiDAR where the terrain is free of vegetation. If using conventional ALS and individual mapping, the data acquisition costs would be multiple times higher than the use of tested technologies.
- All tested LiDAR ground filtering algorithms yielded relatively good results, their performance was however to a great degree affected by the terrain slope and presence of vegetation. Algorithms worked better in areas with tall vegetation than in those with dense vegetation. The overall best results were provided by the PTIN algorithm implemented in LAsTools; some other algorithms however provided superior results in specific environments. For example, SMRF algorithm demonstrated very good performance in the forest environment. The list of algorithms used in the study was of course not comprehensive and other, although at present probably less well known, ground filtering algorithms might be available. The study however very well demonstrates the importance of being able to select a proper algorithm with optimum settings for various landscape types, which should be ideally part of documentation provided in manuals to the individual algorithms.

- As a part of the evaluation of accuracy of data derived from ALS and UAV imagery, DTMs generated from point clouds of both methods were compared. In case of UAV imagery, two separate missions at different times (leaf-on and leaf-off period) were performed to create the DTM in the area containing three different environments (aquatic vegetation, steppe, and forest) to evaluate the possibility of creating DTM from imagery taken at different time points. The overall accuracy of UAV imagery was similar to that of LiDAR-derived DTM, with the best agreement in forest environment and the worst in the environment of aquatic vegetation. The accuracy of both methods would however be sufficient for numerous applications, including e.g. monitoring of spoil banks terrain. The use of UAV imagery is however more susceptible to adverse weather conditions, especially as it must be in many cases (depending on the structure of vegetation) taken in the leaf-off period when the weather conditions are often far from perfect and, moreover, a problem with snow covering the terrain can arise. Airborne LiDAR can on the other hand be used for mapping during all seasons and regardless of the vegetation structure while UAV imagery can be in steppes and deciduous forests successfully used only under leaf-off conditions.
- Utilization of LiDAR data allowed us to perform vegetation filtering and to create scenarios for the calculation of solar potential on the rooftops. We demonstrated that at least in the large extent of entire urban areas, the effect of vegetation on the rooftops solar potential is not significant and if making evaluation of the solar potential on a larger scale, vegetation can be fully excluded from the equation. On a local scale, however, where individual buildings, roofs and parts of the roofs suitable for placement of the photovoltaic panels are being evaluated, the vegetation should always be included into the analysis.

8.6 Further Research

The development of LiDAR systems is still far from being complete and new possibilities of recording, data collection or processing (especially with respect to the use of dual or multispectral airborne LiDAR or lightweight UAV LiDAR systems) keep arising. In the future, we can also expect increasing availability of LiDAR data from various specific environments, which will undoubtedly require development of new (or improvement of the existing) approaches to collection, processing and storage of point cloud data. This is especially true in the fields of filtering and classification algorithms and feature extraction, as well as standardization of the data collection and sharing for extensive areas (such as Europe). Nevertheless, modern high resolution LiDAR data covering extensive areas come with a phenomenon – spatial big data, i.e. the fact that the data are just too bulky, which among other things increases the demands for data processing (Sugumaran et al., 2012; Singh et al., 2016). Where data processing is concerned, research in the fields of automatic classification and detection of individual features on the Earth surface (water bodies, vegetation or single trees, bridge decks, etc.) using deep learning or machine learning methods is ongoing (Guan et al., 2015; Hu and Yuan, 2016; Zhao et al., 2018; Kumar et al., 2019; Verschoof-van and Lambers, 2019).

As this thesis dealt with the topic of laser scanning in environmental science, I would like to focus my future research on the same area, in particular on the point cloud filtering and classification algorithms as well as on the use of LiDAR data originating besides manned aircraft systems also from terrestrial, mobile and UAV platforms for mapping (not only) in the field of environmental research.

At present, I participate in two research topics. The first project aiming at the field of filtering algorithms, is titled “*Contrasting performance of six ground filtering algorithms with LiDAR and UAV based photogrammetric point clouds in complex artificial terrain*”. It focuses on

comparison of LiDAR ground filtering algorithms for both airborne LiDAR and UAV imagery point cloud. The other project focused more on the ecological side, is titled “*The influence of structure of growth on the species diversity and distribution of birds in the Giant Mountains national park*” and deals with the use of ALS point clouds for modelling species diversity and distribution of birds.

8.7 Afterword

The present development and trends in various areas of remote sensing indicate that the availability of three-dimensional spatial data will keep improving. In view of the possibilities represented by laser scanning technologies, we can therefore over time assume that unique datasets will be acquired, reflecting the complex condition of the landscape and will be stored as a “*digital imprint*” for future generations. This principle is even now being used in the fields of archaeology and architecture. The landscape condition stored in this way can in the future represent a valuable source of information for research purposes

Chapter 9

References

- Ackers, S. H., Davis, R. J., Olsen, K. A., and Dugger, K. M. (2015). The evolution of mapping habitat for northern spotted owls (*Strix occidentalis caurina*): A comparison of photo-interpreted, landsat-based, and lidar-based habitat maps. *Remote Sensing of Environment*, 156:361–373.
- Agugiaro, G., Nex, F., Remondino, F., De Filippi, R., Droghetti, S., and Furlanello, C. (2012). Solar radiation estimation on building roofs and web-based solar cadastre. *ISPRS Ann. Photogramm. Remote Sens. Spat. Inf. Sci*, 1:177–182.
- Araya-Muñoz, D., Carvajal, D., Sáez-Carreño, A., Bensaïd, S., and Soto-Márquez, E. (2014). Assessing the solar potential of roofs in Valparaíso (Chile). *Energy and Buildings*, 69:62–73.
- Arnold, N. S., Rees, W. G., Devereux, B. J., and Amable, G. S. (2006). Evaluating the potential of high-resolution airborne LiDAR data in glaciology. *International Journal of Remote Sensing*, 27(6):1233–1251.
- Aryal, R. R., Latifi, H., Heurich, M., and Hahn, M. (2017). Impact of slope, aspect, and habitat-type on LiDAR-derived digital terrain models in a near natural, heterogeneous temperate forest. *PFG – Journal of Photogrammetry, Remote Sensing and Geoinformation Science*, 85(4):243–255.

- Asner, G. P., Owen-Smith, N., Loarie, S. R., Davies, A. B., Roux, E. L., and Levick, S. R. (2015). Habitat differences do not explain population declines of sable antelope in an African savanna. *Journal of Zoology*, 297(3):225–234.
- ASPRS (2013). LAS Specification Version 1.4 – R13. Technical report, The American Society for Photogrammetry & Remote Sensing.
- Axelsson, P. (2000). DEM generation from laser scanner data using adaptive TIN models. *International archives of photogrammetry and remote sensing*, 33(4):110–117.
- Bakx, T. R. M., Koma, Z., Seijmonsbergen, A. C., and Kissling, W. D. (2019). Use and categorization of light detection and ranging vegetation metrics in avian diversity and species distribution research. *Diversity and Distributions*, 25(7):1045–1059.
- Balenović, I., Gašparović, M., Simic Milas, A., Berta, A., and Seletković, A. (2018). Accuracy assessment of digital terrain models of lowland pedunculate oak forests derived from airborne laser scanning and photogrammetry. *Croatian Journal of Forest Engineering: Journal for Theory and Application of Forestry Engineering*, 39(1):117–128.
- Balogun, A. A., Morakinyo, T. E., and Adegun, O. B. (2014). Effect of tree-shading on energy demand of two similar buildings. *Energy and Buildings*, 81:305–315.
- Baltensweiler, A., Walthert, L., Ginzler, C., Sutter, F., Purves, R. S., and Hanewinkel, M. (2017). Terrestrial laser scanning improves digital elevation models and topsoil pH modelling in regions with complex topography and dense vegetation. *Environmental Modelling & Software*, 95:13–21.
- Baltsavias, E. P. (1999a). Airborne laser scanning: basic relations and formulas. *ISPRS Journal of Photogrammetry and Remote Sensing*, 54(2):199–214.

- Baltsavias, E. P. (1999b). Airborne laser scanning: existing systems and firms and other resources. *ISPRS Journal of Photogrammetry and Remote Sensing*, 54(2):164–198.
- Baltsavias, E. P. (1999c). A comparison between photogrammetry and laser scanning. *ISPRS Journal of Photogrammetry and Remote Sensing*, 54(2):83–94.
- Barnes, K. W., Islam, K., and Auer, S. A. (2015). Integrating LIDAR-derived canopy structure into cerulean warbler habitat models. *The Journal of Wildlife Management*, 80(1):101–116.
- Bates, D., Kliegl, R., Vasishth, S., and Baayen, H. (2015). Parsimonious mixed models. *arXiv preprint arXiv:1506.04967*.
- Bazzichetto, M., Malavasi, M., Barták, V., Acosta, A. T. R., Moudrý, V., and Carranza, M. L. (2018). Modeling plant invasion on Mediterranean coastal landscapes: An integrative approach using remotely sensed data. *Landscape and Urban Planning*, 171:98–06.
- Bednarczyk, Z. (2017). Landslide monitoring and counteraction technologies in polish lignite opencast mines. In Mikoš, M., Vilímek, V., Yin, Y., and Sassa, K., editors, *Advancing Culture of Living with Landslides*, pages 33–43, Cham. Springer International Publishing.
- Bell, F. G. and Donnelly, L. J. (2006). *Mining and its Impact on the Environment*. CRC Press.
- Bergen, K. M., Goetz, S. J., Dubayah, R. O., Henebry, G. M., Hunsaker, C. T., Imhoff, M. L., Nelson, R. F., Parker, G. G., and Radeloff, V. C. (2009). Remote sensing of vegetation 3-D structure for biodiversity and habitat: Review and implications for lidar and radar spaceborne missions. *Journal of Geophysical Research: Biogeosciences*, 114(G2):1–13.

- Biljecki, F., Heuvelink, G. B. M., Ledoux, H., and Stoter, J. (2015). Propagation of positional error in 3D GIS: estimation of the solar irradiation of building roofs. *International Journal of Geographical Information Science*, 29(12):2269–2294.
- Boz, M. B., Calvert, K., and Brownson, J. R. S. (2015). An automated model for rooftop PV systems assessment in ArcGIS using LIDAR.
- Brázdil, K. (2012). Technická zpráva k digitálnímu modelu reliéfu 5. generace (DMR 5G). Technical report, Zeměměřický úřad.
- Brown, A. G., Tooth, S., Bullard, J. E., Thomas, D. S. G., Chiverrell, R. C., Plater, A. J., Murton, J., Thorndycraft, V. R., Tarolli, P., Rose, J., Wainwright, J., Downs, P., and Aalto, R. (2017). The geomorphology of the Anthropocene: emergence, status and implications. *Earth Surface Processes and Landforms*, 42(1):71–90.
- Calvert, K. and Mabee, W. (2015). More solar farms or more bioenergy crops? mapping and assessing potential land-use conflicts among renewable energy technologies in eastern Ontario, Canada. *Applied Geography*, 56:209–221.
- Calvert, K., Pearce, J. M., and Mabee, W. E. (2013). Toward renewable energy geo-information infrastructures: Applications of GIScience and remote sensing that build institutional capacity. *Renewable and Sustainable Energy Reviews*, 18:416–429.
- Chalupa, V., Pánek, T., Tábořík, P., Klimeš, J., Hartvich, F., and Grygar, R. (2018). Deep-seated gravitational slope deformations controlled by the structure of flysch nappe outliers: Insights from large-scale electrical resistivity tomography survey and LiDAR mapping. *Geomorphology*, 321:174–187.
- Charaniya, A. P., Manduchi, R., and Lodha, S. K. (2004). Supervised parametric classification of aerial LiDAR data. In *Conference on Computer Vision and Pattern Recognition Workshop*, pages 30–30.

- Charlton, M. E., Coveney, S. J., and McCarthy, T. (2009). Issues in laser scanning. *Laser scanning for the environmental sciences*, 1.
- Chen, Y., Zhu, X., Yebra, M., Harris, S., and Tapper, N. (2017). Development of a predictive model for estimating forest surface fuel load in Australian eucalypt forests with LiDAR data. *Environmental Modelling & Software*, 97:61–71.
- Cho, Y.-C. and Song, Y.-S. (2014). Deformation measurements and a stability analysis of the slope at a coal mine waste dump. *Ecological Engineering*, 68:189–199.
- Clark, M. L., Clark, D. B., and Roberts, D. A. (2004). Small-footprint lidar estimation of sub-canopy elevation and tree height in a tropical rain forest landscape. *Remote Sensing of Environment*, 91(1):68–89.
- Clawges, R., Vierling, K., Vierling, L., and Rowell, E. (2008). The use of airborne lidar to assess avian species diversity, density, and occurrence in a pine/aspens forest. *Remote Sensing of Environment*, 112(5):2064–2073.
- Close, O., Stéphenne, N., and Fripiat, C. (2016). Impact of DEM processing on the geotechnical instability analysis of waste heaps in Wallonia.
- Ćmielewski, B., Dabek, P. B., Patrzalek, C., and Wilczynska, I. (2018). Potential of using unmanned aircraft systems for landslide monitoring: the case of Janowiec landslide in Poland. *Journal of Environmental Science and Management*, 21(1).
- Colgan, M., Baldeck, C., Féret, J.-B., and Asner, G. (2012). Mapping savanna tree species at ecosystem scales using Support Vector Machine classification and BRDF correction on airborne hyperspectral and LiDAR data. *Remote Sensing*, 4(12):3462–3480.

- Coops, N. C., Hilker, T., Wulder, M. A., St-Onge, B., Newnham, G., Siggins, A., and Trofymow, J. A. (2007). Estimating canopy structure of Douglas-fir forest stands from discrete-return LiDAR. *Trees*, 21(3):295–310.
- Cordell, S., Questad, E. J., Asner, G. P., Kinney, K. M., Thaxton, J. M., Uowolo, A., Brooks, S., and Chynoweth, M. W. (2017). Remote sensing for restoration planning: how the big picture can inform stakeholders. *Restoration Ecology*, 25(S2):S147–S154.
- Crow, P., Benham, S., Devereux, B. J., and Amable, G. S. (2007). Woodland vegetation and its implications for archaeological survey using LiDAR. *Forestry*, 80(3):241–252.
- Cunliffe, A. M., Brazier, R. E., and Anderson, K. (2016). Ultra-fine grain landscape-scale quantification of dryland vegetation structure with drone-acquired structure-from-motion photogrammetry. *Remote Sensing of Environment*, 183:129–143.
- Dandois, J. P. and Ellis, E. C. (2013). High spatial resolution three-dimensional mapping of vegetation spectral dynamics using computer vision. *Remote Sensing of Environment*, 136:259–276.
- Davies, A. B. and Asner, G. P. (2014). Advances in animal ecology from 3D-LiDAR ecosystem mapping. *Trends in Ecology & Evolution*, 29(12):681–691.
- Defaix, P. R., van Sark, W. G. J. H. M., Worrell, E., and de Visser, E. (2012). Technical potential for photovoltaics on buildings in the EU-27. *Solar Energy*, 86(9):2644–2653.
- Derenick, J., Miller, T., Spletzer, J., Kushleyev, A., Foote, T., Stewart, A., Bohren, J., and Lee, D. (2008). The Sick LIDAR Matlab/C++ Toolbox: Software for rapidly interfacing/configuring Sick LIDARs. *Technical Report LU-CSE-08-008*.

- Devabhaktuni, V., Alam, M., Shekara Sreenadh Reddy Depuru, S., Green, R. C., Nims, D., and Near, C. (2013). Solar energy: Trends and enabling technologies. *Renewable and Sustainable Energy Reviews*, 19:555–564.
- Devereux, B. and Amable, G. (2009). Airborne LiDAR: Instrumentation, data acquisition and handling. In Heritage, G. L. and Large, A. R. G., editors, *Laser Scanning for the Environmental Sciences*, pages 49–66. Blackwell. ISBN 978-1-4051-5717-9.
- DeWitt, J. D., Warner, T. A., Chirico, P. G., and Bergstresser, S. E. (2017). Creating high-resolution bare-earth digital elevation models (DEMs) from stereo imagery in an area of densely vegetated deciduous forest using combinations of procedures designed for lidar point cloud filtering. *GIScience & Remote Sensing*, 54(4):552–572.
- Doležalová, J., Vojar, J., Smolová, D., Solský, M., and Kopecký, O. (2012). Technical reclamation and spontaneous succession produce different water habitats: A case study from czech post-mining sites. *Ecological Engineering*, 43:5–12.
- Dubayah, R. O. and Drake, J. B. (2000). Lidar remote sensing for forestry. *Journal of Forestry*, 98(6):44–46.
- Dulias, R. (2016). Changes in morphometric parameters of terrain caused by mining. In *The Impact of Mining on the Landscape*, pages 83–93. Springer.
- DxOMark (2016). Lens mounted on Nikon Coolpix A: Tests and reviews. http://www.dxomark.com/Lenses/Nikon/Nikon-Coolpix-A-Lens-mounted-on-Nikon-Coolpix-A__867 [online]. [cit. 2016-06-03].
- Eitel, J. U. H., Höfle, B., Vierling, L. A., Abellán, A., Asner, G. P., Deems, J. S., Glennie, C. L., Joerg, P. C., LeWinter, A. L., Magney, T. S., Mandlburger, G., Morton, D. C., Müller, J., and Vierling, K. T. (2016). Beyond 3-D: The new spectrum of lidar applications

- for earth and ecological sciences. *Remote Sensing of Environment*, 186:372–392.
- Esclapés, J., Ferreiro, I., Piera, J., and Teller, J. (2014). A method to evaluate the adaptability of photovoltaic energy on urban façades. *Solar Energy*, 105:414–427.
- Esposito, S., Mura, M., Fallavollita, P., Balsi, M., Chirici, G., Oradini, A., and Marchetti, M. (2014). Performance evaluation of lightweight LiDAR for UAV applications. In *2014 IEEE Geoscience and Remote Sensing Symposium*, pages 792–795.
- ESRI (2014). ArcGIS desktop: release 10. *Environmental Systems Research Institute, Redlands, CA*.
- Filin, S. (2004). Surface classification from airborne laser scanning data. *Computers & Geosciences*, 30(9-10):1033–1041.
- Flaspohler, D. J., Giardina, C. P., Asner, G. P., Hart, P., Price, J., Lyons, C. K., and Castaneda, X. (2010). Long-term effects of fragmentation and fragment properties on bird species richness in Hawaiian forests. *Biological Conservation*, 143(2):280–288.
- Flood, M. (2001). LiDAR activities and research priorities in the commercial sector. *International Archives of Photogrammetry Remote Sensing and Spatial Information Sciences*, 34(3/W4):3–8.
- Fogl, M. and Moudrý, V. (2016). Influence of vegetation canopies on solar potential in urban environments. *Applied Geography*, 66:73–80.
- Fonstad, M. A., Dietrich, J. T., Courville, B. C., Jensen, J. L., and Carbonneau, P. E. (2013). Topographic structure from motion: a new development in photogrammetric measurement. *Earth Surface Processes and Landforms*, 38(4):421–430.
- Fox, J. and Weisberg, S. (2011). Multivariate linear models in R. *An R Companion to Applied Regression*. Los Angeles: Thousand Oaks.

- Frazer, G. W., Magnussen, S., Wulder, M. A., and Niemann, K. O. (2011). Simulated impact of sample plot size and co-registration error on the accuracy and uncertainty of LiDAR-derived estimates of forest stand biomass. *Remote Sensing of Environment*, 115(2):636–649.
- Freitas, S., Catita, C., Redweik, P., and Brito, M. C. (2015). Modelling solar potential in the urban environment: State-of-the-art review. *Renewable and Sustainable Energy Reviews*, 41:915–931.
- French, J. R. (2003). Airborne LiDAR in support of geomorphological and hydraulic modelling. *Earth Surface Processes and Landforms*, 28(3):321–335.
- Frouz, J., Mudrak, O., Reitschmiedova, E., Walmsley, A., Vachova, P., ˇSimaˇckova, H., Albrechtova, J., Moradi, J., and Kuˇcera, J. (2018). Rough wave-like heaped overburden promotes establishment of woody vegetation while leveling promotes grasses during unassisted post mining site development. *Journal of Environmental Management*, 205:50–58.
- Fu, P. and Rich, P. M. (1999). Design and implementation of the Solar Analyst: an ArcView extension for modeling solar radiation at landscape scales. In *Proceedings of the nineteenth annual ESRI user conference*, volume 1, pages 1–31. San Diego USA.
- Furukawa, Y. and Ponce, J. (2009). Accurate, dense, and robust multiview stereopsis. *IEEE transactions on pattern analysis and machine intelligence*, 32(8):1362–1376.
- Gallay, M., Kaˇnuk, J., and Hofierka, J. (2015). Capacity of photovoltaic power plants in the Czech Republic. *Journal of Maps*, 11(3):480–486.
- Garabedian, J. E., McGaughey, R. J., Reutebuch, S. E., Parresol, B. R., Kilgo, J. C., Moorman, C. E., and Peterson, M. N. (2014).

- Quantitative analysis of woodpecker habitat using high-resolution airborne LiDAR estimates of forest structure and composition. *Remote Sensing of the Environment*, 145:68–80.
- Gautam, B. R., Li, F., and Ru, G. (2015). Assessment of urban roof top solar photovoltaic potential to solve power shortage problem in Nepal. *Energy and Buildings*, 86:735–744.
- Gonçalves, G. and Pereira, L. G. (2010). Assessment of the performance of eight filtering algorithms by using full-waveform LiDAR data of unmanaged eucalypt forest. *Proc. SilviLaser*, pages 187–196.
- Graf, R. F., Mathys, L., and Bollmann, K. (2009). Habitat assessment for forest dwelling species using LiDAR remote sensing: Capercaillie in the Alps. *Forest Ecology and Management*, 257(1):160–167.
- Guan, H., Yu, Y., Ji, Z., Li, J., and Zhang, Q. (2015). Deep learning-based tree classification using mobile LiDAR data. *Remote Sensing Letters*, 6(11):864–873.
- Guo, Q., Su, Y., Hu, T., Zhao, X., Wu, F., Li, Y., Liu, J., Chen, L., Xu, G., and Lin, G. (2017). An integrated UAV-borne lidar system for 3D habitat mapping in three forest ecosystems across China. *International journal of remote sensing*, 38(8-10):2954–2972.
- Habib, A. and Rens, J. V. (2009). Quality assurance and quality control of LiDAR systems and derived data. In *ASPRS LiDAR Committee*, volume 75, pages 1093–1108. ASPRS.
- Haigh, M. J. and Gentcheva-Kostadinova, S. (2002). Ecological erosion control on coal-spoil banks: an evaluation. *Ecological Engineering*, 18(3):371–377.
- Hancock, G. R., Crawter, D., Fityus, S. G., Chandler, J., and Wells, T. (2008). The measurement and modelling of rill erosion at angle of repose slopes in mine spoil. *Earth Surface Processes and Landforms*, 33(7):1006–1020.

- Hanuš, J., Fabiánek, T., and Fajmon, L. (2016). Potential of airborne imaging spectroscopy at CzechGlobe. *Int. Arch. Photogramm. Remote Sens. Spat. Inf. Sci.*, pages 15–17.
- Harabiš, F. (2016). High diversity of odonates in post-mining areas: Meta-analysis uncovers potential pitfalls associated with the formation and management of valuable habitats. *Ecological Engineering*, 90:438–446.
- Harabiš, F., Tichanek, F., and Tropek, R. (2013). Dragonflies of freshwater pools in lignite spoil heaps: Restoration management, habitat structure and conservation value. *Ecological Engineering*, 55:51–61.
- Haralick, R. M., Sternberg, S. R., and Zhuang, X. (1987). Image analysis using mathematical morphology. *IEEE transactions on pattern analysis and machine intelligence*, (4):532–550.
- Harpold, A. A., Marshall, J. A., Lyon, S. W., Barnhart, T. B., Fisher, B. A., Donovan, M., Brubaker, K. M., Crosby, C. J., Glenn, N. F., Glennie, C. L., Kirchner, P. B., Lam, N., Mankoff, K. D., McCreight, J. L., Molotch, N. P., Musselman, K. N., Pelletier, J., Russo, T., Sangireddy, H., Sjöberg, Y., Swetnam, T., and West, N. (2015). Laser vision: lidar as a transformative tool to advance critical zone science. *Hydrology and Earth System Sciences*, 19(6):2881–2897.
- Hawryło, P., Tompalski, P., and Wężyk, P. (2017). Area-based estimation of growing stock volume in Scots pine stands using ALS and airborne image-based point clouds. *Forestry: An International Journal of Forest Research*, 90(5):686–696.
- Hendrychoviá, M. and Kabrna, M. (2016). An analysis of 200-year-long changes in a landscape affected by large-scale surface coal mining: History, present and future. *Applied Geography*, 74:151–159.

- Heritage, G. L. and Large, A. R. G. (2009). Principles of 3D laser scanning. In Heritage, G. L. and Large, A. R. G., editors, *Laser Scanning for the Environmental Sciences*, pages 21–34. Blackwell. ISBN 978-1-4051-5717-9.
- Heurich, M. (2008). Automatic recognition and measurement of single trees based on data from airborne laser scanning over the richly structured natural forests of the Bavarian Forest National Park. *Forest Ecology and Management*, 255(7):2416–2433.
- Hill, R. and Hinsley, S. (2015). Airborne lidar for woodland habitat quality monitoring: Exploring the significance of lidar data characteristics when modelling organism-habitat relationships. *Remote Sensing*, 7(4):3446–3466.
- Hodgson, M. E., Jensen, J., Raber, G., Tullis, J., Davis, B. A., Thompson, G., and Schuckman, K. (2005). An evaluation of lidar-derived elevation and terrain slope in leaf-off conditions. *Photogrammetric Engineering & Remote Sensing*, 71(7):817–823.
- Hofierka, J., Gallay, M., Bandura, P., and Šašák, J. (2018). Identification of karst sinkholes in a forested karst landscape using airborne laser scanning data and water flow analysis. *Geomorphology*, 308:265–277.
- Hofierka, J. and Kaňuk, J. (2009). Assessment of photovoltaic potential in urban areas using open-source solar radiation tools. *Renewable Energy*, 34(10):2206–2214.
- Hofierka, J., Kaňuk, J., and Gallay, M. (2014). The spatial distribution of photovoltaic power plants in relation to solar resource potential: The case of the Czech Republic and Slovakia. *Moravian Geographical Reports*, 22(2):26–33.
- Hofierka, J. and Šúri, M. (2002). The solar radiation model for open

- source GIS: implementation and applications. In *Proceedings of the Open source GIS-GRASS users conference*, volume 2002, pages 51–70.
- Hofton, M. A., Rocchio, L. E., Blair, J. B., and Dubayah, R. (2002). Validation of vegetation canopy lidar sub-canopy topography measurements for a dense tropical forest. *Journal of Geodynamics*, 34(3):491–502.
- Hogarth, J., Hawley, M., and Beale, G. (2017). Instrumentation and monitoring. *Guidelines for Mine Waste Dump and Stockpile Design*.
- Höhle, J. and Höhle, M. (2009). Accuracy assessment of digital elevation models by means of robust statistical methods. *ISPRS Journal of Photogrammetry and Remote Sensing*, 64(4):398–406.
- Holmgren, J. and Persson, øA. (2004). Identifying species of individual trees using airborne laser scanner. *Remote Sensing of Environment*, 90(4):415–423.
- Hopkinson, C., Chasmer, L. E., Sass, G., Creed, I. F., Sitar, M., Kalbfleisch, W., and Treitz, P. (2005). Vegetation class dependent errors in lidar ground elevation and canopy height estimates in a boreal wetland environment. *Canadian Journal of Remote Sensing*, 31(2):191–206.
- Hu, X. and Yuan, Y. (2016). Deep-learning-based classification for DTM extraction from ALS point cloud. *Remote Sensing*, 8(9).
- Hyypä, J., Hyypä, H., Litkey, P., Yu, X., Haggrén, H., Rönholm, P., Pyysalo, U., Juho Pitkänen, J., and Maltamo, M. (2004). Algorithms and methods of airborne laser-scanning for forest measurements. *International Archives of Photogrammetry and Remote Sensing*, 36:8.
- Iglhaut, J., Cabo, C., Puliti, S., Piermattei, L., O’Connor, J., and Rosette, J. (2019). Structure from motion photogrammetry in forestry: a review. *Current Forestry Reports*.

- Izquierdo, S., Rodrigues, M., and Fueyo, N. (2008). A method for estimating the geographical distribution of the available roof surface area for large-scale photovoltaic energy-potential evaluations. *Solar Energy*, 82(10):929–939.
- Jakubowski, M. K., Guo, Q., and Kelly, M. (2013). Tradeoffs between lidar pulse density and forest measurement accuracy. *Remote Sensing of Environment*, 130:245–253.
- Jensen, J. L. R. and Mathews, A. J. (2016). Assessment of image-based point cloud products to generate a bare Earth surface and estimate canopy heights in a woodland ecosystem. *Remote Sensing*, 8(1).
- Jochem, A., Höfle, B., Rutzinger, M., and Pfeifer, N. (2009). Automatic roof plane detection and analysis in airborne lidar point clouds for solar potential assessment. *Sensors*, 9(7):5241–5262.
- Jochem, A., Wichmann, V., and Conrad, O. (2010). LiDAR point cloud processing with SAGA GIS. In *Hamburger Beiträge zur Physischen Geographie und Landschaftsökologie*, volume 19, pages 59–70.
- Johansen, K., Phinn, S., and Witte, C. (2010). Mapping of riparian zone attributes using discrete return LiDAR, QuickBird and SPOT-5 imagery: Assessing accuracy and costs. *Remote Sensing of Environment*, 114(11):2679–2691.
- Johnson, M. D., Fredin, O., Ojala, A. E. K., and Peterson, G. (2015). Unraveling scandinavian geomorphology: the LiDAR revolution. *GFF*, 137(4):245–251.
- Jon, J., Koska, B., and Pospíšil, J. (2013). Autonomous airship equipped by multi-sensor mapping platform. *ISPRS - International Archives of the Photogrammetry, Remote Sensing and Spatial Information Sciences*, XL-5/W1:119–124.

- Julge, K., Ellmann, A., and Gruno, A. (2014). Performance analysis of freeware filtering algorithms for determining ground surface from airborne laser scanning data. *Journal of Applied Remote Sensing*, 8(1):083573.
- Kachamba, D. J., Ørka, H. O., Gobakken, T., Eid, T., and Mwase, W. (2016). Biomass estimation using 3D data from unmanned aerial vehicle imagery in a tropical woodland. *Remote Sensing*, 8(11).
- Kalacska, M., Chmura, G. L., Lucanus, O., Bérubé, D., and Arroyo-Mora, J. P. (2017). Structure from motion will revolutionize analyses of tidal wetland landscapes. *Remote Sensing of Environment*, 199:14–24.
- Kanters, J. and Horvat, M. (2012). Solar energy as a design parameter in urban planning. *Energy Procedia*, 30:1143–1152.
- Kanters, J., Wall, M., and Kjellsson, E. (2014). The solar map as a knowledge base for solar energy use. *Energy Procedia*, 48:1597–1606.
- Kashani, A. G., Olsen, M. J., Parrish, C. E., and Wilson, N. (2015). A review of LIDAR radiometric processing: From ad hoc intensity correction to rigorous radiometric calibration. *Sensors*, 15(11):28099–28128.
- Khan, S., Aragão, L., and Iriarte, J. (2017). A UAV–lidar system to map amazonian rainforest and its ancient landscape transformations. *International journal of remote sensing*, 38(8-10):2313–2330.
- Khosravipour, A., Skidmore, A. K., and Isenburg, M. (2016). Generating Spike-free digital surface models using LiDAR raw point clouds: A new approach for forestry applications. *International Journal of Applied Earth Observation and Geoinformation*, 52:104–114.
- Khosravipour, A., Skidmore, A. K., Isenburg, M., Wang, T., and Hussin, Y. A. (2014). Generating Pit-free canopy height models from

airborne lidar. *Photogrammetric Engineering & Remote Sensing*, 80(9):863–872.

Klouček, T., Lagner, O., and Šimová, P. (2015). How does data accuracy influence the reliability of digital viewshed models? a case study with wind turbines. *Applied Geography*, 64:46–54.

Kodysh, J. B., Omitaomu, O. A., Bhaduri, B. L., and Neish, B. S. (2013). Methodology for estimating solar potential on multiple building rooftops for photovoltaic systems. *Sustainable Cities and Society*, 8:31–41.

Korzeniowska, K., Pfeifer, N., Mandlbürger, G., and Lugmayr, A. (2014). Experimental evaluation of ALS point cloud ground extraction tools over different terrain slope and land-cover types. *International journal of remote sensing*, 35(13):4673–4697.

Koska, B. (2013). Bore-sights and lever-arms determination of sensors mounted on Autonomous Mapping Airship. *Proceeding of 13th International Multidisciplinary Scientific GeoConferences SGEM*, 2:579–586.

Koska, B., Jirka, V., Urban, R., Křemen, T., Hesslerová, P., Jon, J., Pospíšil, J., and Fogl, M. (2017). Suitability, characteristics, and comparison of an airship UAV with lidar for middle size area mapping. *International journal of remote sensing*, 38(8-10):2973–2990.

Koska, B., Křemen, T., and Štroner, M. (2014). Bore-sight calibration of the profile laser scanner using a large size exterior calibration field. In *Earth Resources and Environmental Remote Sensing/GIS Applications V*, volume 9245. International Society for Optics and Photonics.

Kršák, B., Blištan, P., Pauliková, A., Puškárová, P., Kovanič, L., Palková, J., and Zelizňaková, V. (2016). Use of low-cost UAV pho-

- togrammetry to analyze the accuracy of a digital elevation model in a case study. *Measurement*, 91:276–287.
- Kumar, B., Lohani, B., and Pandey, G. (2019). Development of deep learning architecture for automatic classification of outdoor mobile LiDAR data. *International Journal of Remote Sensing*, 40(9):3543–3554.
- Kumhálová, J. and Moudrý, V. (2014). Topographical characteristics for precision agriculture in conditions of the Czech Republic. *Applied Geography*, 50:90–98.
- Lagner, O., Klouček, T., and Šímová, P. (2018). Impact of input data (in) accuracy on overestimation of visible area in digital viewshed models. *PeerJ*, 6:e4835.
- Langhammer, J., Janský, B., Kocum, J., and Minařík, R. (2018). 3-D reconstruction of an abandoned montane reservoir using UAV photogrammetry, aerial LiDAR and field survey. *Applied Geography*, 98:9–21.
- LAStools (2014). Efficient LiDAR processing software. <http://rapidlasso.com/LAStools> [online].
- Lechner, A. M., McIntyre, N., Witt, K., Raymond, C. M., Arnold, S., Scott, M., and Rifkin, W. (2017). Challenges of integrated modelling in mining regions to address social, environmental and economic impacts. *Environmental Modelling & Software*, 93:268–281.
- Lecours, V., Devillers, R., Edinger, E. N., Brown, C. J., and Lucieer, V. L. (2017). Influence of artefacts in marine digital terrain models on habitat maps and species distribution models: a multiscale assessment. *Remote Sensing in Ecology and Conservation*, 3(4):232–246.
- Lefsky, M. A., Cohen, W. B., Parker, G. G., and Harding, D. J. (2002). Lidar remote sensing for ecosystem studies. *Bioscience*, 52(1):19.

- Lefsky, M. A., Harding, D., Cohen, W. B., Parker, G., and Shugart, H. H. (1999). Surface lidar remote sensing of basal area and biomass in deciduous forests of Eastern Maryland, USA. *Remote Sensing of Environment*, 67(1):83–98.
- Leitold, V., Keller, M., Morton, D. C., Cook, B. D., and Shimabukuro, Y. E. (2015). Airborne lidar-based estimates of tropical forest structure in complex terrain: opportunities and trade-offs for REDD+. *Carbon balance and management*, 10(1):3.
- Levinson, R., Akbari, H., Pomerantz, M., and Gupta, S. (2009). Solar access of residential rooftops in four California cities. *Solar Energy*, 83(12):2120–2135.
- Li, Z., Zhang, Z., and Davey, K. (2015). Estimating geographical PV potential using LiDAR data for buildings in downtown San Francisco. *Transactions in GIS*, 19(6):930–963.
- Li, Z., Zhu, Q., and Gold, C. (2004). *Digital Terrain Modeling: Principles and Methodology*. CRC Press.
- Lin, Y., Hyypä, J., and Jaakkola, A. (2011). Mini-UAV-borne LIDAR for fine-scale mapping. *IEEE Geoscience and Remote Sensing Letters*, 8(3):426–430.
- Lisein, J., Pierrot-Deseilligny, M., Bonnet, S., and Lejeune, P. (2013). A photogrammetric workflow for the creation of a forest canopy height model from small unmanned aerial system imagery. *Forests*, 4(4):922–944.
- Liu, K., Shen, X., Cao, L., Wang, G., and Cao, F. (2018). Estimating forest structural attributes using UAV-LiDAR data in Ginkgo plantations. *ISPRS Journal of Photogrammetry and Remote Sensing*, 146:465–482.

- Lovitt, J., Rahman, M. M., and McDermid, G. J. (2017). Assessing the value of UAV photogrammetry for characterizing terrain in complex peatlands. *Remote Sensing*, 9(7).
- Luo, S., Wang, C., Pan, F., Xi, X., Li, G., Nie, S., and Xia, S. (2015). Estimation of wetland vegetation height and leaf area index using airborne laser scanning data. *Ecological Indicators*, 48:550–559.
- Maguya, A. S., Junttila, V., and Kauranne, T. (2014). Algorithm for extracting digital terrain models under forest canopy from airborne LiDAR data. *Remote Sensing*, 6(7):6524–6548.
- Mallet, C. and Bretar, F. (2009). Full-waveform topographic lidar: State-of-the-art. *ISPRS Journal of Photogrammetry and Remote Sensing*, 64(1):1–16.
- Mandlbürger, G., Hauer, C., Höfle, B., Habersack, H., and Pfeifer, N. (2008). Optimisation of LiDAR derived terrain models for river flow modelling. *Hydrology & Earth System Sciences Discussions*, 5(6).
- Martín, A. M., Domínguez, J., and Amador, J. (2015). Applying LIDAR datasets and GIS based model to evaluate solar potential over roofs: a review.
- Mavromatidis, G., Orehounig, K., and Carmeliet, J. (2015). Evaluation of photovoltaic integration potential in a village. *Solar Energy*, 121:152–168.
- May, N. C. and Toth, C. K. (2007). Point positioning accuracy of airborne LIDAR systems: A rigorous analysis. *International Archives of Photogrammetry, Remote Sensing, and Spatial Information Sciences*, 36(3/W49B):107–112.
- Meng, X., Currit, N., and Zhao, K. (2010). Ground filtering algorithms for airborne LiDAR data: A review of critical issues. *Remote Sensing*, 2(3):833–860.

- Meng, X., Wang, L., Silván-Cárdenas, J. L., and Currit, N. (2009). A multi-directional ground filtering algorithm for airborne LIDAR. *ISPRS Journal of Photogrammetry and Remote Sensing*, 64(1):117–124.
- Michoud, C., Carrea, D., Costa, S., Davidson, R., Delacourt, C., Deron, M.-H., Jaboyedoff, M., and Macquaire, O. (2014). Rockfall detection and landslide monitoring ability of boat-based mobile laser scanning along Dieppe coastal cliffs. *Vertical Geology Conference 2014*. University of Lausanne, Switzerland.
- Mikita, T., Janata, P., and Surový, P. (2016). Forest stand inventory based on combined aerial and terrestrial close-range photogrammetry. *Forests*, 7(8).
- Montealegre, A. L., Lamelas, M. T., and de la Riva, J. (2015). A comparison of open-source LiDAR filtering algorithms in a mediterranean forest environment. *IEEE Journal of Selected Topics in Applied Earth Observations and Remote Sensing*, 8(8):4072–4085.
- Moore, I. D., Grayson, R. B., and Ladson, A. R. (1991). Digital terrain modelling: A review of hydrological, geomorphological, and biological applications. *Hydrological Processes*, 5(1):3–30.
- Moudrý, V., Lecours, V., Gdulová, K., Gábor, L., Moudrá, L., Kropáček, J., and Wild, J. (2018). On the use of global DEMs in ecological modelling and the accuracy of new bare-earth DEMs. *Ecological Modelling*, 383:3–9.
- Moudrý, V., Urban, R., Štroner, M., Komárek, J., Brouček, J., and Prošek, J. (2019). Comparison of a commercial and home-assembled fixed-wing UAV for terrain mapping of a post-mining site under leaf-off conditions. *International journal of remote sensing*, 40(2):555–572.

- Næsset, E., Gobakken, T., Holmgren, J., Hyypä, H., Hyypä, J., Maltamo, M., Nilsson, M., Olsson, H., Persson, A., and Söderman, U. (2004). Laser scanning of forest resources: The Nordic experience. *Scandinavian Journal of Forest Research*, 19(6):482–499.
- Næsset, E. and Økland, T. (2002). Estimating tree height and tree crown properties using airborne scanning laser in a boreal nature reserve. *Remote Sensing of Environment*, 79(1):105–115.
- Nagai, M., Chen, T., Shibasaki, R., Kumagai, H., and Ahmed, A. (2009). UAV-borne 3-D mapping system by multisensor integration. *IEEE Transactions on Geoscience and Remote Sensing*, 47(3):701–708.
- Nelson, R. (1997). Modeling forest canopy heights: The effects of canopy shape. *Remote Sensing of Environment*, 60(3):327–334.
- Ni, W., Sun, G., Ranson, K. J., Pang, Y., Zhang, Z., and Yao, W. (2015). Extraction of ground surface elevation from ZY-3 winter stereo imagery over deciduous forested areas. *Remote Sensing of Environment*, 159:194–202.
- Nocerino, E., Menna, F., Remondino, F., and Saleri, R. (2013). Accuracy and block deformation analysis in automatic UAV and terrestrial photogrammetry-lesson learnt. *ISPRS Annals of the Photogrammetry, Remote Sensing and Spatial Information Sciences*, 2(5/W1):203–208.
- Nowak, M. M., Dziób, K., and Bogawski, P. (2019). Unmanned aerial vehicles (uavs) in environmental biology: a review. *European Journal of Ecology*, 4(2):56–74.
- Nyssen, J. and Vermeersch, D. (2010). Slope aspect affects geomorphic dynamics of coal mining spoil heaps in Belgium. *Geomorphology*, 123(1):109–121.
- Pan, W. W., Dou, Y. J., Wang, G. L., Wu, M. X., Ren, R. G., and Xu, X. (2015). Development and test of blimp-based compact LI-DAR power-line inspection system. *The International Archives of*

- Photogrammetry, Remote Sensing and Spatial Information Sciences*, 40(3):155–159.
- Pavelka, K., Pikhartová, L., Faltýnová, M., and Řezníček, J. (2010). Combining of aerial laser scanning data, terrestrial mobile scanned data and digital orthophoto. In *Proceedings of 31st ACRS Conference*, volume 1, pages 351–356.
- Penížek, V., Zádorová, T., Kodešová, R., and Vaněk, A. (2016). Influence of elevation data resolution on spatial prediction of colluvial soils in a luvisol region. *PLOS ONE*, 11(11):1–18.
- Petras, V., Petrasova, A., Jeziorska, J., and Mitasova, H. (2016). Processing UAV and LiDAR point clouds in grass GIS. *The International Archives of Photogrammetry, Remote Sensing and Spatial Information Sciences*, 41:945.
- Petrie, G. and Kennie, T. J. M. (1987). Terrain modelling in surveying and civil engineering. *Computer-Aided Design*, 19(4):171–187.
- Pilarska, M., Ostrowski, W., Bakula, K., Górski, K., and Kurczyński, Z. (2016). The potential of light laser scanners developed for unmanned aerial vehicles-the review and accuracy. *International Archives of the Photogrammetry, Remote Sensing & Spatial Information Sciences*, 42.
- Pingel, T. J., Clarke, K. C., and McBride, W. A. (2013). An improved simple morphological filter for the terrain classification of airborne LIDAR data. *ISPRS Journal of Photogrammetry and Remote Sensing*, 77:21–30.
- Pitkänen, J., Maltamo, M., Hyypä, J., and Yu, X. (2004). Adaptive methods for individual tree detection on airborne laser based canopy height model. *International Archives of Photogrammetry, Remote Sensing and Spatial Information Sciences*, 36(8):187–191.

- Polat, N. and Uysal, M. (2015). Investigating performance of airborne LiDAR data filtering algorithms for DTM generation. *Measurement*, 63:61–68.
- Popelková, R. and Mulková, M. (2018). The mining landscape of the Ostrava-Karviná coalfield: Processes of landscape change from the 1830s to the beginning of the 21st century. *Applied Geography*, 90:28–43.
- R Core Team (2018). R: A language and environment for statistical computing.
- Ramirez Camargo, L., Zink, R., Dorner, W., and StoeGLEHNER, G. (2015). Spatio-temporal modeling of roof-top photovoltaic panels for improved technical potential assessment and electricity peak load offsetting at the municipal scale. *Computers, Environment and Urban Systems*, 52:58–69.
- Rashidi, P. and Rastiveis, H. (2017). Ground filtering lidar data based on multi-scale analysis of height difference threshold. *ISPRS - International Archives of the Photogrammetry, Remote Sensing and Spatial Information Sciences*, XLII-4/W4:225–229.
- Redweik, P., Catita, C., and Brito, M. (2013). Solar energy potential on roofs and facades in an urban landscape. *Solar Energy*, 97:332–341.
- Reitberger, J., Krzystek, P., and Stilla, U. (2008). Analysis of full waveform LIDAR data for the classification of deciduous and coniferous trees. *International journal of remote sensing*, 29(5):1407–1431.
- Reitberger, J., Schnörr, C., Krzystek, P., and Stilla, U. (2009). 3D segmentation of single trees exploiting full waveform LIDAR data. *ISPRS Journal of Photogrammetry and Remote Sensing*, 64(6):561–574.

- Ren, H., Zhao, Y. and Xiao, W., and Hu, Z. (2019). A review of UAV monitoring in mining areas: current status and future perspectives. *International Journal of Coal Science & Technology*.
- Reutebuch, S. E., McGaughey, R. J., Andersen, H.-E., and Carson, W. W. (2003). Accuracy of a high-resolution lidar terrain model under a conifer forest canopy. *Canadian journal of remote sensing*, 29(5):527–535.
- Řezníček, J. and Straková, H. (2013). Documentation of dumps and heaps by use of UAV. *International Multidisciplinary Scientific GeoConference: SGEM: Surveying Geology & mining Ecology Management*, 2:151.
- RIEGL (2019). Riegl - unmanned laser scanning.
- Roussel, J.-R., Caspersen, J., Béland, M., Thomas, S., and Achim, A. (2017). Removing bias from LiDAR-based estimates of canopy height: Accounting for the effects of pulse density and footprint size. *Remote Sensing of Environment*, 198:1–16.
- Ruiz-Arias, J. A., Tovar-Pescador, J., Pozo-Vázquez, D., and Alsamamra, H. (2009). A comparative analysis of DEM-based models to estimate the solar radiation in mountainous terrain. *International Journal of Geographical Information Science*, 23(8):1049–1076.
- Šálek, M. (2012). Spontaneous succession on opencast mining sites: implications for bird biodiversity. *Journal of Applied Ecology*, 49(6):1417–1425.
- Samberg, A. (2007). An implementation of the ASPRS LAS Standard. In *ISPRS Volume XXXVI, Part 3/W52*, pages 363–372, Finland. ISPRS Workshop on Laser Scanning 2007 and SilviLaser 2007.
- Sánchez, E. and Izard, J. (2015). Performance of photovoltaics in non-optimal orientations: An experimental study. *Energy and Buildings*, 87:211–219.

- Sangireddy, H., Stark, C. P., Kladzyk, A., and Passalacqua, P. (2016). GeoNet: An open source software for the automatic and objective extraction of channel heads, channel network, and channel morphology from high resolution topography data. *Environmental Modelling & Software*, 83:58–73.
- Santos, T., Gomes, N., Freire, S., Brito, M. C., Santos, L., and Tenedório, J. A. (2014). Applications of solar mapping in the urban environment. *Applied Geography*, 51:48–57.
- Sarralde, J. J., Quinn, D. J., Wiesmann, D., and Steemers, K. (2015). Solar energy and urban morphology: Scenarios for increasing the renewable energy potential of neighbourhoods in London. *Renewable Energy*, 73:10–17.
- Sasaki, T., Imanishi, J., Fukui, W., and Morimoto, Y. (2016). Fine-scale characterization of bird habitat using airborne LiDAR in an urban park in Japan. *Urban Forestry & Urban Greening*, 17:16–22.
- Sedlák, V., Hofierka, J., Gallay, M., and Kaňuk, J. (2018). Specific solution of 3D deformation vector in mine subsidence: a case study of the Košice-Bankov abandoned magnesite mine, Slovakia. *Archives of Mining Sciences*, 63:511–531.
- Shackelford, N., Miller, B. P., and Erickson, T. E. (2018). Restoration of open-cut mining in semi-arid systems: A synthesis of long-term monitoring data and implications for management. *Land Degradation & Development*, 29(4):994–1004.
- Shan, J. and Aparajithan, S. (2005). Urban DEM generation from raw LiDAR data. *Photogrammetric Engineering & Remote Sensing*, 71(2):217–226.
- Silva, C. A., Klauberg, C., Hentz, Â. M. K., Corte, A. P. D., Ribeiro, U., and Liesenberg, V. (2018). Comparing the performance of ground

filtering algorithms for terrain modeling in a forest environment using airborne LiDAR data. *Floresta e Ambiente*, 25(2).

Šimová, P., Moudrý, V., Komárek, J., Hrach, K., and Fortin, M.-J. (2019). Fine scale waterbody data improve prediction of waterbird occurrence despite coarse species data. *Ecography*, 42(3):511–520.

Simpson, J. E., Smith, T. E. L., and Wooster, M. J. (2017). Assessment of errors caused by forest vegetation structure in airborne LiDAR-derived DTMs. *Remote Sensing*, 9(11).

Singh, K. K., Chen, G., Vogler, J. B., and Meentemeyer, R. K. (2016). When Big Data are too much: Effects of LiDAR returns and point density on estimation of forest biomass. *IEEE Journal of Selected Topics in Applied Earth Observations and Remote Sensing*, 9(7):3210–3218.

Sithole, G. and Vosselman, G. (2004). Experimental comparison of filter algorithms for bare-earth extraction from airborne laser scanning point clouds. *ISPRS Journal of Photogrammetry and Remote Sensing*, 59(1):85–101.

Skaloud, J. and Lichti, D. (2006). Rigorous approach to bore-sight self-calibration in airborne laser scanning. *ISPRS Journal of Photogrammetry and Remote Sensing*, 61(1):47–59.

Slatton, K. C., Carter, W. E., Shrestha, R. L., and Dietrich, W. (2007). Airborne Laser Swath Mapping: Achieving the resolution and accuracy required for geosurficial research. *Geophysical Research Letters*, 34(23).

Smardon, R. C. (1988). Perception and aesthetics of the urban environment: Review of the role of vegetation. *Landscape and Urban Planning*, 15(1):85–106.

- Smith, M. W., Carrivick, J. L., and Quincey, D. J. (2016). Structure from motion photogrammetry in physical geography. *Progress in Physical Geography: Earth and Environment*, 40(2):247–275.
- Snavely, N., Seitz, S. M., and Szeliski, R. (2006). Photo tourism: exploring photo collections in 3D. In *ACM transactions on graphics (TOG)*, volume 25, pages 835–846. ACM.
- Song, J.-H., Han, S.-H., Yu, K. Y., and Kim, Y.-I. (2002). Assessing the possibility of land-cover classification using lidar intensity data. *International archives of photogrammetry remote sensing and spatial information sciences*, 34(3/B):259–262.
- SPAR 3D (2016). Drone LiDAR vs Photogrammetry: A technical guide. <http://www.spar3d.com/news/lidar/drone-lidar-vs-photogrammetry-technical-guide> [online]. [cit. 2016-07-10].
- Steiakakis, E., Kavouridis, K., and Monopolis, D. (2009). Large scale failure of the external waste dump at the "South Field" lignite mine, Northern Greece. *Engineering Geology*, 104(3):269–279.
- Stephenne, N., Fripiat, C., Veschkens, M., Salmon, M., and Pacyna, D. (2014). Use of a LiDAR high resolution digital elevation model for risk stability analysis. *EARSeL eProceedings*, 13(S1):24–29.
- Stereńczak, K., Ciesielski, M., and Balazy, R. and Zawila-Niedźwiecki, T. (2016). Comparison of various algorithms for DTM interpolation from LIDAR data in dense mountain forests. *European journal of remote sensing*, 49(1):599–621.
- Stoker, J. M., Abdullah, Q. A., Nayegandhi, A., and Winehouse, J. (2016). Evaluation of Single Photon and Geiger Mode Lidar for the 3D elevation program. *Remote Sensing*, 8(9).
- Straub, C., Wang, Y., and Iercan, O. (2009). Airborne laser scanning: Methods for processing and automatic feature extraction for natural

- and artificial objects. In Heritage, G. L. and Large, A. R. G., editors, *Laser Scanning for the Environmental Sciences*, pages 115–132. Blackwell. ISBN 978-1-4051-5717-9.
- Sugumaran, R., Burnett, J., and Blinkmann, A. (2012). Big 3d spatial data processing using cloud computing environment. In *Proceedings of the 1st ACM SIGSPATIAL international workshop on analytics for big geospatial data*, pages 20–22. ACM.
- Sulaiman, N. S., Majid, Z., and Setan, H. (2010). DTM generation from LiDAR data by using different filters in open-source software. *Geoinformation Science Journal*, 10(2):89–109.
- Susaki, J. (2012). Adaptive slope filtering of airborne LiDAR data in urban areas for digital terrain model (DTM) generation. *Remote Sensing*, 4(6):1804–1819.
- Svobodová, K., Sklenička, P., Molnářová, K., and Šálek, M. (2012). Visual preferences for physical attributes of mining and post-mining landscapes with respect to the sociodemographic characteristics of respondents. *Ecological Engineering*, 43:34–44.
- Tarolli, P. and Sofia, G. (2016). Human topographic signatures and derived geomorphic processes across landscapes. *Geomorphology*, 255:140–161.
- Tarsha-Kurdi, F., Landes, T., and Grussenmeyer, P. (2008). Extended RANSAC algorithm for automatic detection of building roof planes from LiDAR data. *The photogrammetric journal of Finland*, 21(1):97–109.
- Teledyne (2019). Optech Titan multispectral lidar system - high precision environmental mapping. Technical report, Teledyne Optech, Inc.

- Tinkham, W. T., Huang, H., Smith, A. M. S., Shrestha, R., Falkowski, M. J., Hudak, A. T., Link, T. E., Glenn, N. F., and Marks, D. G. (2011). A comparison of two open source LiDAR surface classification algorithms. *Remote Sensing*, 3(3):638–649.
- Tomašík, J., Mokroš, M., Saloň, Š., Chudý, F., and Tunák, D. (2017). Accuracy of photogrammetric UAV-based point clouds under conditions of partially-open forest canopy. *Forests*, 8(5).
- Tonkin, T. N., Midgley, N. G., Graham, D. J., and Labadz, J. C. (2014). The potential of small unmanned aircraft systems and structure-from-motion for topographic surveys: A test of emerging integrated approaches at Cwm Idwal, North Wales. *Geomorphology*, 226:35–43.
- Tooke, T. R., Coops, N. C., Christen, A., Gurtuna, O., and Prévot, A. (2012). Integrated irradiance modelling in the urban environment based on remotely sensed data. *Solar Energy*, 86(10):2923–2934.
- Tooke, T. R., Coops, N. C., Voogt, J. A., and Meitner, M. J. (2011). Tree structure influences on rooftop-received solar radiation. *Landscape and Urban Planning*, 102(2):73–81.
- Tulldahl, H. M. and Larsson, H. (2014). Lidar on small UAV for 3D mapping. *Proc. SPIE 9250*, 9250.
- van Iersel, W., Straatsma, M., Addink, E., and Middelkoop, H. (2018). Monitoring height and greenness of non-woody floodplain vegetation with UAV time series. *ISPRS Journal of Photogrammetry and Remote Sensing*, 141:112–123.
- Velodyne (2019). Velodyne - smart, powerful lidar solutions for ADAS and autonomy.
- Verschoof-van, d. V. W. B. and Lambers, K. (2019). Learning to look at LiDAR: The use of r-CNN in the automated detection of archaeological objects in LiDAR data from the Netherlands. *Journal of Computer Applications*, 2:10.

- Vierling, K. T., Vierling, L. A., Gould, W. A., Martinuzzi, S., and Clawges, R. M. (2008). Lidar: shedding new light on habitat characterization and modeling. *Frontiers in Ecology and the Environment*, 6(2):90–98.
- Vojar, J., Doležalová, J., Solský, M., Smolová, D., Kopecký, O., Kadlec, T., and Knapp, M. (2016). Spontaneous succession on spoil banks supports amphibian diversity and abundance. *Ecological Engineering*, 90:278–284.
- Vorster, C. and Strecha, C. (2013). Accuracy assessment, time savings and safety—UAS for mining. *GIM International*, 27:5–10.
- Vymazal, J. and Sklenička, P. (2012). Restoration of areas affected by mining. *Ecological Engineering*, 43:1–4.
- Wagner, W., Ullrich, A., Melzer, T., Briese, C., and Kraus, K. (2004). From single-pulse to full-waveform airborne laser scanners: potential and practical challenges. *International Archives of Photogrammetry and Remote Sensing*, 35(B3):201–206.
- Wallace, L., Lucieer, A., Watson, C., and Turner, D. (2012). Development of a UAV-LiDAR system with application to forest inventory. *Remote Sensing*, 4(6):1519–1543.
- Wallace, L., Lucieer, A., and Watson, C. S. (2014). Evaluating tree detection and segmentation routines on very high resolution UAV LiDAR data. *IEEE Transactions on Geoscience and Remote Sensing*, 52(12):7619–7628.
- Wan, P., Zhang, W., Skidmore, A. K., Qi, J., Jin, X., Yan, G., and Wang, T. (2018). A simple terrain relief index for tuning slope-related parameters of LiDAR ground filtering algorithms. *ISPRS Journal of Photogrammetry and Remote Sensing*, 143:181–190.

- Wasowski, J., Bovenga, F., Nutricato, R., Nitti, D. O., and Chiaradia, M. T. (2018). Advanced satellite radar interferometry for deformation monitoring and infrastructure control in open-cast mines and oil/gas fields. *Innovative Infrastructure Solutions*, 3(1):68.
- Wehr, A. and Lohr, U. (1999). Airborne laser scanning—an introduction and overview. *ISPRS Journal of Photogrammetry and Remote Sensing*, 54(2):68–82.
- Wei, H. and Bartels, M. (2014). 3D digital elevation model generation. *3D Imaging, Analysis and Applications*, pages 367–415.
- Weisberg, P. J., Dilts, T. E., Becker, M. E., Young, J. S., Wong-Kone, D. C., Newton, W. E., and Ammon, E. M. (2014). Guild-specific responses of avian species richness to LiDAR-derived habitat heterogeneity. *Acta Oecologica*, 59:72–83.
- Weżyk, P., Szostak, M., Krzaklewski, W., Pająk, M., Pierzchalski, M., Szwed, P., Hawryło, P., and Ratajczak, M. (2015). Landscape monitoring of post-industrial areas using LiDAR and GIS technology. *Geodesy and Cartography*, 64(1):125–137.
- Wilson, J. P. (2012). Digital terrain modeling. *Geomorphology*, 137(1):107–121.
- Wortley, L., Hero, J.-M., and Howes, M. (2013). Evaluating ecological restoration success: A review of the literature. *Restoration Ecology*, 21(5):537–543.
- Xiang, J., Chen, J., Sofia, G., Tian, Y., and Tarolli, P. (2018). Open-pit mine geomorphic changes analysis using multi-temporal UAV survey. *Environmental Earth Sciences*, 77(6):220.
- Yan, W. Y., Shaker, A., and El-Ashmawy, N. (2015). Urban land cover classification using airborne LiDAR data: A review. *Remote Sensing of Environment*, 158:295–310.

- Yang, P., Ames, D. P., Fonseca, A., Anderson, D., Shrestha, R., Glenn, N. F., and Cao, Y. (2014). What is the effect of LiDAR-derived DEM resolution on large-scale watershed model results? *Environmental Modelling & Software*, 58:48–57.
- Yu, X., Hyypä, J., Vastaranta, M., Holopainen, M., and Viitala, R. (2011). Predicting individual tree attributes from airborne laser point clouds based on the random forests technique. *ISPRS Journal of Photogrammetry and Remote Sensing*, 66(1):28–37.
- Zalesky, J. and Capova, K. (2017). Monitoring and assessment of remedial measures in closed open cast mine. In Mikoš, M., Arbanas, Ž., Yin, Y., and Sassa, K., editors, *Advancing Culture of Living with Landslides*, pages 597–605, Cham. Springer International Publishing.
- Zalesky, M., Zalesky, J., Kuklik, P., and Hanek, P. (2008). Monitoring of a large slide and slope reclamation in a former open-pit mine. In *Proceedings of 13th FIG International Symposium on Deformation Measurements and Analysis and 4th IAG Symposium on Geodesy for Geotechnical and Structural Engineering*.
- Zhang, K., Chen, S.-C., Whitman, D., Shyu, M.-L., Yan, J., and Zhang, C. (2003). A progressive morphological filter for removing nonground measurements from airborne LIDAR data. *IEEE Transactions on Geoscience and Remote Sensing*, 41(4):872–882.
- Zhang, S., Li, X., and Chen, Y. (2015). Error assessment of grid-based direct solar radiation models. *International Journal of Geographical Information Science*, 29(10):1782–1806.
- Zhang, W., Qi, J., Wan, P., Wang, H., Xie, D., Wang, X., and Yan, G. (2016). An easy-to-use airborne LiDAR data filtering method based on Cloth Simulation. *Remote Sensing*, 8(6).
- Zhao, R., Pang, M., and Wang, J. (2018). Classifying airborne LiDAR point clouds via deep features learned by a multi-scale convolutional

neural network. *International Journal of Geographical Information Science*, 32(5):960–979.

Zink, R., Ramirez Camargo, L., Reidelstürz, P., and Dorner, W. (2015). *Photogrammetric Point Clouds for GIS-Based High-Resolution Estimation of Solar Radiation for Roof-Top Solar Systems*, pages 293–305. Springer International Publishing, Cham.

Chapter 10

Curriculum Vitae & List of Publications

Personal

Name: Michal Fogl

Date of birth: February 27, 1991 (Czech Republic)

E-mail: fogl@fzp.czu.cz

ORCID: <https://orcid.org/0000-0002-5880-6926>

RG: https://www.researchgate.net/profile/Michal_Fogl

Affiliations

1/2018 – present

Department of Applied Geoinformatics and Spatial Planning,
FES, Czech University of Life Sciences Prague

Member of the TACR project working group

2017 – present

Department of Applied Geoinformatics and Spatial Planning,
FES, Czech University of Life Sciences Prague

*Member of Spatial Science in Ecology and Environment Research
Group*

Education

2015 – present

Department of Applied Geoinformatics and Spatial Planning,
FES, Czech University of Life Sciences Prague

Doctor's degree of Applied and Landscape Ecology

Thesis topic: The Use of Laser Scanning Data in the Environmental Sciences

2013 – 2015

Faculty of Environmental Sciences, Czech University of Life Sciences
Prague

Master's degree of Landscape Engineering

Thesis topic: Rooftop Solar Potential in Different Latitudes: Tree
Structure Influence

2010 – 2013

Faculty of Environmental Sciences, Czech University of Life Sciences
Prague

Bachelor's degree of Landscaping, spec. Water Management

Thesis topic: The Use of Airborne LiDAR Systems in Ecology and
Hydrology

2006 – 2010

Secondary Technical School of Land Surveying and Geodesy in Prague
Geodesy

Participation in Research Projects

2018 – 2019

Detection of infection forest bark beetle (*Ips typographus*) in advance
using unmanned air vehicles

Technology Agency of the Czech Republic

Co-investigator

2018 – 2019

Remote sensing: an effective tool for the study of spatial dynamics of bark beetles at Krkonoše Mountains National Park
Grant Agency of the Czech University of Life Sciences Prague
Co-investigator

2017 – 2018

The influence of structure of growth on the species diversity and distribution of birds in the Giant Mountains national park
Internal Grant Agency of the Faculty of Environmental Sciences
Leader

2015 – 2016

Characteristics of the 3D structure of vegetation and terrain
Hornojiřetínská dump, migration routes and habitat preferences agile frog (*Rana dalmatina*)
Internal Grant Agency of the Faculty of Environmental Sciences
Co-investigator

Courses and Trainings

4/2019 – 5/2019

Department of Forest Management, Geomatics and Forest Economics,
Faculty of Forestry, University of Agriculture in Krakow, Poland
Internship

7/2013 – 8/2013

Ecosystems of Ireland
Ireland, FES, CZU Prague
Intensive summer school

6/2012 – 7/2012

Ecosystems of Northern Europe
Norway, Finland and Sweden, FES, CZU Prague
Intensive summer school

International Conferences

4/2017

The Use of Airborne Laser Scanning Data to Study Birds Habitat Requirements

Fogl M. & Moudrý V.

In: Doctoral Consortium on 3rd International Conference on Geographical Information Systems Theory, Applications and Management, INSTICC.

Porto, Portugal.

Impact Publications (J_{imp})

Comparison of leaf-off and leaf-on combined UAV imagery and airborne LiDAR for assessment of a post-mining site terrain and vegetation structure: Prospects for monitoring hazards and restoration success. (2019). Moudrý V., Gdulová K., **Fogl M.**, Klápště P., Urban R., Komárek J., Moudrá L., Štroner M., Barták V., Solský M. *Applied Geography*, Elsevier. vol. 104, p. 32-41, ISSN 0143-6228.

Suitability, characteristics, and comparison of an airship UAV with lidar for middle size area mapping. (2017). Koska B., Jirka V., Urban R., Křemen T., Hesslerová P., Jon J., Pospíšil J., **Fogl M.** *International Journal of Remote Sensing*, Taylor & Francis. vol. 38, p. 2973-2990, ISSN 0143-1161.

Influence of vegetation canopies on solar potential in urban environments. (2016). **Fogl M.**, Moudrý V. *Applied Geography*, Elsevier. vol. 66, p. 73-80, ISSN 0143-6228.

Other Publications

Identification of infested trees using unmanned aerial vehicles. (2019). Klouček T., Komárek J., Lagner O., **Fogl M.**, Gdulová K. Certified methodology. 66 p., ISBN 978-80-213-2932-4.

Teaching Experience

2015 – present

Department of Applied Geoinformatics and Spatial Planning

Seminars of GIS; Computer Technology Utilization; Cartography and Mapping

